NsG-233-62

UNPUBLISHED PRELIMINARY DATA ; SUI 63-20) OTS:

N64 10178*

123 p. (NASA CR 5 2300; CODE-1

[redacted]

[7]

OTS PRICE

XEROX $ 10.10 ph

MICROFILM $ 3.89 mf.

Department of Physics and Astronomy

STATE UNIVERSITY OF IOWA State U.,

Iowa City, ~~Iowa~~

465 8001

THE MORPHOLOGY OF THE ELECTRON DISTRIBUTION IN THE OUTER RADIATION ZONE AND NEAR THE MAGNETOSPHERIC BOUNDARY AS OBSERVED BY EXPLORER XII *

by

John Wright Freeman, Jr. (Ph. D. Thesis)

A dissertation submitted in partial fulfillment of the requirements for the degree of Doctor of Philosophy in the Department of Physics and Astronomy in the Graduate College of the State University of Iowa

June 1963 123 p refs

Chairman: Professor James A. Van Allen

*Research supported in part by the National Aeronautics and Space Administration under grant (NsG-233-62)

(NASA Grant)

ACKNOWLEDGEMENTS

The author is especially indebted to Drs. J. A. Van Allen and B. J. O'Brien for guidance and encouragement as well as the original design of the S.U.I. Explorer XII experiment and to L. A. Frank, C. D. Laughlin, D. Gurnett, and W. A. Whelpley of S.U.I. for the design and fabrication of various components of the experiment.

Special thanks are due to Drs. S.-I. Akasofu and L. J. Cahill, Jr., for helpful discussions regarding various aspects of this work.

The cooperation of F. B. McDonald, L. R. Davis, and Paul Butler of the Goddard Space Flight Center is gratefully acknowledged.

Thanks also to Mrs. Evelyn Robison who typed the manuscript.

This work was performed under contract NsG-233-62 while the author was a research fellow of the National Aeronautics and Space Administration.

ABSTRACT

The elliptic orbit satellite Explorer XII made possible the routine survey of the heart of the outer radiation zone as well as the region of transition between the magnetosphere and interplanetary space on the sunward side of the earth using a variety of particle and magnetic field detectors. A comprehensive analysis of the data received from the S.U.I. detectors during the entire 112 day lifetime has been performed. Salient features observed include: confirmation of the enhancement of soft electron fluxes and diminution of hard electron fluxes in the outer zone during magnetically disturbed times; the outward motion of the outer zone hard electron maximum during periods of enhancement; confirmation of the general Chapman and Ferraro picture of a well defined magnetosphere with compression of the geomagnetic field during the initial phases of magnetic storms; the existence of a layer of quasi-thermalized plasma immediately outside the magnetosphere; confirmation of the result of Frank and Van Allen that the contours of constant counting rate for $E \geq 40$ keV electrons

10178

tend to protrude outward near 90° from the sub-solar point and draw closer to the earth on the night side; and general support for the result of Gringauz, Kurt, Moroz, and Shklovskii, that there exists a region beyond some 8 R_e on the night side of the earth dominated by very low energy electrons. AUTHOR

TABLE OF TABLES

TABLE OF CONTENTS

I. INTRODUCTION

Early estimates of the soft electron fluxes in the outer zone were based on measurements made with detectors whose primary electron sensitivity was to particles exceeding a MeV in energy. Largely under the impetus of observed auroral electron spectrums and plausibility arguments, it was assumed that the response of these detectors was in the main the result of bremsstrahlung from non-penetrating electrons. Under such assumptions (that the average energy of electrons was of the order of 50 keV), it was generally estimated that the omnidirectional intensity, J_o, of electrons of energy $E > 20$ keV was of the order of 10^9 to 10^{11} electrons/cm^2 sec [Van Allen and Frank, 1959; Arnoldy, Hoffman, and Winckler, 1960; Fan, Meyer, and Simpson, 1961; Vernov, Chudakov, Vakulov, Togachev, and Nikolayev, 1960].

The second Soviet cosmic rocket (Lunik II) provided an indication that existing soft electron flux estimates for the outer zone should be re-evaluated when Vernov and his co-workers [1960] reported an intensity of $\sim 5 \times 10^5$ 1 to 2 MeV electrons/cm^2 sec and Gringauz [1960] and his co-workers reported less than 10^7 electrons of energy $E > 200$ eV/cm^2 sec out to 61,000 km (geocentric distance).

Using data from an Anton 302 Geiger tube and an ionization chamber flown on Explorer VI, Arnoldy, Hoffman, and Winckler, in a preliminary report [1960] showed an apparent decrease in the outer zone intensity during periods of intense magnetic activity. They attributed the response of these detectors to bremsstrahlung from electrons of energy of the order of 50 keV. Also using Explorer VI data from a scintillation counter Rosen and Farley [1961] observed an enhancement of the soft electron component of the outer zone during magnetically disturbed times. Van Allen [1961] and Forbush, Pizzella, and Venkatesan [1962], using Explorer VII data, reported an apparent diminution in the hard component of the outer zone with magnetic activity.

However, the question of absolute fluxes for electrons in the 50 keV energy range in the outer zone was not settled unambiguously until the launching of Explorer XII, which carried on the State University of Iowa experiment an electron spectrometer with pass bands in the 50 keV and 100 keV range as well as total energy flux detectors capable of sensing electron energy fluxes consisting of electrons of energies as low as a few hundred eV. In a preliminary paper based on Explorer XII data from 5 September 1961, O'Brien, Van Allen, Laughlin, and Frank [1962]

reported that the omnidirectional intensity of electrons of energy greater than 40 keV was of the order of 10^8 electrons/cm^2/sec of energy between 1.6 and 5 MeV, 2 x 10^5 electrons/cm^2 sec; also see Rosser, O'Brien, Van Allen, Frank, and Laughlin [1962]. More recently, Frank, Van Allen, Whelpley, and Craven [1963], using Explorer XIV data, have derived the following sample estimates of the outer radiation zone electron intensities at 39,000 km geocentric distance:

$$J_o\ (E_e \geq 40\ \text{keV}) = 1.5 \times 10^8/\text{cm}^2\ \text{sec}$$
$$J_o\ (E_e \geq 230\ \text{keV}) \leq 1.5 \times 10^6/\text{cm}^2\ \text{sec}$$
$$J_o\ (E \geq 1.6\ \text{MeV}) = 2 \times 10^5/\text{cm}^2\ \text{sec}.$$

In addition to yielding new measurements on the average absolute electron intensities on the outer radiation zone, Explorer XII, during its 112-day lifetime, provided extensive data on the temporal and spatial variations of the electron fluxes in the outer zone as well as the region of interaction between the magnetosphere and the solar wind. It is to the presentation and analysis of these data that this paper is addressed.

II. THE EXPERIMENT

Explorer XII (1961 Upsilon, see Figure 1) was launched at 0321 U.T. on August 16, 1961, into an orbit with apogee approximately 83,600 km, perigee 6,700 km (geocentric distance), inclination 33°, and period 26.5 hours. Her spin axis extended to right ascension 47.0° and declination -27.5°. The sun angle with the spin axis, χ, varied from 105° after launch to a maximum of 135° in mid-October. Her spin rate increased from 27.8 RPM to 30.5 RPM in mid-October, at which time it was increasing.

The angle between the satellite-earth line at apogee and the earth-sun line projected on the equatorial plane of the earth, i.e., the longitudinal difference between the apogee sub-satellite point and sub-solar point, varied from -4° on August 16 to +103° on December 6, when the active life of the satellite ended (see Figure 2). Similarly, the latitudinal difference between the apogee sub-satellite point and the sub-solar point varied slowly from +28° to -18°. These angles are referenced to the apogee sub-satellite point and are considered positive or negative in the standard latitude and longitude sense. Hence, during the first few weeks, apogee was within 30° of the solar direction. Due to the earth's rotation about the sun, apogee moved away from the

solar direction at a rate of 0.95 degree/day. By the time that transmission ended on December 6, 1961, it had reached approximately 100° from the solar direction.

The State University of Iowa detector complement of Explorer XII consists of the following charged particle detectors:

SpL -- an electron energy spectrometer channel with pass band 40 keV $\leq$ E $\leq$ 50 keV. Here, electrons are magnetically focussed into a mica-window, Anton 213 G.M. tube surrounded except for the entrance aperture by 3.5 g/cm^2 of lead [C. D. Laughlin, private communication].

SpH -- a second energy channel for the above spectrometer with pass band 80 keV $\leq$ E $\leq$ 100 keV.

SpB -- a background detector for the above two spectrometer channels. This detector is an Anton 213 G.M. tube surrounded completely by at least 3.5 gm/cm^2 of lead. Van Allen [1963] estimates an efficiency, ϵ, of 3×10^{-4} counts/second per electron/cm^2 second for 10 MeV monoenergetic electrons incident on this detector. Below this energy the estimated electron efficiency falls monotonically to 10^{-5} at 2 MeV. Protons of E $\geq$ 40 MeV are detectable with high efficiency.

302 -- an Anton 302 G.M. tube sensitive directly to electrons E $\geq$ 1.6 MeV and protons E $\geq$ 20 MeV [L. A. Frank, private communication] and indirectly through bremsstrahlung to electrons of E $\gtrsim$ 30 keV.

CdSTE -- a CdS crystal energy flux detector sensitive to energy fluxes exceeding 1 erg/cm^2 sec ster consisting of electrons

of energy E $\geq$ 200 eV or protons of energy E $\geq$ 1 keV or ions of similar energy. This detector consists of a bare photoconductive single crystal of CdS mounted in a cylindrical lead shield situated behind a series of beam-collimating and light-baffling apertures. The aperture provides a zero-absorber, circular solid angle of 10^{-2} steradians. An additional 0.66 steradian of the crystal solid angle is covered by approximately 1 g/cm^2 of magnesium and the remaining 12 steradians by at least 2.6 g/cm^2 of lead (see Figure 3) /Freeman, 1961/.

CdSB -- a CdS crystal energy flux detector identical to CdSTE except for a small "broom" magnet which removes electrons of energy E $\geq$ 250 keV and protons of energy E $\geq$ 400 eV from the beam incident on the crystal. The magnet provides a field of 500 gauss which with the detector geometry reduces the electron flux from a T ℓ^{204} source by better than 90%. The magnet is 5 g/cm^2 thick and subtends a solid angle of 0.5 steradian at the crystal. This solid angle lies within the 0.66 steradian cone of the 1 g/cm^2 shielding.

CdSOM -- a CdS crystal detector identical to CdSTE except for a 2 mm thick (0.55 g/cm^2) transparent quartz window. This detector serves as a light and x-ray background detector for the other two CdS detectors.

Note that the energy per particle lower limit of sensitivity quoted above for electrons and protons incident on the CdSTE detector is not sharp, but merely represents declining efficiency due to crystal surface effects. An upper limit also occurs when

particle energy reaches the point of complete penetration of the crystal. For a typical crystal this occurs at about 200 keV for electrons and 8 MeV for protons. Figure 4 shows a sensitivity curve for electrons. Previous investigation has shown that the maximum sensitivity (see caption of Figure 4 for definition of sensitivity) is nearly the same for electrons, protons, alpha particles, and x-rays [Freeman, 1961]. Unless otherwise stated, maximum efficiency particles will always be assumed to determine the CdS derived energy flux. This means that quoted energy fluxes are lower limits.

For the selected CdS crystals used in the flight modules, crystal conductivity is very nearly linear with energy input. The current resulting from the crystal photoconductivity is monitored by a neon-glow tube relaxation oscillator whose output frequency is linear with crystal current.

The calibrated sensitivities of the CdSTE and CdSB detectors are nearly the same for maximum efficiency particles; however, when the responses of the two detectors are compared, the response of CdSB is always normalized to that of CdSTE in order that relative energy fluxes can be compared directly. The dark current of the CdSB detector in flight was higher than during laboratory calibrations. This shift in dark current has not been adequately

explained; however, there is no evidence to indicate a corresponding drift in the detector efficiency.

The CdS detectors are also sensitive omnidirectionally to penetrating radiation such as electrons $E \gtrsim 3$ MeV, protons $E \gtrsim 30$ MeV, and x-rays $E \gtrsim 200$ keV. Table I gives a compilation of the detector details.

All of the above detectors are directional detectors, except the 302 and SpB.

These directional detectors are mounted with their look axes normal to the spin axis of the satellite as shown diagramatically in Figure 5.

Since the count accumulation interval is 10.24 seconds and the spin rate approximately 30 RPM, the satellite rotates about its axis approximately 5 times during each accumulation interval. During these 5 rotations, the directional detectors have repeatedly swept out a band on the celestial sphere whose plane is normal to the spin axis of the satellite. For the CdS detectors and the spectrometer channels, this band is approximately 12° and 6° wide, respectively. Thus, the count-rates of these detectors represent directional time averages over the specified region of the sky taken over a period of 10.24 seconds. This makes precise directional resolution impossible; however,

generalizations can be made regarding the relationship between count-rates and the magnetic field direction. If α is the angle between the magnetic field vector $\overrightarrow{F}$ and the spin axis of the satellite (as shown in Figure 5) and ϕ is the azimuthal angle between the detector direction and the plane containing the $\overrightarrow{F}$ and the spin axis, then θ, the angle between the detector direction and the field vector $\overrightarrow{F}$ is given by

$$\cos \theta = \sin \alpha \cos \phi \, . \tag{1}$$

Here ϕ may be given by

$$\phi = \frac{2\pi t}{T} + \zeta \tag{2}$$

where t is time, T is the period of the satellite spin, approximately 2 seconds, and ζ is an arbitrary angle.

From this, it can be seen that the limits of θ are determined by α through

$$\cos \theta = \pm \sin \alpha \, . \tag{3}$$

Figure 6 illustrates graphically the values of θ swept out by the directional detectors, during one complete revolution, for all possible values of α. Note that when α has the value of 90°, all values of θ are sampled, i.e., particles having all possible pitch angles can enter the directional detectors. As α increases

or decreases from 90° particles with very low pitch angles are progressively excluded from the detectors. For example at $\alpha = 45°$ only particles with pitch angles greater than 45° and less than 135° can be sampled. At $\alpha = 0°$ or 180° only particles moving normal to the magnetic field can be seen by the directional detectors.

Whether or not a charged particle moving along a line of geomagnetic force with constant magnetic moment will be reflected before encountering the earth's atmosphere can be determined by specifying the equatorial pitch angle of the particle. For each line of force a critical angle, θ_D, exists such that all particles having equatorial pitch angles less than θ_D will be "dumped" and all particles having equatorial pitch angles greater than θ_D will be "trapped". Figure 6 also gives these critical angles, θ_D, for four L values superimposed on the θ vs α pattern. By inspection of Figure 6 it is possible to determine for each α whether or not the limits of θ include pitch angles which lie within the dumping cones. For example, beyond $L = 4$, α must have a value of $90 \pm 8°$ or the extreme angular excursion of θ will fall short of the dumping cone; that is, the directional detectors will see only trapped radiation.

Similarly for $L \geq 6$ and $86° \leq \alpha \leq 94°$ all the directional detector response will be due to trapped radiation, etc.

As the satellite spins and the detectors sweep through values of θ the time during which various pitch angles are exposed to the detectors is <u>not</u> in general independent of θ. The time average obtained over the 10.24 second accumulation interval is in fact a weighted average over the pitch angles within the limits specified above. The weight factors attached to various values of θ are a function of α. Some samples of the manner in which the weight functions vary over θ for different α's are given in Figure 7. The detectors are considered to have an opening angle of 6° and the time which is plotted is the total time during each accumulation interval that a particle having a pitch angle, θ, can enter the detector. It is seen that low pitch angles tend to be favored in the time averaging process.

The parameter, α, which is so crucial to the above discussion, is provided by an onboard magnetometer built under the direction of Dr. L. J. Cahill, Jr., of the University of New Hampshire. The magnetometer consists of three orthogonally mounted saturable core magnetometers. Each one is capable of measuring the component of the magnetic field along its axis in the range from

1 to 1000 gammas. The direction of the component is also indicated. The direct telemetry introduces an uncertainty in each component measurement of $\pm$ 12 gammas. In final form, the magnetic data provides the magnitude of the magnetic field vector, $\vec{F}$, the angle α, and the angle ψ, between the planes formed by the spin axis and the field vector and the spin axis and the direction of the sun [Cahill and Amazeen, 1962].

At the time of writing, the value of α is only available for a limited number of passes. An inspection of these passes, however, shows that α behaves in a regular and predictable manner due to the highly inertial property of the satellite spin axis in a space fixed coordinate system. Because of the relative proximity of the satellite orbit to the magnetic equator, α changes very slowly within the magnetosphere. During a typical inbound pass α drops gradually from approximately 100° at 65,000 km to approximately 80° at 30,000 km. During an outbound pass α increases slowly from about 60° to some value usually less than 80° over a similar radial range. (A sample of the way α varies during an inbound pass is shown in Figure 20.)

From this, together with the foregoing discussion, we can conclude that the angular sweep of the directional detectors

generally includes the dumping cone at some time during an inbound pass although the total time averaging process is generally weighted in favor of trapped radiation pitch angles at greater distances. An examination of three inbound passes for which the α data indicates an expected transition from inclusion to exclusion of the dumping cone in the θ sweep shows no coincident changes in the directional detector response. For these reasons and because of the lack of routine α data at the time of writing, we will assume that the directional detector responses within the magnetosphere are predominantly the result of geomagnetically trapped radiation.

The Explorer XII telemetry format is such that a new readout of the counts accumulated during a 10.24 second accumulation interval is obtained once every 79 seconds for each SUI detector. Each new readout is defined as a data-point. Thus if one takes a three-data-point average of the count-rate of a given detector, the average covers a time interval of approximately 4 minutes, although the time during which the detector was actually being monitored is only approximately 30 seconds. In order to speed automatic data reduction and data analysis, three-data-point averages have been taken where continuous data permits. Admittedly, some time and space resolution has been lost by this

averaging process; however, cases where high temporal and spatial variations are suspected have been hand-plotted with every data point.

SUI Explorer XII data is received in digitized form on magnetic tape from Goddard Space Flight Center. It is processed by the SUI IBM 7070 computer with a program which finds frame synchronization by searching for the SUI sync word and rejects noisy data by requiring perfect redundancy between redundantly telemetered detector count-rates.

For purposes of automatic plotting and more detailed data analysis, a second program was written which was designed to operate on the output of the first. This program computes the three (or less if there occurs a sequence break in the data) data-point averages for the count-rate of each SUI detector. Where necessary and possible, it corrects the detector count-rates for dead time and scaling factors and background. It computes, using an eccentric dipole approximation, the magnetic coordinates for each data point. It provides the data from each detector on a separate output for automatic graphing purposes. Finally, it merges and sorts the data from all tracking stations to provide a chronologically-ordered output. The final ordered output for each detector contains the following parameters:

(1) The identification of the detector.

(2) The universal data and time to the nearest second.

(3) The telemetry station number.

(4) The geocentric position of the satellite.

(5) The geographic longitude.

(6) The magnetic latitude.

(7) The radial distance from the earth's dipole center.

(8) The scalar value of the magnetic field.

(9) The McIlwain L parameter.*

(10) The average count rate per 10 second taken over up to as many as three data points.

(11) The logarithm of the average count rate per 10 second (necessary for automatic plotting).

(12) The number of data points over which the average was taken.

---

*The magnetic coordinates generated by the eccentric dipole program have been compared with the output of the current McIlwain program employing the Jensen and Cain coefficients. The L values were found to agree to within a few per cent for distances beyond approximately two earth radii.

The above data are punched on IBM cards. The cards then are separated into successive inbound and outbound passes. Count-rate data from each pass are plotted as a function of geocentric position using an IBM 514 reproducing punch as a card reader and a Moseley model 30 AB card translator and Moseley autograph electronic grapher.

III. THE OUTER ZONE

A. General Features.

To illustrate some of the general properties of the outer zone as revealed by the SUI Explorer XII detectors, we will present the data from a pass during a period of relative magnetic quiet. It will become clear in later pages of this section that the effects of what appear to be small magnetic disturbances from ground based stations are greatly magnified when direct observations of the particle energy content and radial extent of the magnetosphere are considered. A magnetically quiet time is a rare occasion. The apparent commonness of magnetically undisturbed periods is a misconception fostered by the relative insensitivity of the ground based observations.

As representative of a "quiet time" pass we have chosen the inbound pass on September 18 and 19, 1961. During this pass the K_p index is less than or equal to 1^+ and $D_{st}(H)$ value computed from San Juan and Honolulu is negative and less than 10 γ ($1\ \gamma = 10^{-5}$ gauss).* For the 19th of September the magnetic character figure assigned is 0.0 and the K_p sum is 5^-

*D_{st} from San Juan and Honolulu, courtesy of S.-I. Akasofu.

/Compilations of Solar-Geophysical Data, C.R.P.L.-F, 207 Part B, November 1961/. Three flares of importance 2 and one flare of importance 1^+ were reported at approximately noon on the 18th of September. However these flares were probably responsible for the mild increase in magnetic activity which started early on the 20th /Compilations of Solar-Geophysical Data, C.R.P.L.-F, Part B, October 1961/.

The Explorer XII, SUI, data for the 18-19 September inbound pass are illustrated in Figure 8. Note that between the radial range 80,000 km and 15,000 km the satellite is within approximately 15° of the geomagnetic equator; hence the observed detector responses can be thought of as radial profiles of radiation intensity along the magnetic equator.

We observe the following general features in Figure 8:

(a) There exists a sharp outer boundary around 70,000 km beyond which the SpL-SpB and SpH-SpB count rates (the spectrometer channels corrected for background) fall to zero. It will be shown in Section IV, for a similar pass with onboard magnetometer data, that this boundary delineates the region of the dominant geomagnetic field or magnetosphere and the interplanetary medium. Only within this boundary can durable geomagnetic trapping take place since only within this region is the magnetic field ordered.

(b) Inside the boundary the SpL-SpB and SpH-SpB average count-rates rise rapidly to values between 1 and 10 counts/second. These rates, while exhibiting large temporal and/or spatial variations, remain at or below 10 counts/second until the satellite passes within 20,000 km at which time they again continue to rise. Since the plotted data points are time averages over three data points or a total accumulation interval of approximately 30 seconds, the large excursions in count-rate have been averaged out; however the remaining fluctuations are well outside statistical error.

(c) Typically near the outer edge of the zone (45,000 to 68,000 km) the SpL-SpB rate exceeds the SpH-SpB rate while at middle distances (20,000 to 45,000 km) they are indistinguishable. Approaching the region 15,000 to 20,000 km there is an apparent turnover in the spectrum with SpH-SpB exceeding SpL-SpB. The geometric factors of the two spectrometer channels are identical to within 20% /C. D. Laughlin, private communication/.

A count-rate of 10 counts/second for the SpL and SpH detectors corresponds to an averaged directional flux of approximately 5×10^5 electrons/cm^2 sec ster. For the SpH energy of 100 keV this is an averaged directional energy flux of approximately 0.1 erg/cm^2 sec ster.

(d) Beyond approximately 80,000 km the CdS detectors are saturated by sunlight reflected from the earth. Between 80,000 km and 73,500 km there is a small local increase in the CdS total energy detector response. The significance of this increase will be discussed in Section IV. Inside 73,500 km the CdSTE and CdSB detectors show a slow steady increase as the satellite moves inward. This increase in energy flux is correlated with the gradual increase in the SpL-SpB and SpH-SpB rates and is attributed to the combination of primary and secondary radiation from electrons of these or higher energies entering from the collimated and/or non-collimated directions. The CdSTE detector indicates an energy flux of the order of 1 to 10 erg/cm^2 sec ster between the magnetospheric boundary and 16,000 km if the observed response be due entirely to collimated electrons.

(e) CdSOM (completely surrounded by at least 0.55 g/cm^2 of material) indicates a local broad peak at about 32,000 km. This peak is related in position to the similar peak in the SpB count rate. We can therefore conclude that this peak represents the penetrating component of the outer zone.

(f) Unlike the SpL and SpH count rates the 302 count rate varies by nearly 4 orders of magnitude during the pass. The rate in-

creases monotonically into about 31,000 km at which time a small plateau is observed followed by a local peak at 24,000 km. On some passes the plateau resolves into a second local peak (see Figure 1, Rosser et al. [1962]).

(g) The SpB count rate shows only one broad peak. This maximum is coincident with the 302 plateau and not with the 302 maximum.

An interpretation of the 302 and SpB response for a similar pass on August 16 and 17 has been given by Rosser, O'Brien, Van Allen, Frank, and Laughlin [1962] and for a third similar pass by O'Brien, Van Allen, Laughlin, and Frank [1962]. Both papers show, relying essentially on the energy flux measurements of the CdSTE detectors, that the 302 counting rate near the outer zone peaks is due predominantly to penetrating electrons ($E \geq 1.5$ MeV). Early interpretations of outer zone 302 data from the satellite Explorers IV, VI, and VII were based on the assumption that the 302 count rate resulted from bremsstrahlung from a large flux of electrons of energy $E \geq 20$ keV. The SpL and SpH detectors show that the particle fluxes in the 50 and 100 keV range are of the order of 5×10^5 electrons/cm^2 sec ster, several orders of magnitude too low to account for the 302 rate of 10^4 counts/sec. The possibilities remaining are electrons of energy $E \leq 40$ keV or energy $E \geq 100$ keV or protons of energy

$E \geq 20$ MeV. Rosser et al. disposed of the electrons of energy $E \leq 40$ keV by arguing that to obtain the maximum 302 rate, an omnidirectional intensity of the order of 10^{13} electrons/cm^2 sec each of 30 keV energy would be required. This would result in an energy flux of $\sim 5 \times 10^5$ ergs/cm^2 sec. This is at least four orders of magnitude greater than the maximum energy flux ever observed by the CdSTE detector. To eliminate as a possibility bremsstrahlung from electrons of energy $E \geq 100$ keV, Rosser et al. assume a monoenergetic flux of 500 keV electrons. This would require a flux of $\sim 2 \times 10^9$ electrons/cm^2 sec to produce the 302 peak rate observed on the August 17 pass. According to Rosser et al., such a flux would give a CdSTE rate of ~ 50 counts/sec, whereas the observed rate is approximately 7 counts/sec. The foregoing analyses rely on the 302 electron efficiency curve given by Frank [1961].

The conclusion that the maximum 302 rates observed do not result from high energy subpenetrating electrons has recently been given absolute experimental confirmation by Frank, Van Allen, Whelpley, and Craven [1963] who have shown, using a set of variously shielded 213 G.M. tubes, that the omnidirectional flux of electrons of energy $E \geq 230$ keV was $\leq 1.5 \times 10^6$/cm^2 sec in the heart of the outer zone at 5 October 1962, while at the same

time the 302 count rate was 10^5 counts/second. Using Frank's 302 efficiency curve (Figure 1, O'Brien et al. [1962]) and assuming a monoenergetic beam of 500 keV electrons, an omnidirectional flux of 10^{10} electrons/cm^2 sec would be required to provide the observed 302 rate. This is 4 orders of magnitude greater than the observed rate for $E \geq 230$ keV electrons.

The remaining possibilities for the source of the 302 maximum outer cone count rate are directly penetrating electrons, $E \geq 1.5$ MeV or protons, $E \geq 23$ MeV. Protons can be ruled out on the basis of scintillation counter measurements by Bame, Conner, Hill, and Holly [1963] and Davis and Williamson [1962]. We conclude that the 302 rate is a measure of the penetrating electron component, $E \geq 1.5$ MeV. SpB is assumed to respond predominantly to the bremsstrahlung from energetic electrons.

Table II gives a summary of the resulting electron fluxes found for the various detectors at four radial distances during this pass. Using the electron spectrometer channels as two points on a differential energy spectrum we can determine the exponent of the energy, γ, for a power law spectrum, i.e.,

$$N(E) = N_o E^{\gamma} .$$

The values of the exponent, γ, are also shown in Table II. Outside 20,000 km γ is negative and increases in absolute magnitude with

increasing radial distances. Using the same detectors, O'Brien [1962] has shown that this variation in γ is typical. See Figure 3, O'Brien and Laughlin [1962].

If one assumes the power law approximation to be a satisfactory fit to the real spectrum near the low energy end, it should be possible to employ the CdSTE energy flux measurement to determine the low energy cut-off giving the best agreement between the integrated energy flux and the observed energy flux. Such a calculation for the 65,000 km data point, $\gamma = -3.5$, yields a low energy cut-off in the electron spectrum at approximately 2 keV. There are two factors which make this number tentative:

1. The contribution to the CdSTE energy flux from very low energy protons ($E \leq 500$ eV) is undetermined. The low CdS crystal efficiency for such particles makes it unlikely; however, if this flux is significant, the low energy electron cut-off energy may be higher.

2. 2 keV is in the region of low energy declining sensitivity for the CdSTE detector; therefore the energy flux estimated from the detector is too low and consequently the 2 keV cut-off energy may be too high.

For the other values of γ given in Table II the additional two powers of E resulting from the integration and the multiplication by the energy in converting from particle flux to energy flux result in a spectrum whose integrated energy flux is restricted by the high rather than the low energy cut-off.

It is interesting to note that the SpB (also CdSOM) maximum at 32,000 km does not coincide with the 302 maximum which occurs at 24,000 km. The high energy end of the electron spectrum must soften between 32,000 and 25,000 km. Inside 20,000 km the SpH-SpB rate begins to exceed the SpL-SpB rate, indicating a hardening of the middle portion of the electron spectrum. The detailed electron spectrum must undergo some remarkable changes with radial distance in this region of space. In order to avoid possibly confusing flux variations due to more than one source, the following sections of this paper which deal with magnetic storm time variations will be restricted to data from the region of the magnetosphere outside the point of inversion of the SpL, SpH spectrum, that is, typically outside 20,000 km or L = 3.

Using our September 18-19 pass as an example, we can summarize the following general features of the electron fluxes within the magnetosphere on the day side of the earth:

1. The radial distribution of the soft electron component ($E \leq 100$ keV) is unrelated to that of hard electron component ($E \geq 1.5$ MeV), the hard electron component being concentrated toward lesser radial distances.

2. The 50 keV and 100 keV electron fluxes undergo temporal and/or spatial variations of nearly an order of magnitude over intervals of 5 minutes and/or 1000 km. These soft electron fluxes, in contrast to the hard electron fluxes, are characterized by much fine structure.

3. There is a general tendency for the soft electron spectrum to soften at greater radial distances and harden at lesser distances.

4. There exists a radial distance, typically 70,000 km, beyond which the 50 keV and 100 keV electron fluxes fall below the minimum observable value, $\sim 3 \times 10^4$ electrons/cm^2 ster averaged.

B. Storm-Time Variations in the Outer Zone.

1. The Experimental Results.

The first major magnetic storm encountered by Explorer XII began with a sudden commencement at 1715 U.T. on the 29th of August, 1961. The storm had a duration of approximately seven days and a maximum K_p of 6. It was assigned a degree of activity of m (moderate) [Lincoln, 1962]. See Figure 12 for D_{st} and K_p values.

Figures 9, 10, and 11 illustrate the S.U.I. Explorer XII data for selected sequences of passes during different stages of this storm.

Figure 9 shows the changes which took place in the electron spectrometer count-rates throughout the storm. We see that the 50 keV electron channel (SpL) shows an enhancement of typically an order of magnitude during the interval of not more than 10 hours from the August 30 inbound to the August 30 outbound. A subsequent pass occurring late in the recovery phase shows a depletion of the previous enhancement. The greatest enhancement appears to occur near the outer region of the magnetosphere (i.e., from 50,000 to 65,000 km). The 100 keV electron channel (SpH) shows a similar although less striking main phase enhancement, again the greatest variation occurring in the outer regions. Again there is a depletion during the recovery phase.

This enhancement of the soft electron component of the spectrum during the main phase is verified by part (a) of Figure 10 which shows a CdSTE detector response corrected for penetrating radiation through the subtraction of the CdSOM response. The CdSB detector shows no storm-time variation apart from the penetrating component.

Part (b) of Figure 10 shows that the penetrating contribution to the CdS detector responses undergoes an exactly opposite variation with a diminution during the main phase and a subsequent enhancement above the pre-storm levels during the late recovery phase.

Figure 11 verifies this result by showing the 302 and SpB rates, both of which are measures of the penetrating electron component. The post-storm enhancement is most clearly indicated by the SpB count-rate which shows a nearly two order of magnitude enhancement in the penetrating electron flux during the interval from 1400 hours on August 30 to 2100 hours on September 3.

It is now of interest to determine the extent to which the storm-time variations described for this storm are found in the remaining storms during the lifetime of Explorer XII. To this end we present Figure 12 which shows a time history of the hard and soft electron maximum rates found during approximately 100 passes through the outer zone. The SpL-SpB rate is taken to be representative of the soft electron and the 302 rate represents the hard electron flux. The maximum SpL-SpB rates found at or outside the heart of the outer zone, i.e., L values greater than 3, have been used to avoid confusion with variations in the slot region. After September 20, when the SpB detector no longer functioned,

contamination to the SpL detector from penetrating radiation was estimated by the 302 count-rate. Cases where the question could not be resolved with a high degree of confidence were discarded. For most passes the issue does not arise because the soft electron maximum rate occurs at distances well outside the position of the 302 peak.

Also shown in Figure 12 are the K_p indices taken from the 3 hour interval including the SpL peak data point, the D_{st} (H) values generated from the hourly scalings of the San Juan and Honolulu magnetograms, and the magnetic latitude and the L value coordinates of the spacecraft at the time the 302 maximum is observed.

It is necessary to establish at the outset that the variations of the 302 maximum rates for each pass are the result of true time modulations in the trapped radiation flux and not merely apparent variations introduced by the continual change of satellite orbit with respect to the orientation of the magnetic field of the earth. For the SpL rates the analogous problem need not concern us because the high fluxes of soft electrons extend to much greater radial distances and, therefore, fill a greater volume of space. The great relatively uniform radial and volumetric extent of this soft electron belt assures that the low inclination satellite

obtains a fair sample of the relative intensity. It is for this reason, as well as the fact that we do not know how the lines of force are distorted at great distances during a storm, that we have chosen to plot in Figure 12, the maximum values observed during a pass rather than fluxes repeatedly observed on a given line of force.

The hard electron outer zone is confined to a smaller region of space. We argue for the following reasons that time variations in this component do exist and are predominantly responsible for the modulation of the 302 peak rates shown in Figure 12.

(a) Figure 13 shows on a trajectory plot the logarithm of the number of counts/10 seconds for two inbound passes nearly coincident in magnetic coordinate space, approximately 10 days apart. We see that near 5 R_e, within 3° of the magnetic equator, when the two trajectories are only 1° apart, the 302 count-rates differed on the two passes by 2 orders of magnitude. Further, the maximum rates obtained on the two passes differed by well over one order of magnitude. Note that the major discrepancies between the rates on the two passes occur at greater radial distances with relatively good agreement occurring at closer distances. Also note that the greater maximum value lies at a greater radial distance.

(b) Returning to Figure 12 we note that the high 302 peak rates occur on higher L values than the lower peak rates. This is shown explicitly in Figure 14 in which the maximum 302 rates for each pass are plotted as a function of the L values on which they occur. The higher peak rates occur at higher L values. If this effect is due to a peculiarity of the satellite orbit such that the passes on higher L values tend to be closer to the magnetic equator, such a trend should be revealed by plotting the absolute value of the magnetic latitudes at which the peak rates occur as a function of the simultaneous L values. This has been done in Figure 15. It is seen that the absolute values of the magnetic latitudes at which the peak 302 rates are reported are essentially randomly distributed in the L region over which the peaks occur. Thus we are able to eliminate the magnetic latitude as parameter responsible for the correlation between 302 peak rate and L value. An identical argument allows the elimination of magnetic longitude. The only possible remaining coordinate which can explain the gross change in magnitude and radial position of the 302 peak rate is time.

(c) Figure 16 is a trajectory plot in magnetic coordinate space showing the logarithms of the 302 counting rates for a series of passes before, during, and after the onset of the great magnetic storm of 30 September 1961. If the hard electron component of the

outer zone is time stable over a period of ten days, it should be possible to draw contour diagrams of the 302 count-rates by using the rates given on these trajectories as well as their reflections about the magnetic equator. An inspection of this diagram indicates that such an endeavor would lead to a spatial distribution without symmetry about the magnetic equator, whereas it will be shown that if temporal instabilities are allowed, the trajectory plots are merely the result of a general storm-time pattern exhibited by this as well as other storms.

(d) For the magnetic storm at the end of August (already presented as an introductory example of storm-time variations) the graphs showing the SpB and 302 count-rates vs radial distance (see Figure 11) also give the magnetic latitudes at which the maximum count-rates were observed. Changes are observed in these maximum rates between the main phase and recovery phase even though the magnetic latitudes are nearly the same.

Having established the existence of time variations for the 302 peak rate, we must derive an estimate of the fluctuations superimposed upon these by magnetic latitude differences. This is readily accomplished by comparing the 302 peak-rates for successive inbound and outbound sweeps through the heart of the outer zone.

For such successive cuts the time differences is only that required for the satellite to pass through perigee; rarely more than four hours. Those cases where data exist on both sweeps are found in Figure 12 as two 302 peak rate bars closely spaced. Examples occur on August 24 and September 10, 11, 18, 23, 28, etc. Several cases exist where the difference of absolute magnitudes of the two successive magnetic latitudes is about 10°. In all of these cases the difference in 302 peak rates is much less than a factor of 2. The case in which the discrepancy is the greatest is that of September 28. Here the inbound pass cut the magnetic shell containing the peak at +3° magnetic latitude, the the following outbound pass at -21° magnetic latitude. The resulting difference in the maximum 302 rates observed was less than a factor of 3. In general, it can be concluded that magnetic latitude variations are small compared with the temporal variations.

We are now in a position to proceed with a detailed analysis of the storm-time variations in Figure 12. This figure bears out the hypothesis of an enhanced soft electron flux with increased magnetic activity. In addition to the end of August magnetic storm, the end of October storm provides an example of this. The entire time period covered by Figure 12 shows a positive correlation between the SpL maximum rate and the K_p index.

Figure 17 shows this correlation. The correlation coefficient between the logarithm of the SpL peak rates and the K_p indices given in Figure 17 is 0.73.

As can be seen, particularly for the end of August storm, the time constant for the decay of the enhanced soft electron flux (~ 5 days) is the same as that for the recovery phase of the storm as seen in the K_p and the D_{st} (H) values.

We draw attention to the great magnetic storm occurring near the end of October. This storm is often considered to have commenced around noon on the 28th of October; however, considerable magnetic activity preceded this time and the most intense outer zone SpL rate observed during the life of Explorer XII occurred early on the 27th. The magnetic morphology of this storm does not appear to be clear. There are no flares reported of importance greater than 1, later than October 20, and yet the main phase D_{st} (H) value reached the most negative value observed during the active lifetime of Explorer XII, -175 γ. The only solar flares reported after October 20 are class 1 flares on the 27th at 0807 U.T. and 0840 U.T., and on the 29th at 0036 U.T. In spite of these apparent anomalies the storm illustrates a close correlation between the peak SpL rate and the K_p index. Correlation between the peak SpL rate and the D_{st} (H) values is less perfect.

Figure 12 gives additional support to the hypothesis that the 302 rate is generally anti-correlated with magnetic activity. Starting, for example, with the end of August storm, we note the depletion and subsequent build-up during the recovery phase. The time constant for the build-up is the same as that for the magnetic recovery phase and the soft electron depletion. The small storm which commences on the 11th of September has the effect of removing the accumulating electrons. A rapid build-up follows the small storm which starts on September 24. The most dramatic storm-time depletion of the penetrating component occurs on October 1 when the 302 peak rate drops by two orders of magnitude with the onset of the great magnetic storm.

Figure 16 is the trajectory plot for a series of passes illustrating the spatial pattern for this depletion. As discussed previously when the removal of the trapped electrons takes place, the point at which the maximum occurs shifts inward. There is apparently less distortion of the count-rates on lines of force which have their equatorial crossings closer to the earth. Unfortunately the satellite is near apogee during the initial phase and early main phase of the storm so it is impossible to determine exactly when the removal of the hard electrons occurred.

From the October 1 inbound pass shown in Figure 16 we can be certain that the removal was substantially complete by noon on the 1st of October, some 18 hours after the start of the main phase. During the late recovery phase of this storm the typical 302 enhancement is observed.

The 302 peak-rate pattern for the storm occurring on October 26, 27, 28, 29, 30, and 31 is less clear although as we have discussed previously the storm itself has an atypical pattern.

From the overall viewpoint the relationship between the 302 peak rate and the K_p index and D_{st} is not as definite as that for the SpL peak rate. Figure 18 shows the scatter diagram for the 302 peak rate vs K_p. It is possible that the lack of a definitive relationship here results from the long time lag in hard electron storm-time modulation. This demonstrates the importance of examining these variations on an individual storm-time basis.

2. Discussion.

The main results of the foregoing section may be summarized as follows:

(a) The outer zone soft electron component is positively correlated with K_p.

(b) An initial storm effect is a depletion of the high energy electron component.

(c) The enhancement of the hard component follows that of the soft component by several days.

(d) The time constant for the depletion of the storm-time enhanced soft component is the same as that of the slow component of the recovery phase of the magnetic storm.

(e) Soft electron enhancement seems to occur more or less uniformly throughout the magnetosphere (beyond L = 3) with rapid spatial and/or time variations being a predominant characteristic.

(f) The late storm enhancement of the hard component occurs predominantly between L = 3.5 to L = 5 and the greater the enhancement, the greater the L value at which the maximum value occurs.

(g) Fine structure is generally absent in the high energy component.

O'Brien [1962] has shown, using Injun I measurements of the $E \geq 40$ keV electrons in the dumping cone at 1000 km altitude, and Explorer XII measurements of the equatorial trapped electron flux, that the typical dumped electron flux in the auroral zone ($\sim 5 \times 10^4$ electron cm^{-2} sec^{-1} $ster^{-1}$) is sufficient to empty a tube of force in 10^4 seconds if the source is turned off and if the equatorial pitch angles of all the electrons within the

tube of force are altered so that they lie within the dumping cone and the loss rate remains unaltered. This approach is admittedly artificial since it assumes the lifetime of particles at large pitch angles is limited by dumping. It does, however, serve to show that a strong source exists for particles brought within the dumping cone.

As was discussed in Section II, we assume that the average particle fluxes reported by the S.U.I. Explorer XII directional detectors are predominantly due to particles with equatorial pitch angles outside the dumping cone. Under this assumption and by way of the data exhibited in Figure 12, we are able to place an extreme upper limit on the "lifetime" of fluxes of 50 keV electrons lying on steeper equatorial pitch angles than those dealt with in the analysis by O'Brien.

If we take the end of August storm and assume an impulsive injection of 50 keV electrons we see that the flux of these electrons has been reduced by an order of magnitude after approximately five days. This five day "lifetime" does not exclude the possibility that the actual trapping lifetime for 50 keV electrons is actually much shorter and that what is being measured is the lifetime of the source function. It also does not exclude the possibility that diffusion mechanisms are tending to deplete a given region of space with the five day time constant. Nor does it

eliminate the possibility that acceleration mechanisms are operating continuously tending to move the electrons to a higher position on the energy spectrum and thus out of the pass band of the low energy channel of the spectrometer. Some support would appear to be given to this last hypothesis by the fact that the hard electron component is increasing continually during the five day period when the SpL rate is decreasing. An attempt to determine whether there is a time lag between the enhancement in the 50 keV electron channel and that in the 100 keV electron channel was suggestive of this result but inconclusive. Recently McIlwain [1963] has demonstrated a greater time delay of enhancement with increasing electron energy using Explorer XV data.

Regarding item (f) above, Figures 13, 14, and 16 present a picture of increasing stability of the trapped hard electron flux with decreasing L value. The modulation of intensity occurs predominantly at higher L values (L = 4 to 5) while the fluxes at lower L values (L = 3 to 4) tend to be more stable.

The result that the position of the 302 maximum moves to lower L values as the maximum decreases when taken together with the general diminution of the 302 maximum during the main phase is consistent with the result of Forbush, Pizzella, and

Venkatesan [1962] that the values of L_{max} (for an identical 302 on Explorer VII) showed a marked tendency to decrease with increasing U (southward equatorial geomagnetic field of the ring current). They state: "On the average, L_{max} decreased from L = 4.0 to L = 3.0 for an increase of 100 γ in U." From Figure 12 we see that during the September 30, October 1 storm, the Explorer XII 302 L_{max} decreased from 4.5 to 3.0 for a drop in D_{st} (H) from 0 to -100 γ. The remarkable consistency between these two sets of data lends credence to conclusions about the time variations of the hard component of the outer zone derived from the data taken by a low altitude, circular orbit, satellite such as Explorer VII.

The 302 storm-time variations described here are in complete qualitative agreement with those obtained by Arnoldy, Hoffman, and Winckler [1960] using a nearly identical instrument flown on Explorer VI.

IV. THE MAGNETOSPHERIC BOUNDARY

A. Particle Observations near the Boundary.

To illustrate the morphology of the particle flux observed near the magnetospheric boundary we shall discuss the data from the inbound pass of Explorer XII on the 13th of September, 1961. This pass is chosen because it presents examples of several of the characteristic features and because the onboard magnetometer data has been made available. A preliminary study of this pass has been published [Freeman, Van Allen, and Cahill, 1963].

At 18h 19m U.T. on September 13, 1961, the sun was at right ascension 171.5°, declination +3.7°, and the satellite at right ascension 172.3°, declination +3.0°. Hence the satellite was almost precisely on the sub-solar point at the moment of crossing the magnetospheric interface [see later section, Observations].

1. Geo-Solar Conditions.

No flares of importance greater than 1^+ were reported for the three days prior to September 13, although there were six class 1 flares and one 1^+ flare on the 10th of September

/Compilations of Solar-Geophysical Data, C.R.P.L.-F Part B, October 1961/. At 15h 56m U.T. on September 13, there occurred a geomagnetic sudden commencement which resulted in a K_s index at 4 at Wingst and Gottingen. The K_p index remained at or below 4 until 24 hours later, at which time it rose to 6 /ibid., November 1961/. The magnitude of the sudden commencement at Guan and San Juan (Figure 19) was 10 to 25 gammas in the horizontal component. The positive phase continued for over two days. Both Fort Churchill (68.7° geomagnetic north) and Meanook (61.8° geomagnetic north) magnetograms show very little magnetic activity on the 13th of September. /Data courtesy of Canadian Department of Mines and Technical Services./

In contrast to these mild indications of solar activity and of perturbations of the geomagnetic field at the surface of the earth, there was found to be a high level of disturbance in magnetic and particle phenomena at the boundary of the magnetosphere.

2. Observations.

Figure 20 shows the counting rates of the five particle detectors and the magnetic field measurements as a function of geocentric radial distance on the inbound pass of

September 13, 1961. The following features are noteworthy:

(1) The output of the CdS total energy flux detector (CdSTE) steadily increased as the satellite moved inward from apogee. There was an apparently significant drop in flux more or less coincident with the s.c. as reported on the earth. The maximum value of the spin-averaged energy flux, 50 ergs $(cm^2 \text{ sec sterad})^{-1}$, occurred at 55,000 km. Thereafter the measured flux diminished rapidly in the vicinity of the interface then increased again within the trapping region.

(2) For radial distances greater than 40,000 km there was no discernible increase in the output of CdSB above the value attributable to starlight and dark current.

(3) The low energy ($40 \leq E \leq 50$ keV) channel of the electron spectrometer (SpL) showed no increase of counting rate above that due to galactic cosmic rays until about 52,000 km. (Note that in Figure 20, the counting rates of both low energy (SpL) and high energy (SpH) spectrometer channels were corrected for the contribution of non-collimated particles by subtracting the rates of the background detector SpB.) The counting rate then rose sharply to a peak at 45,000 km. The rate then decreased and later rose again in the heart of the outer zone.

(4) The net rate of the high energy spectrometer channel (SpH) ($80 \leq E \leq 100$ keV) was also negligible at radial distances greater than 52,000 km. It then rose in the distance range 52,000 to 47,000 km and continued at about a constant value for lesser radial distances.

(5) The rate of the omnidirectional 302 detector was indiscernibly different from its interplanetary value at radial distances greater than 52,000 km. It then rose sharply within a range of ~ 1000 km and continued to rise monotonically, though less rapidly, as the satellite moved toward the earth.

(6) During passage inward from 70,000 km (magnetometer data beyond this range unavailable at time of plotting) to 52,400 km, the scalar magnitude of the magnetic field $|F|$ fluctuated between 20 and 100 gammas, and large fluctuations in vector direction also occurred. There occurred a local maximum in $|F|$ near 53,700 km, then a rapid decrease until 52,400 km. There the magnitude rose abruptly, within 200 km, from 25 to 120 gammas and the field direction changed abruptly within a radial range of about 100 km. As the satellite continued inward the direction of the field was steady and approximately that expected for a dipole field. Just inside the interface the magnitude of the

field was 60 gammas above that of the reference field [Finch and Leaton, 1955]. The abrupt change in direction and magnitude of the magnetic field at about 52,200 km (8.2 earth radii) is interpreted as defining the boundary of the magnetosphere. Inside the magnetosphere mild fluctuations in magnitude and direction were observed but the fractional changes were much smaller than those outside.

3. Correlation Between Magnetic Field and Particle Measurements.

It has been proposed by Cahill [1962] that the magnetic field measurements give direct evidence for the compression of the geomagnetic field under the impact of solar plasma and that the discontinuity in magnetic parameters at 8.2 earth radii (at the sub-solar point, as noted above) defines the physical boundary between the inner region in which the magnetic field energy density is dominant and the outer region in which the plasma energy density is dominant. We consider that the particle measurements support this interpretation in the following manner:

(1) The sharp rise in counting rates of the G.M. tube and of both the spectrometer channels at 8.2 earth radii gives

evidence that durable geomagnetic trapping of charged particles is possible at lesser radii but is impossible at greater radii due to the disordered nature of the field at greater radii [Van Allen and Frank, 1959a, 1959b; Rosser et al., 1962].

(2) The CdS total energy flux detector shows the presence of high energy fluxes of charged particles in the region of disordered field outside the interface. In the following section it is argued that the combination of all of the charged particle measurements with the various detectors shows that the particles being measured are very likely electrons having an energy spectrum very much softer than those inside the interface and that, indeed, they may very well constitute the observable component of a quasi-thermalized solar plasma.

It will be recalled that, as mentioned in Section II, our belief that the measured particles inside 8.2 earth radii are trapped is presumptive in character. It is seen from the value of α in Figure 20, that according to Figure 3, the spectrometer channels are sweeping through the theoretical dumping cone while the local peak in SpL-SpB inside the boundary is observed. We are therefore not able to determine what fraction of the observed flux may impinge on the atmosphere in the high latitude regions.

In spite of this, for the reasons given in Section II and on the basis of the general body of knowledge on the geomagnetically trapped radiation, we assume the observed fluxes are predominantly due to trapped radiation.

4. The Intensity Peak of Low Energy Electrons within the Trapping Region.

Attention is drawn to the local maxima in the outputs of SpL-SpB and CdSTE at about 45,000 km (Figure 20). We have seen that the radial distribution of 50 keV electrons generally tends to be uniform to within an order of magnitude throughout the outer zone. However, in the entire body of Explorer XII data there are several cases of such a peak located near the magnetospheric boundary. Figure 21 shows a second example of such a peak.

The presence of these peaks appears to be associated with the compression of the magnetosphere, i.e., a closer than normal boundary position. It is possible that there occurs some betatron acceleration of low energy trapped electrons into the energy range of observability (~ 50 keV in the present case) when the boundary of the magnetosphere is compressed. However, for the 13th of September case the strengthening of the field was

by only a small factor, $\sim$ 2 (see Figure 20), and hence it may very well be that transient, wave-like processes which were not observed in this experiment, were of greater efficacy [Judge and Coleman, 1962].

5. Nature of the Particles Observed Outside of the Magnetospheric Boundary.

Direct experimental evidence places certain restrictions on the nature of the particles which were responsible for the large peak in energy flux which was observed with CdSTE outside of the magnetospheric boundary as follows:

(1) Since the peak was not observed with the CdSB detector, the particles must be predominantly electrons of energy $E \leq 250$ keV or protons of energy $E \leq 400$ eV or ions of corresponding magnetic rigidity.

(2) The lack of a discernible response by the 302 in the region in question (52,000 to 80,000 km) places the following upper limits on the omnidirectional intensity of monoenergetic electrons:

J_o 2×10^{10} $(cm^2\ sec)^{-1}$ for E = 20 keV;

J_o 3×10^{8} $(cm^2\ sec)^{-1}$ for E = 30 keV;

J_o 3×10^{7} $(cm^2\ sec)^{-1}$ for E = 40 keV;

J_o 3×10^{5} $(cm^2\ sec)^{-1}$ for E = 100 keV;

etc. [Frank, 1962].

Corresponding upper limits on spin-averaged unidirectional energy fluxes are (dividing omnidirectional intensities by 4π):

50 ergs $(cm^2$ sec sterad$)^{-1}$ for E = 20 keV;

1 erg $(cm^2$ sec sterad$)^{-1}$ for E = 30 keV;

0.15 erg $(cm^2$ sec sterad$)^{-1}$ for E = 40 keV;

0.004 erg $(cm^2$ sec sterad$)^{-1}$ for E = 100 keV.

(3) The lack of discernible response by either the low energy (SpL) or high energy (SpH) channel of the magnetic spectrometer places an upper limit on the spin-averaged unidirectional intensity of electrons $40 \leq E \leq 50$ keV of the order of 10^4 $(cm^2$ sec sterad$)^{-1}$ and of electrons $80 \leq E \leq 100$ keV of the order of 10^4 $(cm^2$ sec sterad$)^{-1}$.

The combination of the above evidence makes it appear exceedingly unlikely that an appreciable proportion of the observed energy flux of 50 ergs $(cm^2$ sec sterad$)^{-1}$ could have been due to electrons of energy greater than 30 keV.

There remains the problem of distinguishing between electrons of $E < 30$ keV and protons of $E < 400$ eV. Our attempt to do this has its foundations in the Chapman-Ferraro theory of the impingement on the geomagnetic field of a neutral ionized stream of solar gas, or plasma. The following observational

evidence provides some measure of confidence in the applicability of the Chapman-Ferraro theory, if the disordered magnetic field outside of 52,400 km be ignored:

(1) There is a sharp discontinuity in $|F|$ (at a mean distance of 52,200 km) from 25 to 125 gammas.

(2) Just inside the interface $|F|$ is approximately twice the Finch-Leaton extrapolation of the surface field of the earth, which assumes no electrical currents external to the earth.

(3) The disturbance of the surface magnetic field is of the order of 1/16th of 125 gammas (Figure 19).

Employing these considerations and the approximate relation (inelastic impact) for the dynamic pressure of the solar stream,

$$p = nmv^2 = F^2/8\pi ,$$

one finds that the dynamic pressure is of the order of 5×10^{-8} dyne cm^{-2}, a result which might correspond to a plasma of $n = 6$ protons cm^{-3}, each having mass $m = 1.67 \times 10^{-24}$ g and moving rectilinearly at $v = 700$ km sec^{-1}. These exemplary values are generally consistent with the recent direct measurements on the solar wind at points remote from the earth by Neugebauer and Snyder [1962].

The energy flux in such a plasma stream (almost entirely due to the proton component) is

$$nmv^3/2 \sim 2 \text{ ergs } (cm^2 \text{ sec})^{-1}$$

across a stationary surface perpendicular to the velocity vector. If CdSTE were pointed out such a beam there would be 6×10^{-2} ergs sec^{-1} incident on its effective area of 0.03 cm^2. If such an energy flux were ascribed to the solid angle 10^{-2} steradian, a unidirectional energy flux 6 ergs $(cm^2 \text{ sec sterad})^{-1}$ would be calculated. Despite the sensitivity of this result to the assumed value of v and the corresponding uncertainty in its magnitude, for the following reasons it is extremely improbable that the actual reading of CdSTE in the region outside of the interface could have been due to the direct impact of "raw" solar plasma.

(1) The observed energy flux was the spin-averaged value of the output of a sharply directional detector (10^{-2} sterad or 12° opening angle) whose axis was orthogonal to the spin axis of the satellite. The spin axis of the satellite was at an angle of 122° to the satellite sun-line. (See section on Experimental Details.) Hence it was very unlikely that the detector axis would

have encountered the flow vector of the solar plasma; and even if it had done so the flux contribution would have had little weight on purely geometric grounds. It would have been further reduced by two instrumental effects:

(a) The crystal sensitivity for protons of energy less than 400 eV (ones of greater energy were eliminated by the null result from CdSB) was less by a factor of 5 to 10 than the "maximum" value used for computing the fluxes shown in Figure 20; and

(b) A sharp peak in flux as would occur by the rotation of the detector axis through a narrowly collimated beam would be considerably suppressed by the finite response time of the crystal.

(2) The flux (Figure 20) decreased with increasing distance from the interface beyond 55,000 km.

(3) During the history of Explorer XII no such fluxes were observed except in intimate association with the magnetospheric interface.

On the above grounds it is suggested that the response of CdSTE in the region beyond the interface was due to more-or-less "thermalized" plasma, in which approximate equipartition of energy between the electronic and protonic components had resulted, somehow, from the interaction of the plasma with the geomagnetic field.

On the crude model that such a body of quasi-thermalized plasma at the sub-solar point acts as a pressure-transmitting "piston" between the arriving, directional solar beam and the geomagnetic field, a further interpretative step may be taken. The energy density in this "piston" of ionized gas is inferred from the discontinuity in magnetic pressure at the interface to be

$$5 \times 10^{-8} \text{ erg cm}^{-3} = NMV^2/2 .$$

If it be supposed that the kinetic velocity vectors of the electrons and of the protons in the gas are isotropically distributed then the CdSTE detector's mean directional energy flux,

$$50 \text{ ergs } (\text{cm}^2 \text{ sec sterad})^{-1} = NMV^3/8\pi .$$

From the two relationships of the preceding paragraph it is inferred that the r.m.s. velocity of the particles which are responsible for the energy flux must be

$$V \sim 1.3 \times 10^{10} \text{ cm sec}^{-1} .$$

The inferred velocity is that of an electron of kinetic energy 56 keV or of a proton of kinetic energy 100 MeV. Protons of any such energy are completely intolerable, both observationally and theoretically.

The inferred electron energy of 56 keV, the corresponding number density 0.6 cm^{-3} and omnidirectional intensity 10^{10} $(cm^2\ sec)^{-1}$ are totally inconsistent with the direct observational evidence from the 302 and SpL detectors as cited earlier. But it should be noted that the inferred velocity of the particles

$$V = \frac{(\text{Observed Mean Directional Energy Flux})\ (\Omega)}{(\text{Observed Discontinuity in Magnetic Pressure})}$$

where Ω is the solid angle within which the observed mean directional energy flux is assumed to exist. The corresponding value of particle kinetic energy is proportional to the square of the right hand side of this equation. Since there are clearly uncertainties by factors of the order of unity in each of the three essential quantities (especially Ω) it is evident that an r.m.s. particle velocity as low as

$$V \sim 3 \times 10^9 \text{ cm sec}^{-1}$$

can be tolerated. Protons remain hopeless. The corresponding values of energy, number density, and omnidirectional intensity of <u>electrons</u> are respectively:

$$E = 2.6 \text{ keV}$$
$$N = 10 \text{ cm}^{-3}$$
$$J_o = 3 \times 10^{10} (\text{cm}^2\ \text{sec})^{-1}.$$

Such a set of results is consistent with all observational evidence and can be reconciled more-or-less reasonably with rudimentary theoretical considerations.

The ways in which the observed, spin-averaged directional flux and $|F|$, α, and γ vary with distance from the interface and/or with time (Figure 20) are taken to represent the imperfections, in the real physical situation, of the simple model which envisions a layer of thermalized (unmagnetized) plasma acting as the pressure-transmitting agent or "piston" between the impinging solar stream on the outside and the geomagnetic field on the inside. The disordered structure may be, in part, caused by magnetic fields due to electrical currents in the original solar stream, a feature not present in the simple model. Also, it is clear that the observed irregularities, though plotted against radial distance, are actually an indistinguishable mixture of temporal and spatial variations.

6. Observations of the Soft Electron Flux External to the Boundary on Other Occasions.

Due to the unique orientation of the spin axis of the satellite, as expected from geometrical considerations, the sunlit earth always came within the field of view of the CdS detectors when the satellite was beyond approximately 65,000 km while outbound

and beyond 80,000 km while inbound. Because of their photosensitivity, the CdS detectors were saturated with earthlight and hence rendered useless for particle detection during this portion of the orbit. The occurrences when examination of the plasma flux is possible are thus restricted to inbound passes during which geo-solar conditions are such that the magnetospheric boundary lies well within approximately 75,000 km. There are forty such cases for which good data are available during the active life of the satellite. In each of the forty cases the CdSTE detector indicates the presence of an energy flux above the threshold for the detector, ~ 0.5 erg/cm^2 sec ster.

If, as we have proposed, this energy flux results from the electronic component of the thermalized solar plasma we should expect to observe a relationship between the intensity of this energy flux and some other parameter representative of the solar plasma pressure. Such a parameter is the radial position of the magnetospheric boundary as determined by the termination of trapped radiation (see Section IV-B). Specifically one would expect to see the highest CdSTE external fluxes during passes when the magnetospheric boundary is at its closest distances to the earth. Figure 22 shows that there is some evidence for

believing that this is the case. Here the maximum CdSTE count-rate external to the boundary (excluding the region dominated by earth-light) on each of the forty passes is plotted as a function of the observed boundary position for the same pass. At or beyond 70,000 km the maximum CdSTE rate observed is 2.7 c/s, at or beyond 65,000 km, 9.5 c/s, and at or beyond 50,000 km, 17 c/s.

It is of interest to determine whether or not this external flux is related to the standard surface parameter for solar plasma activity, K_p. Figure 23 shows the forty CdSTE maximum count-rates plotted vs K_p. It is seen that the times of greatest variability in the energy flux are the times of higher K_p index. This is qualitatively consistent with the concept of K_p as a measure of the rate-of-change of solar plasma pressure rather than the plasma pressure itself.

An attempt has been made to find time-coincident variations in external CdSTE flux and sudden changes in the auroral intensities based on all-sky camera films from College, Alaska, Pullman, Washington, Choteau, Montana, and Hanover, New Hampshire. In the available data there are four cases where the satellite is in a position to monitor the CdSTE energy flux beyond the boundary during periods of intense auroral activity. None of these cases

show any abrupt changes in the CdSTE flux simultaneous with changes in auroral intensity.

7. Radial Termination of the External Flux.

Note that in Figure 22 thirteen of the forty data points are solid dots rather than open dots. The distinguishing feature of each of these thirteen passes is that the CdSTE energy flux outside the boundary shows one or more sharp decreases at a radial distance of 10,000 to 20,000 km beyond the boundary. Figures 20, 24, 25, 26, and 27 illustrate five of these passes. Table III shows the pertinent characteristics of each of the thirteen passes. From Figure 22, they tend to occur predominantly on passes with close boundary positions. This is to be expected since the boundary must be some 20,000 km inside the point at which the CdSTE detector saturates from earthlight in order for the discontinuities in the CdSTE to be observed.

We propose that the sharp decrease in the CdSTE energy flux observed on these thirteen passes represents the location of a shock front generated by the supersonic flow of solar plasma past the magnetosphere as has been discussed by Axford [1962], Dessler [1962], Kellogg [1962], and others. In particular,

Kellogg predicts that the stand-off distance should be 26, 18, or 15 thousand km for Mach numbers of 2, 4, and ∞, respectively. On the basis of Explorer X measurements of the solar plasma Mach numbers between 2 and 5.5 have been observed experimentally. Since our observation of the stand-off distance is restricted to times of closer than normal boundary conditions, i.e., higher Mach numbers, the agreement between Kellogg's estimates, and our median value of 13,000 km seems to be quite good considering the uncertainties in the theory.

B. Gross Boundary Motion.

1. Multiple Boundaries and Shock Fronts.

An occasional feature of the CdSTE extramagnetospheric response is the occurrence of more than one pronounced maximum. On these occasions the changes in the energy flux are very sharp and the levels tend to be quite stable between the changes, i.e., the energy flux vs radial distance has a waveform similar to a square wave. This is illustrated in Figures 26 and 27 which show the detector response for inbound passes on the 11th of September and the 11th of October, respectively. Both

passes occur during the initial phase of moderate magnetic storms while the San Juan horizontal component is steadily increasing.

We suggest that the apparent existence of multiple shock fronts may be due to the increasing pressure from the solar plasma forcing the shock front inward past the satellite following the initial encounter. A second encounter then occurs when the satellite again catches up with the front after quasi-equilibrium has again been established.

Focusing attention on the 11 October inbound pass we interpret the sequence of events as follows:

(a) At 75,092 km (0604 U.T.) the inbound satellite encounters a shock front and the energized electrons inside the front are detected by a rise in the CdSTE count-rate.

(b) At 72,637 km (0644 U.T.) the enhanced solar plasma pressure compresses the magnetosphere to the extent that the original shock front moves inward past the satellite exposing it once again to the interplanetary medium with a consequential drop in the CdSTE response. Note that the CdSTE count-rate is 50% higher the second time it is outside the shock front, this being consistent with the enhancement of the solar plasma.

(c) At 68,417 km (0743 U.T.) the spacecraft again encounters the shock front whose position has now become quasi-stabilized through the balance of magnetic and corpuscular energy density. The resultant response is a second increase in the CdSTE count-rate.

(d) At approximately 55,500 km (0945 U.T.) the satellite encounters the boundary between the magnetosphere and the external shock region. This is evidenced by the subsequent sharp rise in the SpL count-rate. The characteristic decrease in the CdSTE rate is also observed as the satellite approaches the boundary. Inside the boundary the ratio of the SpL to CdSTE rates increases by some 2 to 3 orders of magnitude and CdSTE response follows that of the SpL. During this time CdSB shows no change in count-rate.

We further propose that an analogous situation occurred during the 11th of September inbound pass (Figure 26). In this case motion of the magnetospheric boundary as well as the shock front is apparently evident. The boundary motion is derived from the data as follows:

(a) At 53,000 km (1300 U.T.) the CdSTE response drops and the SpL-SpB rate rises sharply, presumably indicating the presence of trapped energetic electrons.

(b) At 51,000 km (1320 U.T.) the ratio of SpL-SpB count-rate to CdSTE count-rate again becomes less than unity as it was outside the initial boundary. Hypothetically the magnetospheric boundary has pushed inward past the satellite and we are again observing the thermalized plasma lying between the boundary and inside the shock front. Note that the peak CdSTE rate in this region is slightly greater than the peak rate during the first approach to the boundary. This substantiates our idea that the plasma pressure has increased.

(c) Again at 50,000 km (1330 U.T.) the CdSTE flux drops and the SpL-SpB rate takes on the character of the durable trapping region.

If this interpretation is correct a lower limit of ~ 2 km/sec can be set on the boundary velocity during the interval of rapid motion.

An alternative explanation for the above sequence of data is that the CdSTE peak at 50,000 km represents a bubble of plasma trapped within the magnetosphere. For an entirely analogous set of data during the 1st of October inbound pass the onboard magnetometer data does show a sudden change in the magnetic field to a definitely non-dipolar form in a region

2,500 km thick located approximately 4,000 km inside the initial magnetospheric boundary [Cahill, private communication]. Konradi [1963] has shown that a narrow peak of geomagnetically trapped protons is found in the region between the "bubble" and boundary, and that the radius of gyration of these protons exceeds the thickness of the region over which they are observed. This proves that rapid temporal (i.e., motional) variations are superimposed on the spatial observations of the boundary region, but it does not prove conclusively that the region of enhanced CdSTE flux and unstable magnetic field is not a time stationary region within the magnetosphere. Such a problem can only be completely resolved by two or more satellites distributed radially.

2. Storm-Time Boundary Motion and Gross Boundary Position.

We have seen (see Figure 20) that the sharp cut-off in the SpL count-rate readily delineates the magnetospheric boundary. Employing statistically significant counts above background for this detector together with the experience gained through a detailed study of the data from all the detectors we have estimated the radial position of the magnetospheric boundary for the first

two and one-half months of the satellite life. This time-history of the boundary position along with the D_{st} (H) values from San Juan and Honolulu are given in Figure 28. The following important features are revealed:

(a) The average boundary position on the sunward side of the earth is 66,000 km.

(b) Positive or above normal D_{st} values are accompanied by closer-than-average boundary positions, the maximum inward excursion being about 15,000 km. See for example the time regions 23-26 August, 7-8 September, 11 September, 21-24 September, and 9-11 October, etc. The correlation is good even on a small scale as is illustrated by the data points at 0000 U.T. on the 23rd of September and the 9th and 10th of September. Note that while barely visible on the D_{st} curve, the sudden commencement at 1556 U.T. on the 13th of September had the effect of reducing the boundary position by 18,000 km or nearly three earth radii.

(c) The closer-than-average boundary position present during the initial phase appears to persist throughout the main phase. This conclusion, somewhat less certain than those pertaining to the initial phase and recovery phase, is based on the data points at the apex of the main phase for the 1 October and 28 October storms.

(d) The recovery phase of magnetic storms is accompanied by an outward motion of the boundary, the radial extent of this motion exceeding satellite apogee, 83,500 km, for large storms such as those occurring on 1 October and 28 October. The pattern is discernible as well for small and moderate storms such as those of 19 August, 11 September, 25 September, 11 October, and 25 October.

It is clear then that gross boundary motion features have their surface equatorial field counterparts as was suggested originally by Chapman and Ferraro [1931], the initial phase, or positive D_{st} values resulting from the compression of the magnetosphere by the enhanced solar plasma flow, which storm time properties have now been directly verified [Neugebauer and Snyder, 1962], and the recovery phase outward boundary motion presumably resulting from the relief of solar plasma pressure against the ring-current-enhanced outer geomagnetic field. Akasofu has shown employing a realistic ring current model based on the outer zone proton belt reported by Davis et al. [1962] that the observed values of the positional change in the boundary position are consistent with reasonable

changes in solar wind pressure and ring current strength /private communication/.

During the interval covered by the data in Figure 28 there is no systematic difference between the radial boundary positions found in inbound and outbound passes, i.e., there is no significant difference in the observed boundary positions due to small changes in the magnetic latitude or the probe-earth-sun geocentric angle at least out to 75° from the sub-solar point. There may, however, be a gradual increase in the mean boundary position.

Following the period covered by Figure 28 (i.e., as the satellite apogee approaches probe-earth-sun angles near and beyond 90°), a remarkable sequence of events takes place:

(a) During the first half of November telemetry is poor and gaps in the data make boundary position estimates on the basis of the 50 keV electron flux difficult to obtain.

(b) During the second half of November the radial profile of the SpL count-rate loses its characteristic sharp cut-off. The sudden termination gives way to a sloping decrease which occasionally extends out to apogee.

(c) Toward the end of November, and during the first week in December (longitudinal difference between the sub-satellite point at apogee and the sub-solar point greater than 90°), the outbound passes (greater probe-earth-sun angle) begin to show a decrease to background rate in the SpL count-rate at geocentric distances as close as 45,000 km. The subsequent inbound portions of the passes, however, register high fluxes as far out as apogee.

Recently Frank, Van Allen, and Macagno [1963] have shown, using data from Explorer XIV, that the radial termination of soft electron ($E \geq 40$ keV) fluxes occurs closer to the earth on the night side of the earth than on the day side and that near the magnetic equator in a region near 90° from the sub-solar point high fluxes of electrons of energy $E \geq 40$ keV are found as far out as 100,000 km geocentric distance. The S.U.I. Explorer XII data generally support these findings although we wish to emphasize that we do not equate radial termination of the 50 keV electron flux on the night side with the magnetospheric boundary as we have done for the day side of the earth.

C. Very Soft Electrons on The Night Side.

Figure 29 shows the CdSTE detector response along with the SpL count-rate for an outbound pass through the region behind the earth. Note that as the satellite approaches apogee the SpL response is increasing. The subsequent inbound pass shows a continuing high rate near apogee and on in.

Also note that the ratio of CdSTE response to the SpL response is greater than unity throughout the pass. This, together with the good correlation between response of the two detectors, in all probability, indicates a high flux of very soft (500 eV $\lesssim$ E $\lesssim$ 40 keV) electrons present at great distances on the night side of the earth near the magnetic equator!

Specifically, if the CdSTE energy flux be due to 10 keV electrons the particle flux is $\sim 10^9$ electrons/cm^2 sec ster (average). These intensities and energies of electrons on the night side of the earth are suggestively similar to those observed to produce visible aurorae [McIlwain, 1960; Davis, Berg, and Meredith, 1960; McDiarmid, Rose, and Budzinski, 1961].

Using data primarily from a system of three-electrode "ion traps" on Lunik II, Gringauz and collaborators

/Gringauz, Bezrukikh, Ozerov, Rybchinskii, 1960; Gringauz and Ryton, 1960; Gringauz, Balondina, Bordovsky, and Shutte, 1962/ discovered omnidirectional intensities $J_o \sim 2 \times 10^8$ $(cm^2\ sec)^{-1}$ of electrons of $E > 200$ eV in the radial distance range from the center of the earth 61,400 to 81,400 km (55,000 to 75,000 km above the surface of the earth). Gringauz et al. regarded these observations as establishing the existence of a "third radiation belt". It has been estimated by us /Freeman, Van Allen, and Cahill, 1963/ that the Lunik II observations were at a geocentric angle of 125° ($\pm$ 10°) eastward from the sub-solar point.

We believe that the aforementioned Soviet findings support our hypothesis that the CdSTE energy flux response at a westward geocentric angle with the sub-solar point of approximately 125° in the region beyond which higher energy trapped radiation is observed is due predominantly to very soft electrons. A large measure of consistency is hereby introduced to these two sets of measurements and the Soviet finding of a region of soft electrons on the night side of the earth is experimentally confirmed.

V. SUMMARY

Figure 30 is a graphic representation of our present concept of the magnetosphere.

The outstanding conclusions of the preceding sections may be summarized as follows:

(1) The radial extent of 50 keV and 100 keV electrons is typically terminated at 10 earth radii on the day side of the earth.

(2) The value of this radial extent shows storm-time modulations consistent with a compression of the geomagnetic field during the initial phase and main phase and a subsequent expansion to a position beyond the pre-storm value during the recovery phase.

(3) The radial extent of the 50 keV electrons is typically terminated some 2 earth radii closer to the earth on the night side.

(4) The large scale presence of the 50 keV and 100 keV electrons within the magnetosphere shows a positive correlation with the K_p index with the greatest enhancement occurring during the main phase of magnetic storms and with the decrease occurring in a time interval characteristic of the storm recovery phase.

(5) This storm-time enhancement of the soft electron flux generally occurs over the entire region covered by our investigation,

i.e., from 20,000 km to the magnetospheric boundary, although sometimes local maxima are observed close to the boundary.

(6) The hard electron component ($E \geq 1.5$ MeV) concentrated between 3 and 5 earth radii shows a diminution with the onset of magnetic activity and a subsequent recovery to above pre-storm levels with a time constant the same as the recovery phase of the storm.

(7) As the post-storm enhancement occurs, the radial distance at which the maximum is found increases.

(8) On the day side of the earth, in a region of radial thickness 10,000 to 20,000 km, outside the magnetospheric boundary an energy flux of charged particles of the order of tens of ergs/cm^2 sec ster is observed. The dominant contribution to this flux is very likely by electrons whose particle energies are of the order of 1 to 10 keV and whose intensities are of the order of $10^9/cm^2$ sec ster.

(9) On some occasions the radial termination of these particles is very sharp and at such a distance beyond the boundary ($\sim$ 15,000 km) to provide agreement with estimates for the standoff distance of a shock front. It appears likely that these electrons form the pressure-transmitting component of a quasi-

thermalized plasma resulting from the impingement of an enhanced solar plasma wind on the geomagnetic field.

(10) On the night side of the earth a similar energy flux also believed to consist of very soft electrons is found beyond the region of intense trapping. No apparent termination of this flux is evident in the Explorer XII data although the untimely death of the satellite limits a proper exploration of this point.

(11) We believe that these particles can be clearly cross-identified with the "third radiation belt" of Gringauz et al. The suggestion that they may comprise the high-latitude auroral particles is intriguing.

(12) The Explorer XII data are in general agreement with the findings of Frank and Van Allen that the constant counting rate contours for 50 keV electrons protrude outward in a region near 90° from the sub-solar point and draw closer to the earth on the night side.

TABLE I

S.U.I. Detector Characteristics on Explorer XII

Detector	Symbol	Solid Angle (Steradians)	Geometric Factor	Directly Detectable Particles through Quoted Solid Angles	Minimum Detectable Flux
Anton 302 G.M. Tube	302	4π	0.75 cm^2	Electrons $E \geq 1.6$ MeV Protons $E \geq 20$ MeV	$\sim 0.15/cm^2$ sec
Electron Spectrometer Channels	SpL	--	$10^{-5} cm^2$ ster	Electrons 40 keV $\leq E \leq$ 50 keV	$\sim 3 \times 10^4/cm^2$ sec ster
	SpH	--	$10^{-5} cm^2$ ster	Electrons 80 keV $\leq E \leq$ 100 keV	$\sim 3 \times 10^4/cm^2$ sec ster
	SpB	4π	0.15 cm^2	Electrons $E \geq 20$ MeV Protons $E \geq 40$ MeV	$\sim 0.6/cm^2$ sec
CdS Total Energy Flux Detector	CdSTE	10^{-2}	3×10^{-4}	Electrons 200 eV $\leq E \leq$ 500 keV Protons 1 keV $\leq E \leq$ 10 MeV Light	$\frac{\sim 1 \text{ erg}}{cm^2 \text{ sec ster}}$
CdS Proton Energy Detector	CdSB	10^{-2}	3×10^{-4}	Protons 1 keV $\leq E \leq$ 10 MeV Light	$\frac{\sim 1 \text{ erg}}{cm^2 \text{ sec ster}}$
CdS Light Monitor	CdSOM	10^{-2}	3×10^{-4}	Light	--

TABLE II

Electron Fluxes During the 18-19 September Inbound Pass

Geocentric Distance (km)	50 keV $\left(\frac{\text{electrons}}{\text{cm}^2 \text{ sec ster}}\right)$ (average)	100 keV $\left(\frac{\text{electrons}}{\text{cm}^2 \text{ sec ster}}\right)$ (average)	$E \geq 1.6$ keV $\left(\frac{\text{electrons}}{\text{cm}^2 \text{ sec}}\right)$	$E \geq 5$ MeV $\left(\frac{\text{electrons}}{\text{cm}^2 \text{ sec}}\right)$	γ
20,000	5×10^5	5×10^5	3.5×10^3	1.3×10^1	0
35,000	2.8×10^5	2.5×10^5	2.5×10^3	3.3×10^2	-0.14
50,000	4.5×10^5	1.7×10^5	4.0×10^1	-	-1.3
65,000	1.0×10^5	1.0×10^4	-	-	-3.4

TABLE III

Data for Thirteen Examples of Energy Flux Outside the Magnetospheric Boundary Showing Sudden Termination

DATE	UT	K_p	Boundary Position (km)	Maximum Energy Flux* (ergs/cm^2 sec ster) (average)	Radial Thickness of Energy Flux (km)
Aug. 26	2150	3^+	60,000	8	13,500
Aug. 30	0550	4^-	64,000	10	12,000
Sept. 1	1100	3^-_+	62,500	6	10,000, 14,000
Sept. 11	1256	2^+	53,000	33	11,500, 13,000, 15,000
Sept. 13	1800	3^-	52,000	42	13,000
Sept. 20	0718	3^-	64,000	27	15,000
Sept. 22	1345	3^-	55,000	50	12,500
Sept. 24	1813	5	56,000	36	12,000
Oct. 1	0843	7^-	62,000	34	7,000, 11,000, 13,000
Oct. 9	0253	2^-	59,000	60	12,000
Oct. 11	0800	3^-	55,000	80	14,000, 20,000
Oct. 28	2340	7^-_+	62,000	39	11,000
Nov. 16	1926	0^+	58,000	22	11,000

*This energy flux estimate is a lower limit.
It is considered accurate for 10 keV electrons to within a factor of 2.

REFERENCES

Arnoldy, R. L., R. A. Hoffman, and J. R. Winckler, "Observations of the Van Allen Radiation Regions during August and September 1959", Part I, J. Geophys. Research 65, 1361-1375 (1960).

Axford, W. I., "The Interaction between the Solar Wind and the Earth's Magnetosphere", J. Geophys. Research 67, 3791-3796 (1962).

Bame, S. J., J. P. Conner, H. H. Hill, and F. E. Holly, "Protons in the Outer Zone of the Radiation Belt", J. Geophys. Research 68, 55-64 (1963).

Cahill, L. J., "A Study of the Outer Geomagnetic Field", Proc. Third International Space Science Symposium, Washington, D. C., April 1962 (to be published, North Holland Publishing Co., Amsterdam).

Cahill, L. J., and P. G. Amazeen, "The Boundary of the Geomagnetic Field", U. N. H. Research Report 62-1 (1962).

Davis, L. R., O. E. Berg, and L. H. Meredith, "Direct Measurements of Particle Fluxes in and near Auroras", pp. 721-735, Space Research, Proceedings of the First International Space Science Symposium, edited by H. Kallman Bijl, North Holland Publishing Co., Amsterdam, 1960.

Davis, L. R., and J. M. Williamson, "Low-Energy Trapped Protons", Paper Presented at Third International Space Science Symposium and COSPAR Plenary Meeting, Washington, D. C., April 1962.

REFERENCES (continued)

Dessler, A. J., "Further Comments on Stability of Interface between Solar Wind and Geomagnetic Field", J. Geophys. Research 67, 4892-4894 (1962).

Fan, C. Y., P. Meyer, and J. A. Simpson, "Dynamics and Structure of the Outer Radiation Belt", J. Geophys. Research 66, 2607-2640 (1961).

Finch, H. F., and B. R. Leaton, "The Earth's Main Magnetic Field --Epoch 1955.0", Monthly Notices of the Royal Astronomical Society (Geophysical Supplement), Vol. 7, No. 6, November 1957, pp. 314-317.

Forbush, S. E., G. Pizzella, and D. Venkatesan, "The Morphology and Temporal Variations of the Van Allen Radiation Belt, October 1959 to December 1960", J. Geophys. Research 67, 3651-3668 (1962).

Frank, L. A., "Efficiency of a Geiger-Mueller Tube for Non-Penetrating Electrons", J. Franklin Institute 273, 91-106 (1962).

Frank, L. A., J. A. Van Allen, and E. Macagno, "Charged Particle Observations in the Earth's Outer Magnetosphere", SUI Research Report 63-10 (to be published in J. Geophys. Research, June 15, 1963).

Frank, L. A., J. A. Van Allen, W. A. Whelpley, and J. D. Craven, "Absolute Intensities of Geomagnetically Trapped Particles with Explorer 14", J. Geophys. Research 68, 1573-1579 (1963).

REFERENCES (continued)

Freeman, J. W., "A Satellite Borne Cadmium Sulfide Total Corpuscular Energy Detector", SUI Research Report 61-2, February 1961 (unpublished);
also see Freeman, J. W., "Detection of an Intense Flux of Low-Energy Protons or Ions Trapped in the Inner Radiation Zone", J. Geophys. Research 67, 921-928 (1962).

Freeman, J. W., J. A. Van Allen, and L. J. Cahill, Jr., "Explorer XII Observations of the Magnetospheric Boundary and the Associated Solar Plasma on the 13th of September 1961", J. Geophys. Research 68, 2121-2130 (1963).

Gringauz, K. I., V. G. Kurt, V. I. Moroz, and I. S. Shklovskii, "Results of Observations of Charged Particles Observed Out to R = 100,000 km with the Aid of Charged-Particle Traps on Soviet Space Rockets", Soviet Astronomy (AJ) 4, 680-695 (1961) (originally Astronomicheskii Zhurnal 37, 716-735 (1960));
see also Gringauz, K. I., V. V. Berzruhikh, V. D. Ozerov, and R. E. Rybchinskii, "A Study of the Interplanetary Ionized Gas, High Energy Electrons, and Corpuscular Radiation from the Sun by Means of the Three-Electrode Trap for Charged Particles on the Second Soviet Cosmic Rocket", Soviet Physics, Doklady 5, 361-364 (1961) (originally Doklady Akaf. Nauk. SSSR 131, 1301-1304 (1960)).

REFERENCES (continued)

Gringauz, K. I., V. V. Bezrukikh, V. D. Ozerov, and R. E. Rybochinski, "A Study of the Interplanetary Ionized Gas, High Energy Electrons, and Corpuscular Radiation from the Sun by Means of the Three-Electrode Trap for Charged Particles on the Second Soviet Cosmic Rocket", Soviet Physics, Doklady 5, 361-364 (1961) (originally Doklady Akaf. Nauk. SSSR 131, 1301-1304 (1960)).

Gringauz, K. I., S. M. Bolavdina, G. A. Bordovsky, and N. M. Shutte, "To The Results of the Charged Particle Three-Electrode Trap Experiments in the Second Radiation Belt and in the Outermost Belt of Charged Particles", Third International Space Symposium, Washington, D. C., April 1962 (to be published, North Holland Publishing Co., Amsterdam).

Kellogg, P. J., "Flow of Plasma Around the Earth", J. Geophys. Research 67, 3805-3811 (1962).

Konradi, A., "Study of the Outer Region of the Trapped Radiation", Paper Presented at the 44th Annual Meeting of the American Geophysical Union, Washington, D. C., April 1963.

Lincoln, J. Virginia, "Geomagnetic and Solar Data", J. Geophys. Research 67, 381-387 (1962).

McDiarmid, I. B., D. C. Rose, and E. Budzinski, "Direct Measurement of Charged Particles Associated with Auroral Zone Radio Absorption", Canadian J. Phys. 39, 1888-1900 (1961).

REFERENCES (continued)

McIlwain, C. E., "Direct Measurements of Particles Producing Visible Auroras", J. Geophys. Research 65, 2727-2747 (1960).

McIlwain, C. E., "Spatial and Temporal Measurements of Electrons with Explorer XV", Paper Presented at The Goddard Symposium, Washington, D. C., March 1963.

Neugebauer, M., and C. W. Snyder, "Mission of Mariner II: Preliminary Observations", Science, December 7, 1962, Vol. 138, No. 3545.

O'Brien, B. J., "Lifetimes of Outer-Zone Electrons and Their Precipitation into the Atmosphere", J. Geophys. Research 67, 3687-3706 (1962).

O'Brien, B. J., and C. D. Laughlin, "Electron Precipitation and the Outer Radiation Zone", Paper Presented at the COSPAR Third International Space Symposium, Washington, D. C., May 1962; also SUI Research Report 62-9.

O'Brien, B. J., J. A. Van Allen, C. D. Laughlin, and L. A. Frank, "Absolute Electron Intensities in the Heart of the Earth's Outer Radiation Zone", J. Geophys. Research 67, 397-403 (1962).

Rosen, A., and Thomas A. Farley, "Characteristics of the Van Allen Radiation Zones as Measured by the Scintillation Counter on Explorer VI", J. Geophys. Research 66, 2013-2028 (1961).

REFERENCES (continued)

Rosser, W. G. V., B. J. O'Brien, J. A. Van Allen, L. A. Frank, and C. D. Laughlin, "Electrons in the Earth's Outer Radiation Zone", J. Geophys. Research 67, 4533-4542 (1962).

Van Allen, J. A., "Composition and Origin of the Geomagnetically Trapped Radiation", SUI Research Report 61-19 (1961).

Van Allen, J. A., "Spatial Distribution and Time Decay of the Intensities of Geomagnetically Trapped Electrons from the High Altitude Nuclear Burst of July 1962", SUI Research Report 63-11 (1963).

Van Allen, J. A., and L. A. Frank, "Radiation Around the Earth to a Radial Distance of 107,400 km", Nature (London) 183, 430-434 (1959a).

Van Allen, J. A., and L. A. Frank, "Radiation Measurements to 658,300 km with Pioneer IV", Nature (London) 184, 219-224 (1959b).

Vernov, S. N., A. E. Chudakov, P. V. Vakulov, Yu. I. Logachev, and A. G. Nikoloyev, "Radiation Measurements during the Flight of the Second Soviet Space Rocket", Space Research, edited by H. Kallman Bijl, pp. 845-851, North Holland Publishing Company, 1175 pp., Amsterdam, 1960. Originally Dokl. Akad. Nauk. SSSR 130, 517-520 (1960).

FIGURE CAPTIONS

Figure 1. Explorer XII.

Figure 2. The Longitudinal difference between apogee and the earth-sun line throughout the active life of Explorer XII.

Figure 3. Cross-sectional drawing of the 10^{-2} steradian CdS energy flux detector. The overall detector length is about 15 cm; the weight is 160 grams.

Figure 4. The actual efficiency curve for CdSTE; crystal sensitivity versus electron energy. The sensitivity is defined as the ratio of the crystal current (for a 150 volt bias voltage) to the incident electron energy flux in ergs/cm^2 sec.

Figure 5. Diagram showing the relationship between the SUI detector look axes, the spin axis, the solar direction, and the magnetic coordinates used in describing the magnetometer output.

Figure 6. Relationship between the values of θ swept out during each revolution and α. Also shown are the values of θ which lie within the dumping cone at the magnetic equator for four values of L.

Figure 7. Total time for each revolution during which a particle having pitch angle θ can enter a detector whose total opening angle is 6°.

FIGURE CAPTIONS (continued)

Figure 8. Explorer XII inbound pass, 18-19th of September 1961. The data points given here are 3 point averages (see section on Experimental Details) and SpL and SpH have both been corrected for background counts by subtraction of SpB. CdSB has been normalized to energy scale of CdSTE.

Figure 9. (a) SpL-SpB for three passes associated with the August 30th magnetic storm.

(b) SpH-SpB for three passes associated with the August 30th magnetic storm.

Figure 10. (a) CdSTE for three passes associated with the August 30th magnetic storm.

(b) CdSOM for three passes associated with the August 30th magnetic storm.

Figure 11. (a) 302 for three passes associated with the August 30th magnetic storm.

(b) SpB for three passes associated with the August 30th magnetic storm.

Figure 12. A time history of the maximum values for each pass for the hard and soft components of the outer zone. The SpL peak rate (corrected for background where possible) is taken to represent the soft component and the 302 peak rate is taken to represent the hard component. Also shown is the K_p index from the three-hour interval including the SpL data point, the D_{st} (H) value computed

FIGURE CAPTIONS (continued)

from the hourly scalings of the San Juan and Honolulu magnetograms, and the L values and magnetic latitude at which the 302 peak rates are observed.

Figure 13. Trajectory plots of two Explorer XII inbound passes whose trajectories were nearly coincident in magnetic coordinate space. The logarithm of the 302 counts/10 seconds is given for various points along the trajectories.

Figure 14. The 302 peak rate points shown in Figure 12 are plotted as a function of the L value at which they occurred.

Figure 15. The magnetic latitudes of the 302 peak rate points shown in Figure 12 plotted as a function of the simultaneous L value.

Figure 16. The trajectories in magnetic coordinate space of six passes through the outer zone associated with the September 30th storm. The logarithms of the 302 count-rates are indicated at various points along the trajectories. The crosses indicate the points on the trajectories where the maximum 302 rate occurred.

Figure 17. The correlation between the maximum outer zone SpL count-rates and the K_p index.

Figure 18. Scatter diagram showing the 302 peak rates from Figure 12 plotted as a function of the K_p indices.

FIGURE CAPTIONS (continued)

Figure 19. The San Juan magnetogram for September 13-14, 1961, showing the sudden commencement at 15h 56m U.T. on September 13 and the mild, prolonged "initial" phase.

Figure 20. Particle and magnetic field measurements with Explorer XII for the inbound pass on September 13, 1961. The CdSB detector count-rate has been normalized to the energy scale of the CdSTE detector. The counting rates of both CdS detectors are nearly linear with energy flux. Both spectrometer channels (SpL and SpH) have been corrected for background counts by the subtraction of the counting rate of the background detector SpB. The CdS optical monitor (not shown) indicated that during this pass the CdS detectors did not have any bright objects within their field of view. If F denotes the scalar magnetic field strength; α the angle between the F-vector and the spin-axis of the satellite; and γ the dihedral angle between the plane containing the F-vector and the spin axis and the plane containing the spin axis and the satellite-sun line (see section on Experimental Details).

Figure 21. The SpL count-rate for the inbound pass on the 16th and 17th of September, 1961.

Figure 22. Correlation between the maximum CdSTE response beyond the magnetospheric boundary and the geocentric position of the magnetospheric boundary. The solid

FIGURE CAPTIONS (continued)

dots represent passes on which there is a sharp radial discontinuity or termination of the CdSTE response beyond the boundary.

Figure 23. The maximum CdSTE response beyond the magnetospheric boundary plotted as a function of the K_p index.

Figure 24. The count-rate of the CdSTE and SpL detectors for the inbound pass on September 22. Note the softening of the electron spectrum immediately inside the boundary as indicated by the ratio of the SpL to CdSTE count-rates.

Figure 25. The count-rates of the CdSTE and SpL detectors for the inbound pass on the 8th and 9th of October.

Figure 26. The count-rates of the CdSTE and SpL detectors for the inbound pass on the 11th of September. Note the apparent multiple boundary (see text).

Figure 27. The count-rates of the CdSTE and SpL detectors for the inbound pass on the 11th of October.

Figure 28. The time history of the radial position of the magnetospheric boundary as determined by radial termination of counts above background in the SpL detector. Also shown is the D_{st} (H) value from the San Juan and Honolulu magnetograms.

FIGURE CAPTIONS (continued)

Figure 29. The CdSTE and SpL count-rates for the December 2nd outbound pass; an example of a pass at geocentric earth-sun-satellite angles of greater than 90°.

Figure 30. A pictorial diagram showing an equatorial cut of geomagnetosphere. Regions in which hard, soft, and very soft electrons are found in abundance are indicated. The general shapes of the various regions are consistent with all satellite and space probe data which have been made available to date.

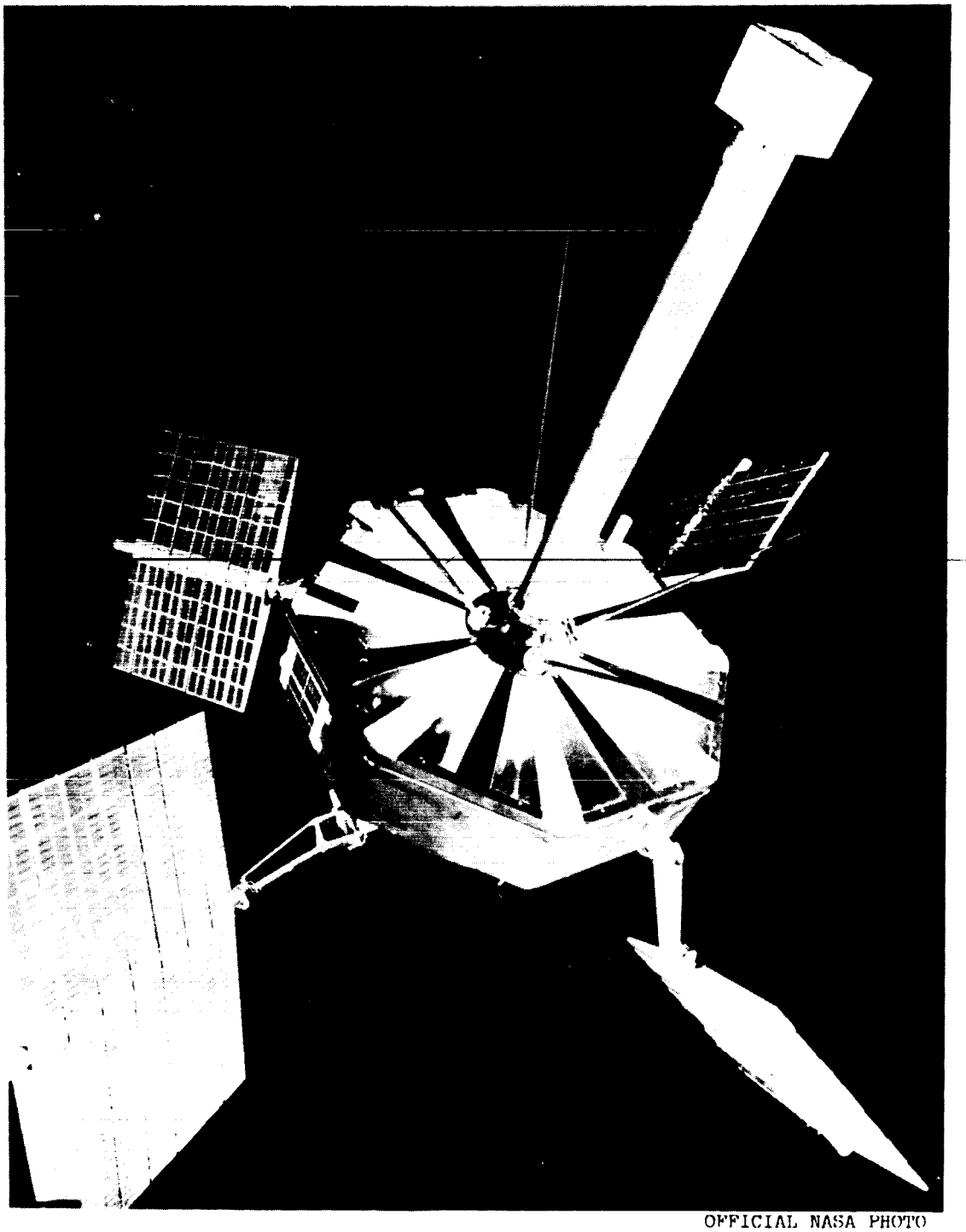

OFFICIAL NASA PHOTO

EXPLORER XII (S-3)
Energetic Particles Satellite, Launched August 15, 1961

Figure 1

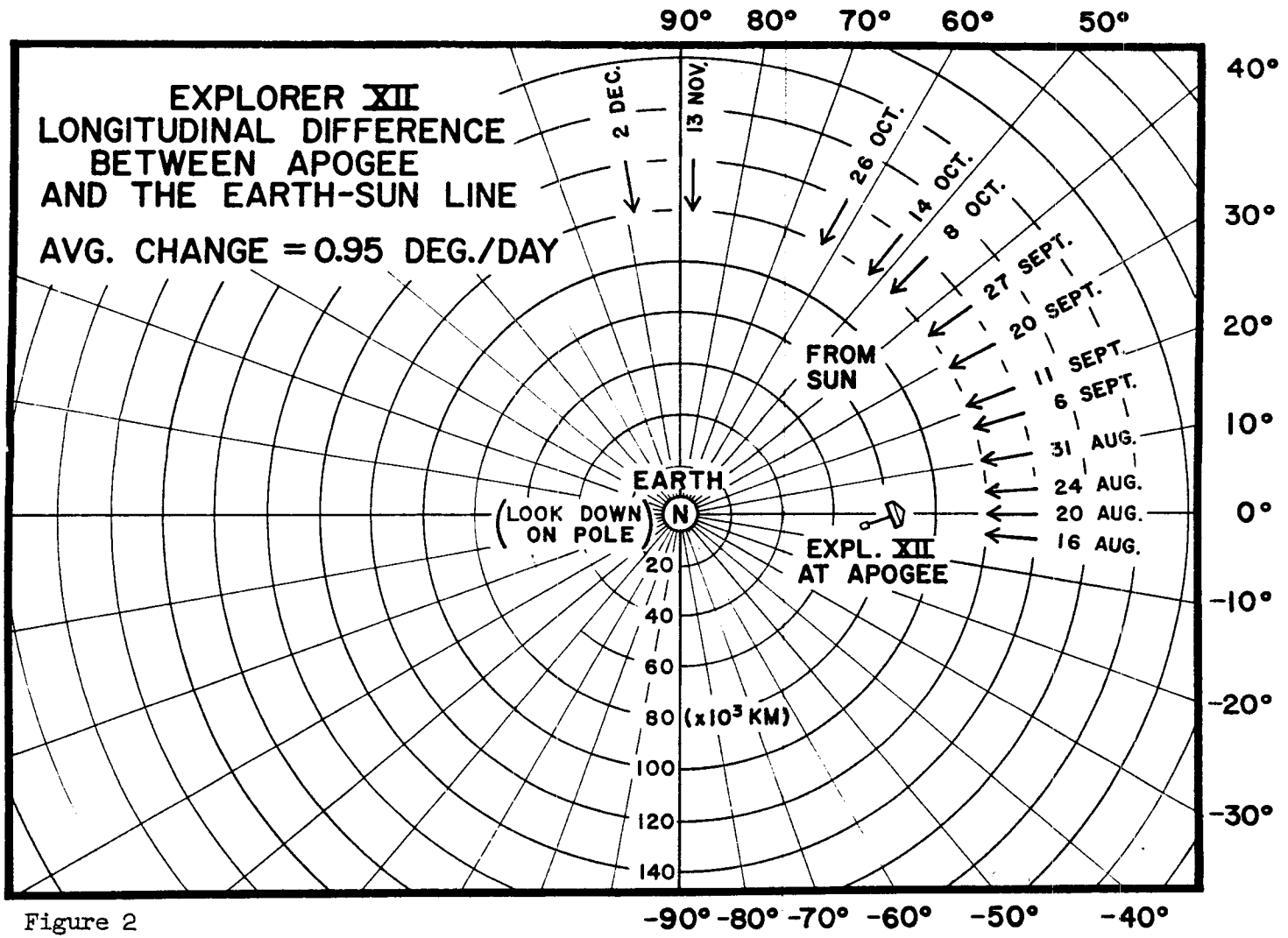
EXPLORER XII
LONGITUDINAL DIFFERENCE
BETWEEN APOGEE
AND THE EARTH-SUN LINE
AVG. CHANGE = 0.95 DEG./DAY
90° 80° 70° 60° 50°
40°
30°
20°
10°
0°
-10°
-20°
-30°
-90° -80° -70° -60° -50° -40°
2 DEC.
13 NOV.
26 OCT.
14 OCT.
8 OCT.
27 SEPT.
20 SEPT.
11 SEPT.
6 SEPT.
31 AUG.
24 AUG.
20 AUG.
16 AUG.
FROM SUN
EARTH
N
LOOK DOWN ON POLE
EXPL. XII AT APOGEE
20
40
60
80
100
120
140
(x10³ KM)

Figure 2

CDS DETECTOR ASSEMBLY

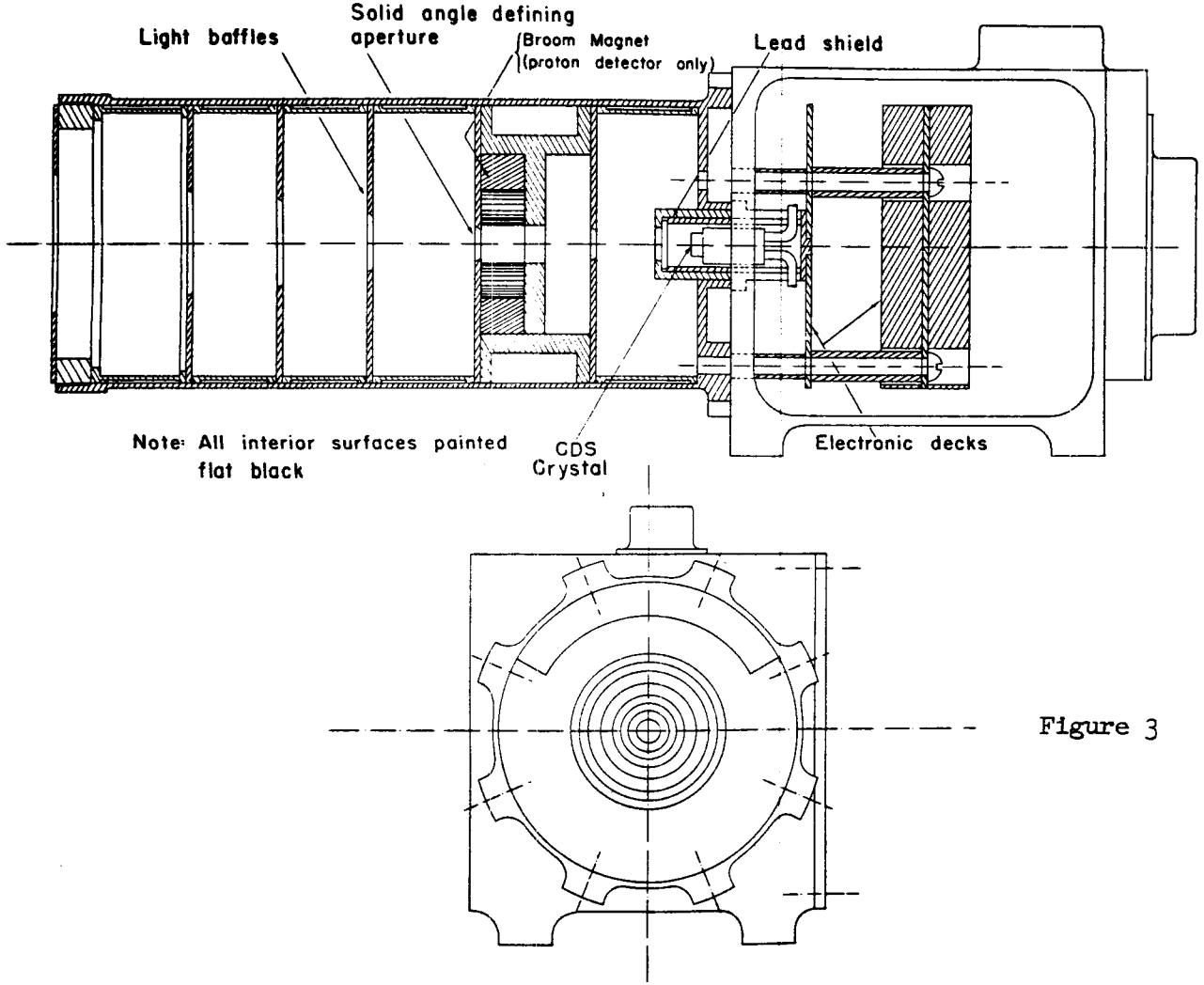

Figure 3

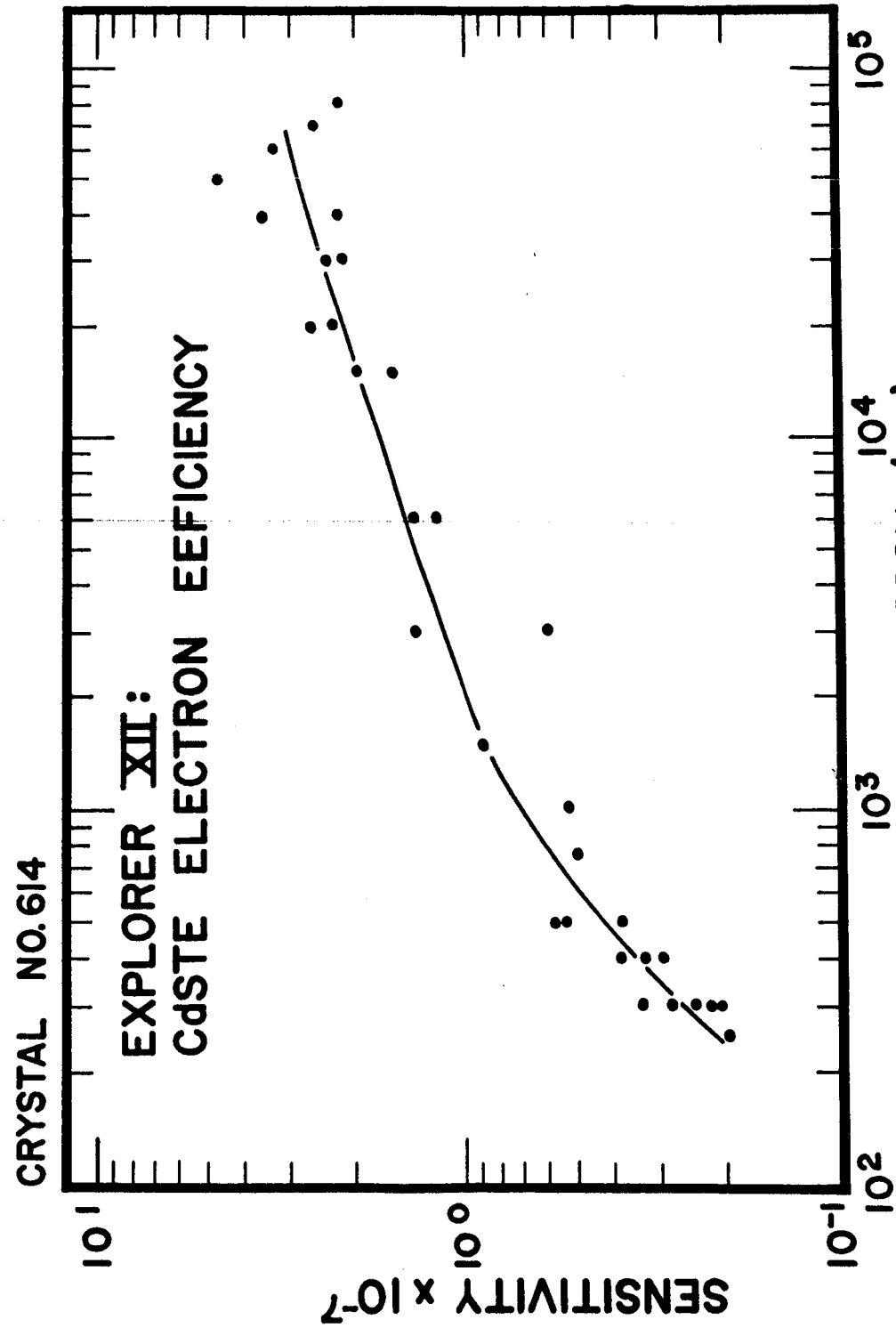
CRYSTAL NO.614
EXPLORER XII:
CdSTE ELECTRON EEFICIENCY
SENSITIVITY x 10⁻⁷
ELECTRON ENERGY (ev)
10¹
10⁰
10⁻¹
10²
10³
10⁴
10⁵

Figure 4

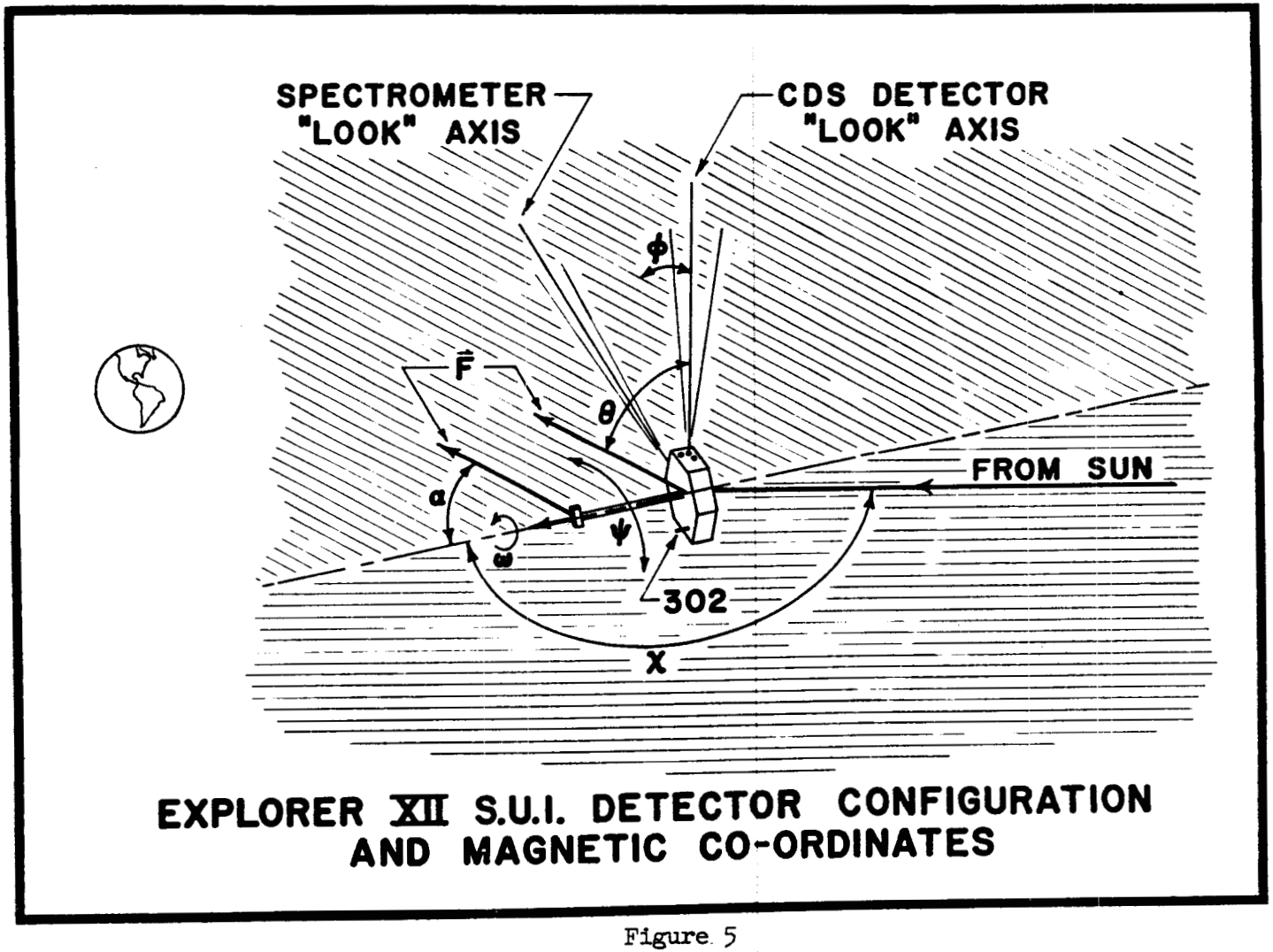
SPECTROMETER
"LOOK" AXIS
CDS DETECTOR
"LOOK" AXIS
φ
F
θ
α
ω
ψ
FROM SUN
302
X
EXPLORER XII S.U.I. DETECTOR CONFIGURATION
AND MAGNETIC CO-ORDINATES

Figure 5

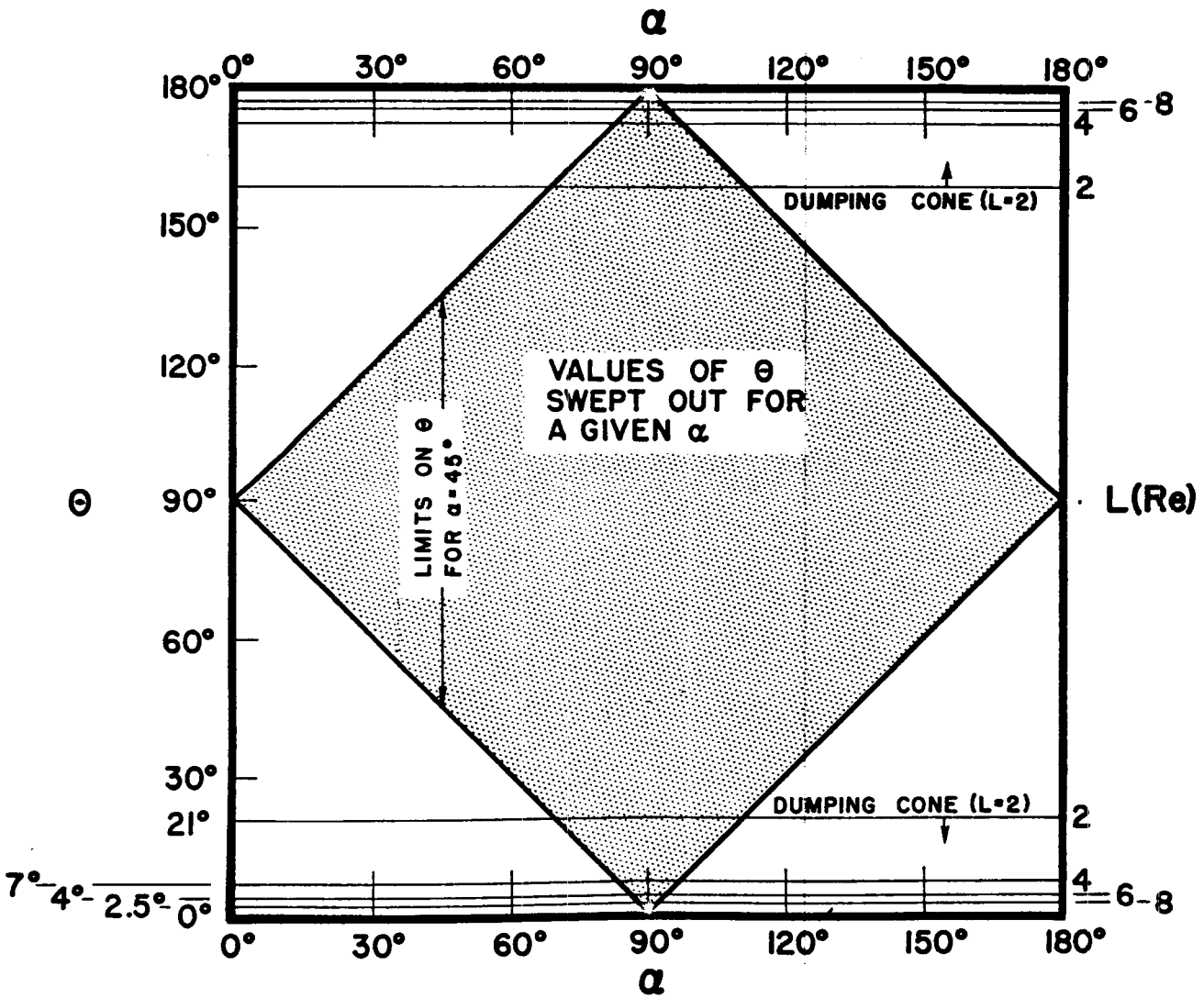

Figure 6

LIMITS OF THE DUMPING CONE, θ_D, AT THE MAGNETIC EQUATOR

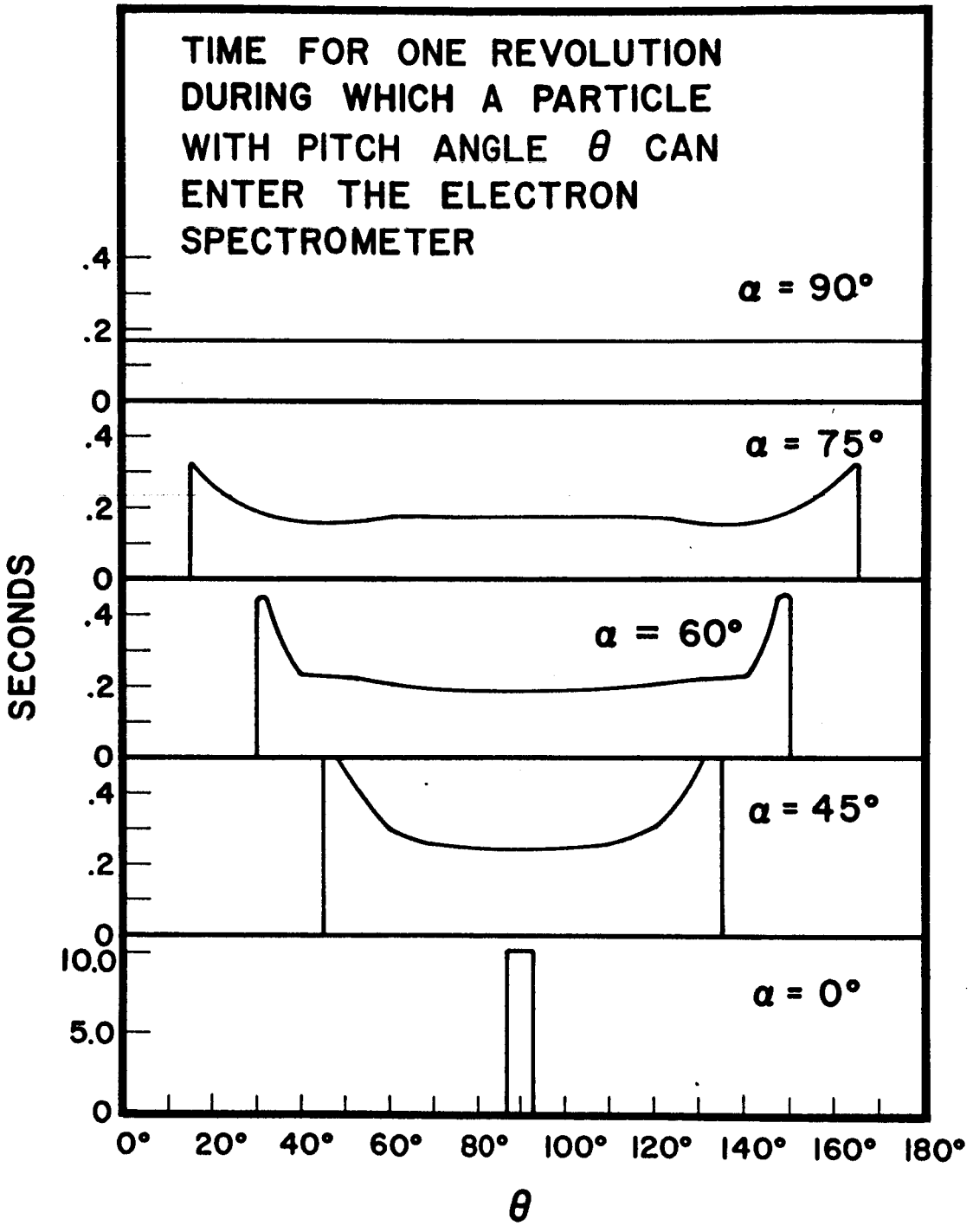
TIME FOR ONE REVOLUTION DURING WHICH A PARTICLE WITH PITCH ANGLE θ CAN ENTER THE ELECTRON SPECTROMETER
α = 90°
α = 75°
α = 60°
α = 45°
α = 0°
SECONDS
.4
.2
0
10.0
5.0
0°
20°
40°
60°
80°
100°
120°
140°
160°
180°
θ

Figure 7

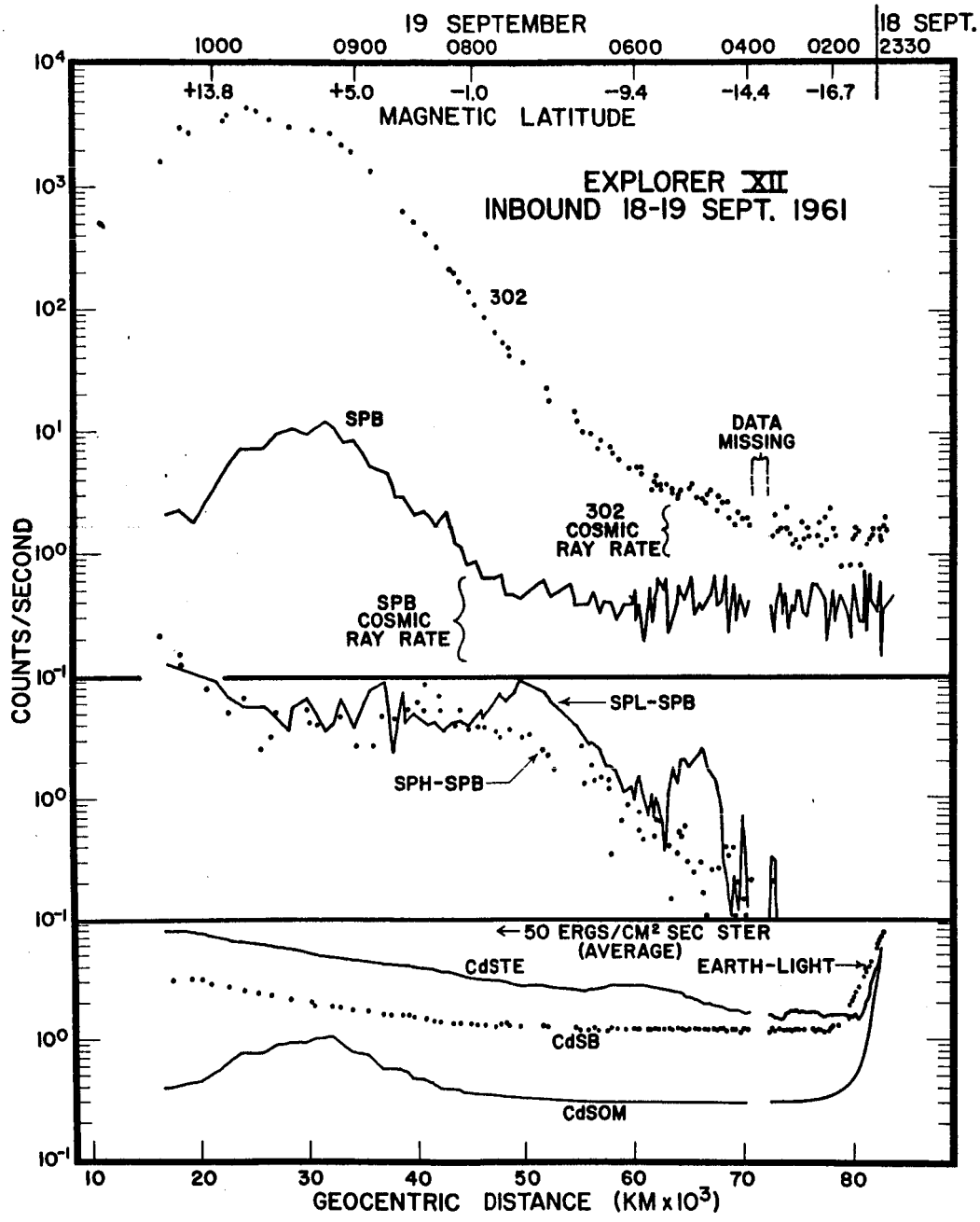
19 SEPTEMBER
18 SEPT.
1000
0900
0800
0600
0400
0200
2330
+13.8
+5.0
-1.0
-9.4
-14.4
-16.7
MAGNETIC LATITUDE
EXPLORER XII
INBOUND 18-19 SEPT. 1961
302
SPB
DATA MISSING
302 COSMIC RAY RATE
SPB COSMIC RAY RATE
SPL-SPB
SPH-SPB
50 ERGS/CM² SEC STER (AVERAGE)
CdSTE
EARTH-LIGHT
CdSB
CdSOM
COUNTS/SECOND
GEOCENTRIC DISTANCE (KM x 10³)

Figure 8

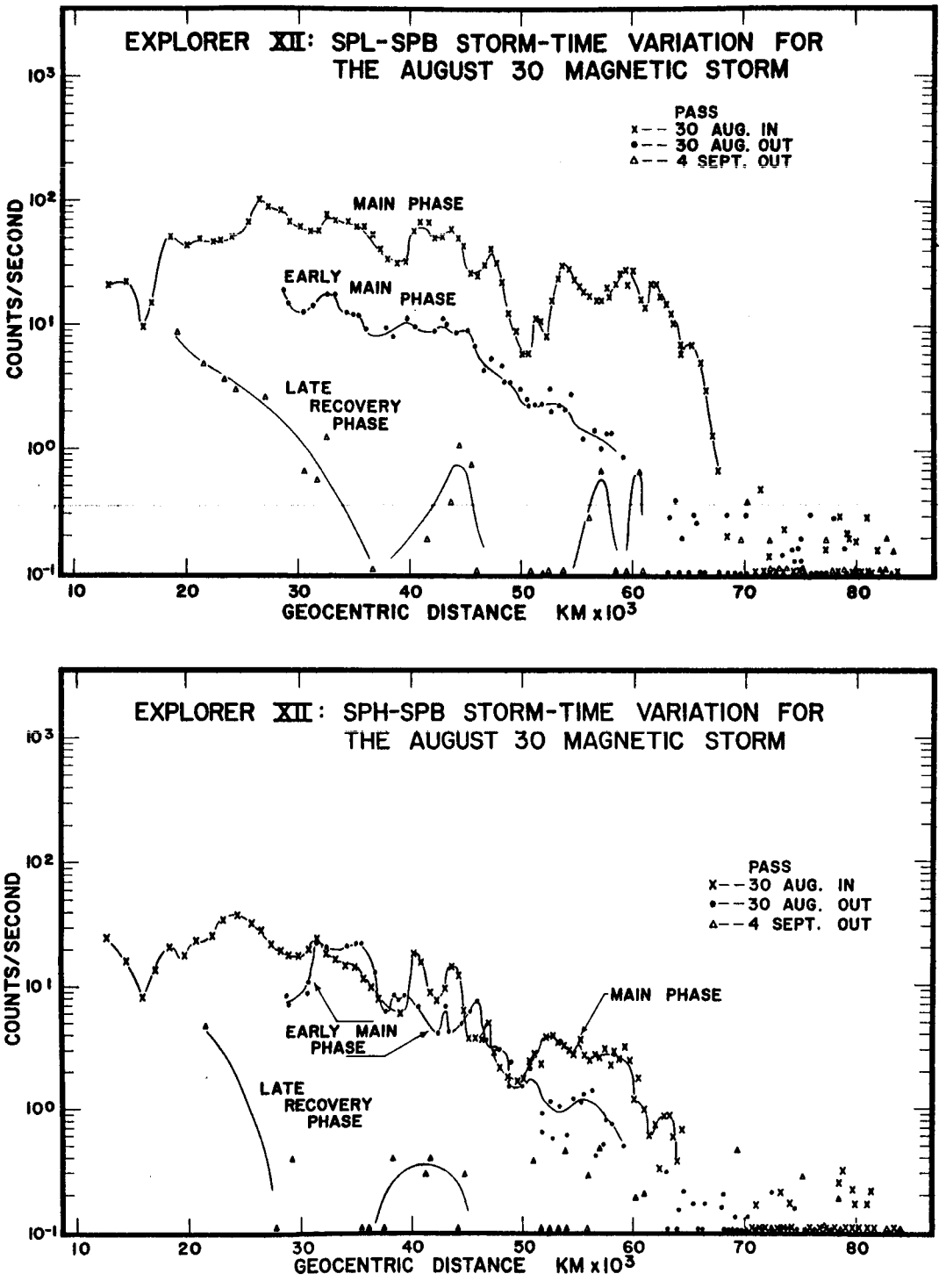
EXPLORER XII: SPL-SPB STORM-TIME VARIATION FOR THE AUGUST 30 MAGNETIC STORM
PASS
x-- 30 AUG. IN
•-- 30 AUG. OUT
Δ-- 4 SEPT. OUT
MAIN PHASE
EARLY MAIN PHASE
LATE RECOVERY PHASE
COUNTS/SECOND
GEOCENTRIC DISTANCE KM x10³
EXPLORER XII: SPH-SPB STORM-TIME VARIATION FOR THE AUGUST 30 MAGNETIC STORM
PASS
x--30 AUG. IN
•--30 AUG. OUT
Δ--4 SEPT. OUT
MAIN PHASE
EARLY MAIN PHASE
LATE RECOVERY PHASE
COUNTS/SECOND
GEOCENTRIC DISTANCE KM x10³

Figure 9

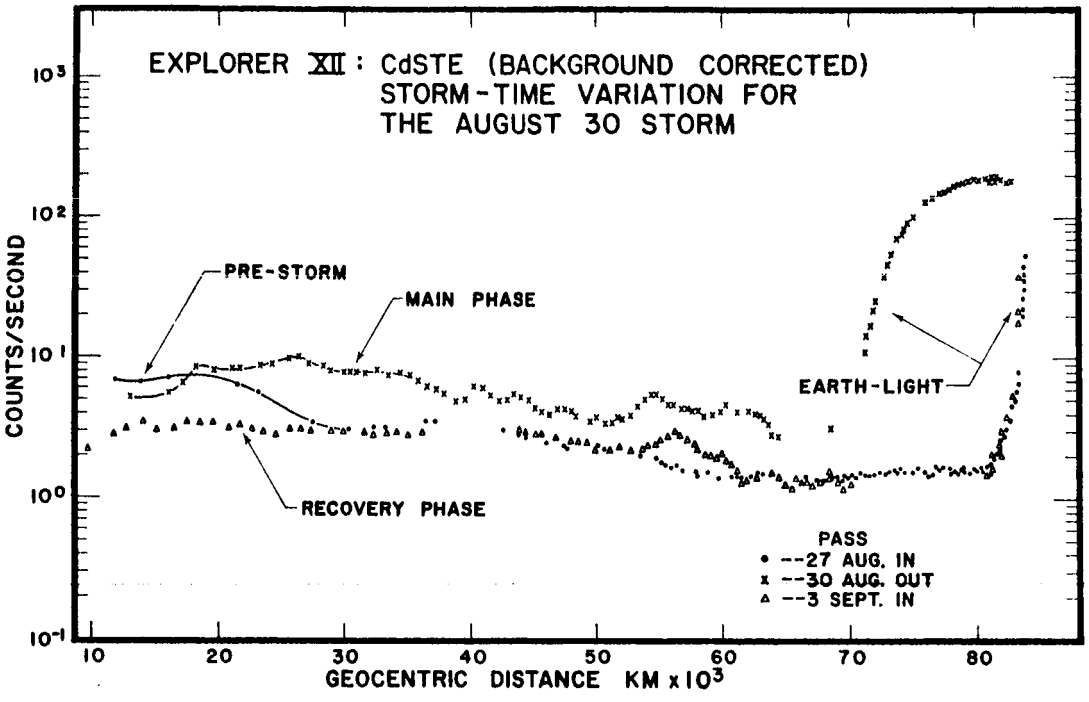
EXPLORER XII : CdSTE (BACKGROUND CORRECTED)
STORM-TIME VARIATION FOR
THE AUGUST 30 STORM
COUNTS/SECOND
PRE-STORM
MAIN PHASE
RECOVERY PHASE
EARTH-LIGHT
PASS
• --27 AUG. IN
x --30 AUG. OUT
△ --3 SEPT. IN
GEOCENTRIC DISTANCE KM x 10³

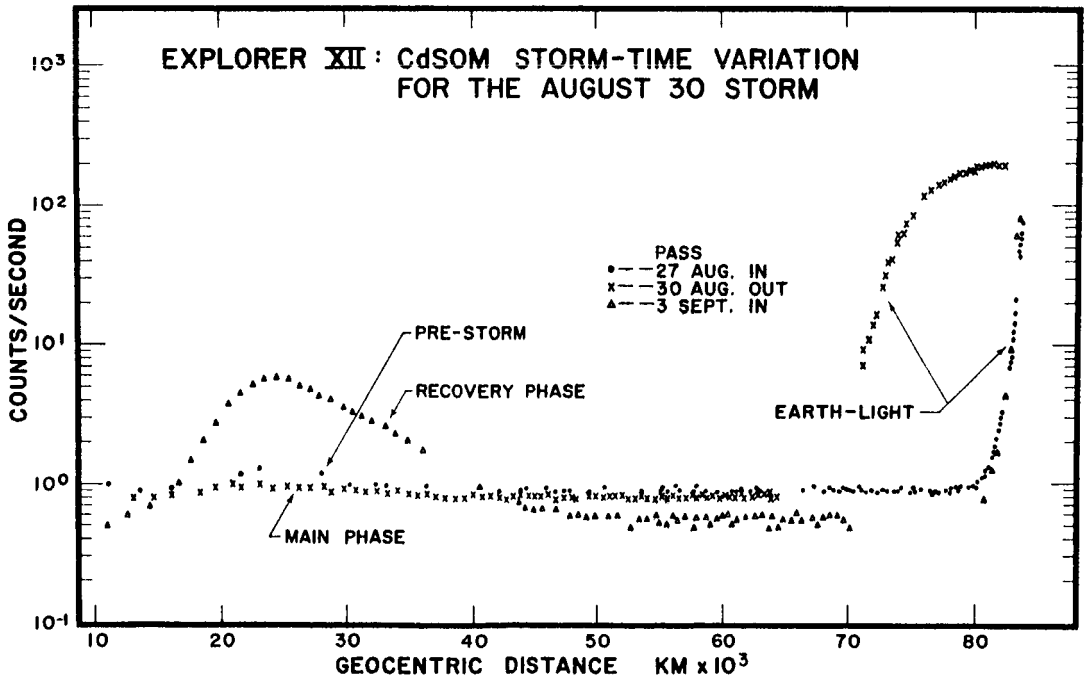
EXPLORER XII : CdSOM STORM-TIME VARIATION
FOR THE AUGUST 30 STORM
COUNTS/SECOND
PASS
•--27 AUG. IN
x--30 AUG. OUT
△--3 SEPT. IN
PRE-STORM
RECOVERY PHASE
MAIN PHASE
EARTH-LIGHT
GEOCENTRIC DISTANCE KM x 10³

Figure 10

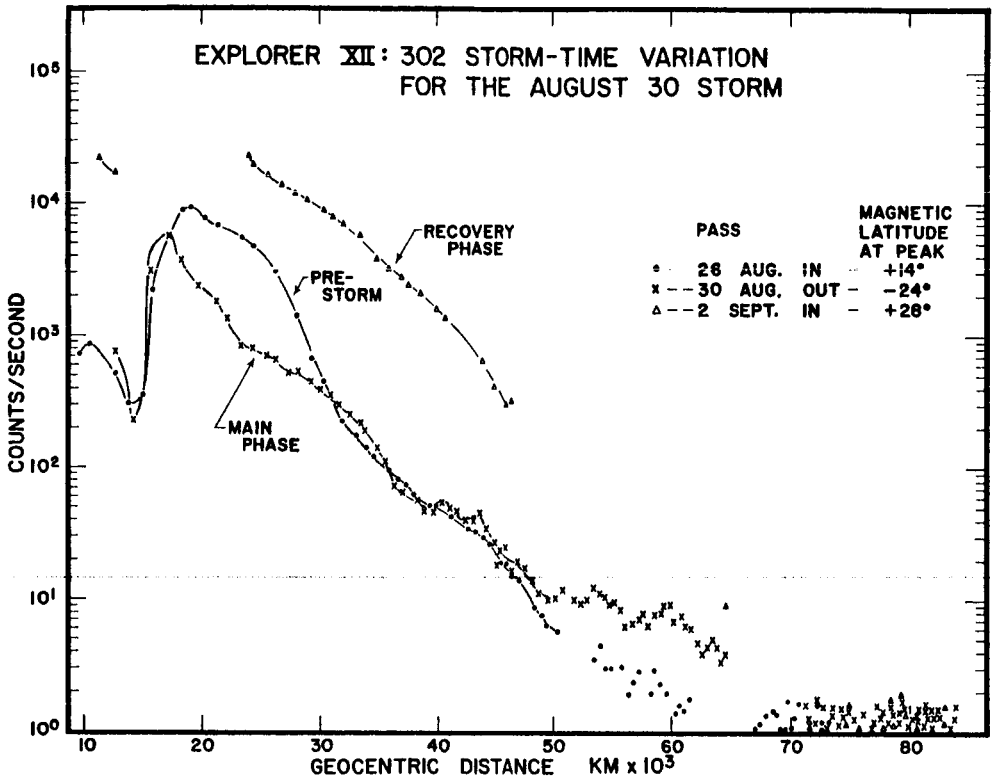
EXPLORER XII: 302 STORM-TIME VARIATION
FOR THE AUGUST 30 STORM
COUNTS/SECOND
GEOCENTRIC DISTANCE KM x 10³
RECOVERY PHASE
PRE-STORM
MAIN PHASE
PASS
MAGNETIC LATITUDE AT PEAK
26 AUG. IN +14°
30 AUG. OUT −24°
2 SEPT. IN +28°

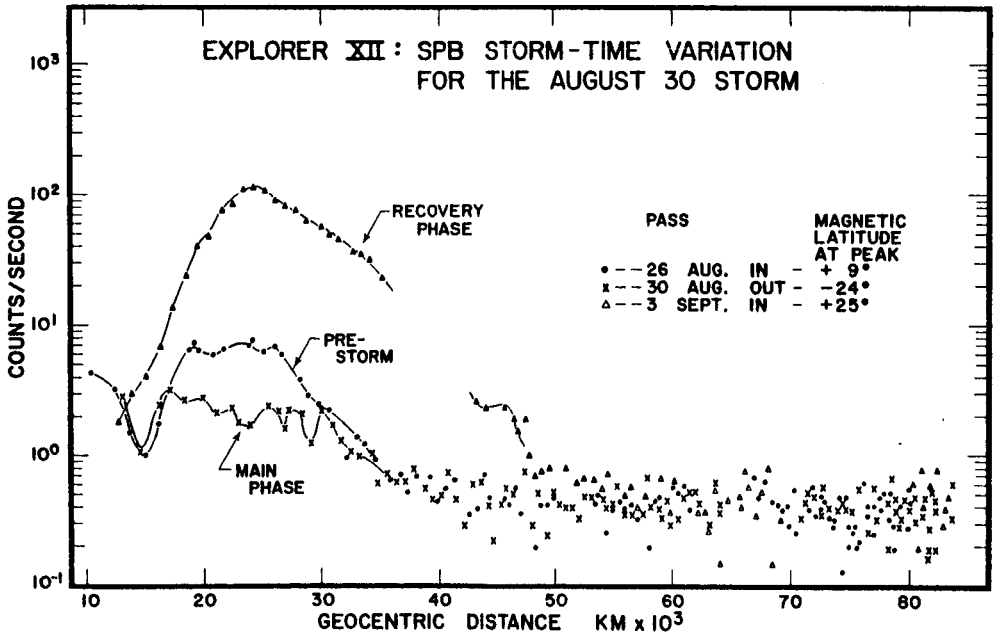
EXPLORER XII: SPB STORM-TIME VARIATION
FOR THE AUGUST 30 STORM
COUNTS/SECOND
GEOCENTRIC DISTANCE KM x 10³
RECOVERY PHASE
PRE-STORM
MAIN PHASE
PASS
MAGNETIC LATITUDE AT PEAK
26 AUG. IN + 9°
30 AUG. OUT −24°
3 SEPT. IN +25°

Figure 11

EXPLORER XII

OUTER ZONE HARD AND SOFT ELECTRON MAXIMUM COUNT-RATES COMPARED WITH THE MAGNETIC PARAMETERS $D_{st}(H)$ AND K_p.

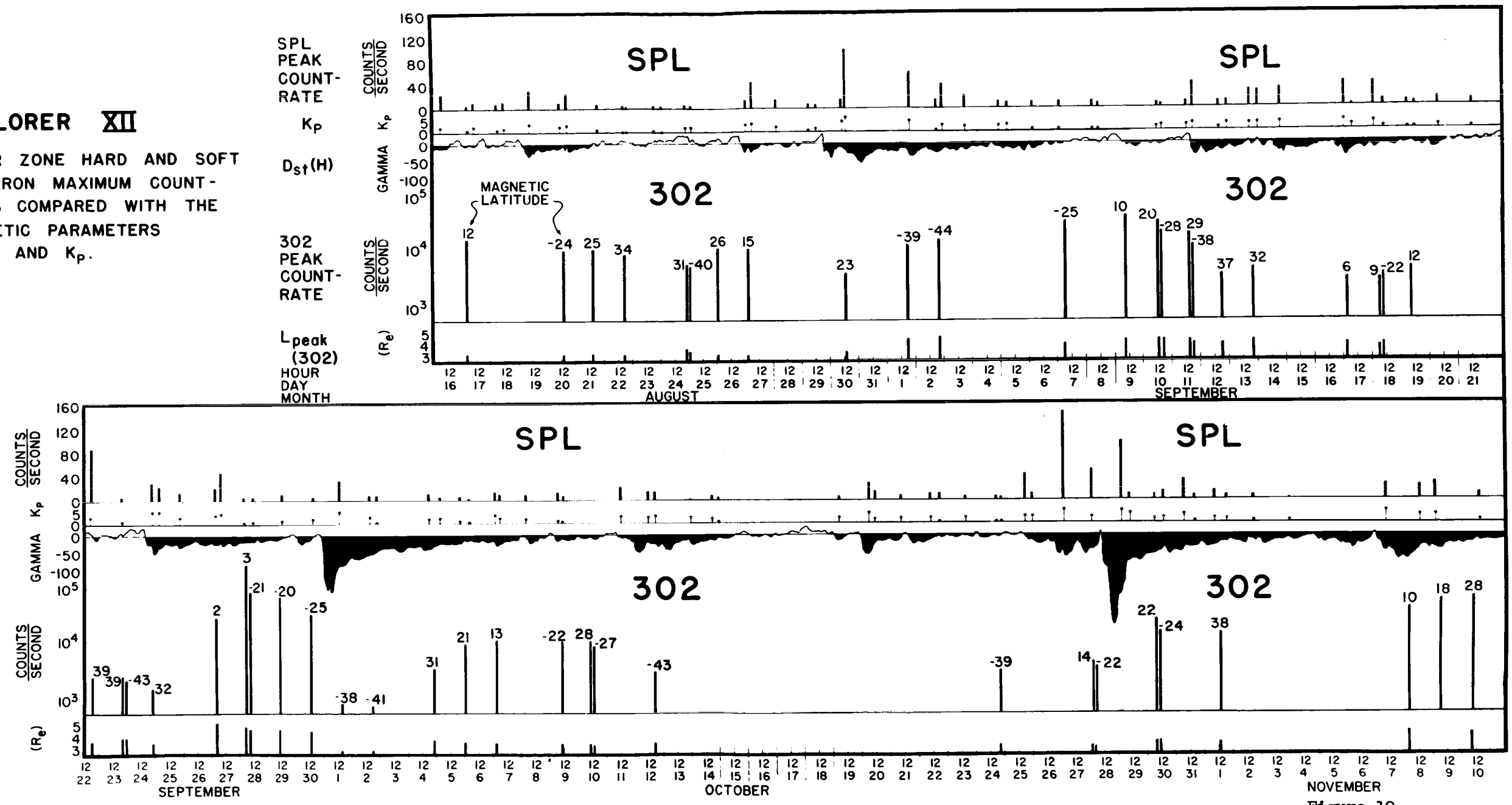

Figure 12

EXPLORER XII

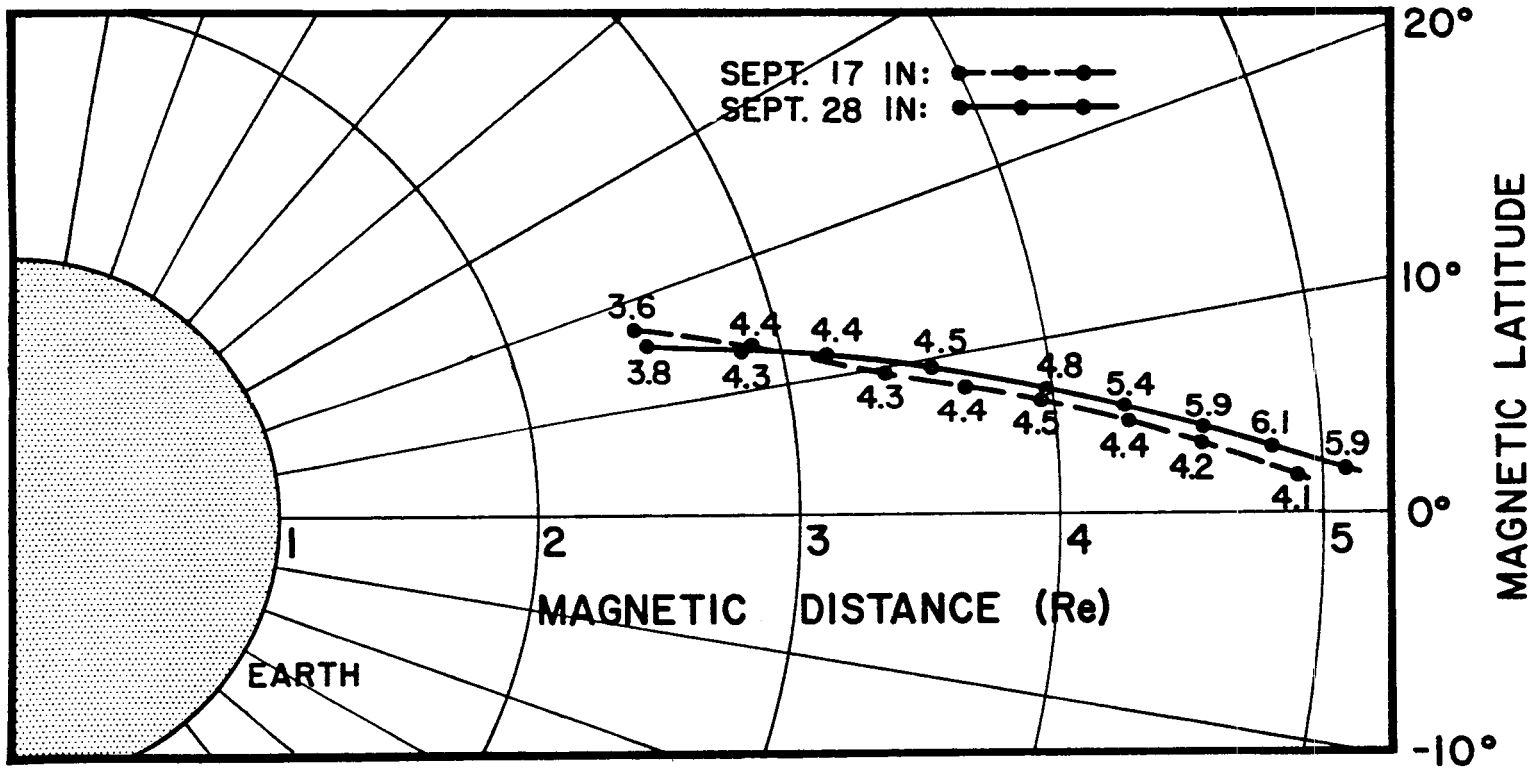

TRAJECTORY PLOT OF THE LOG OF 302 COUNTS PER 10 SECONDS FOR TWO PASSES NEARLY COINCIDENT IN MAGNETIC COORDINATE SPACE

Figure 13

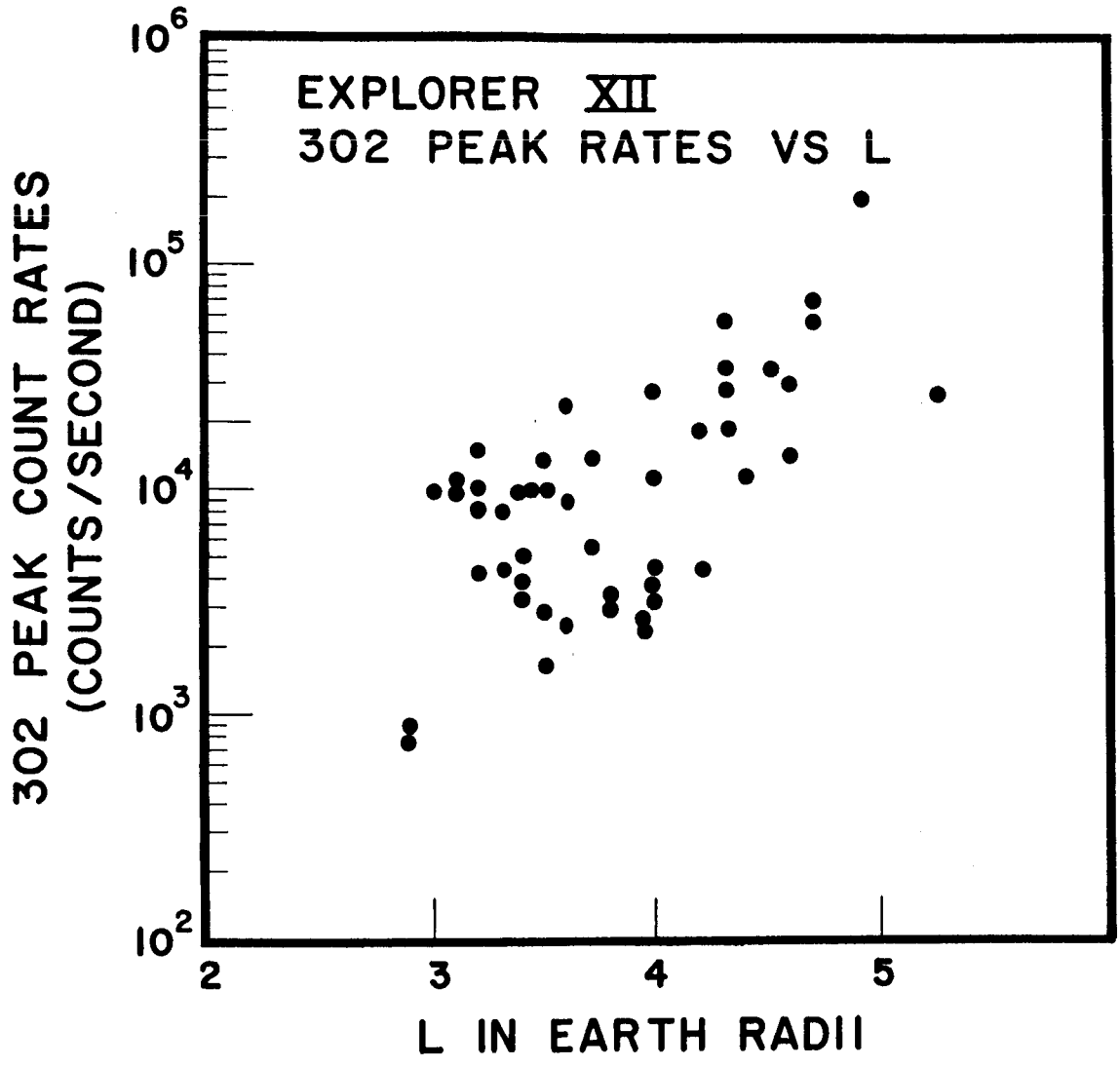
EXPLORER XII
302 PEAK RATES VS L
302 PEAK COUNT RATES (COUNTS/SECOND)
10^6
10^5
10^4
10^3
10^2
2
3
4
5
L IN EARTH RADII

Figure 14

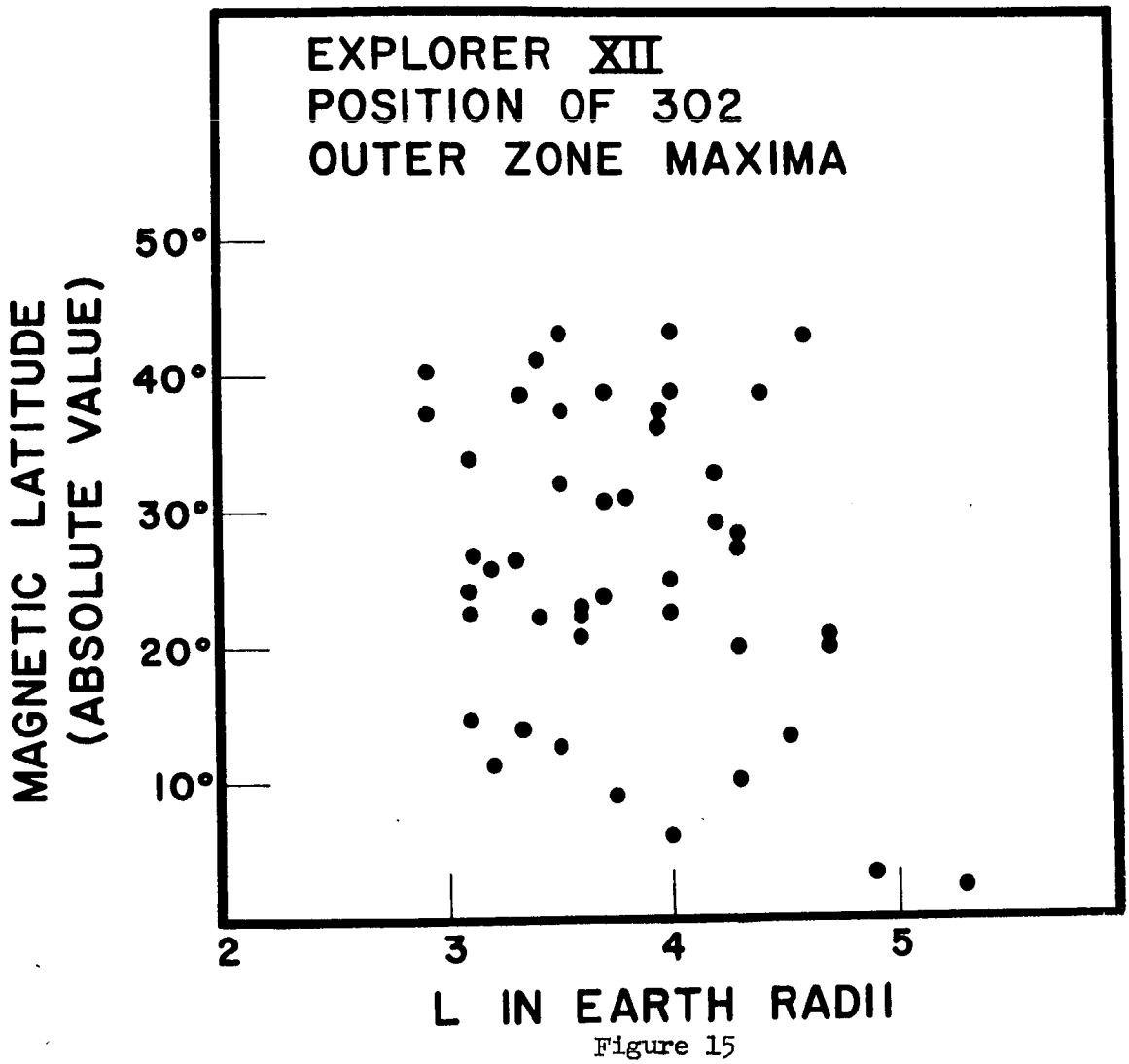
EXPLORER XII
POSITION OF 302
OUTER ZONE MAXIMA
MAGNETIC LATITUDE
(ABSOLUTE VALUE)
50°
40°
30°
20°
10°
2
3
4
5
L IN EARTH RADII

Figure 15

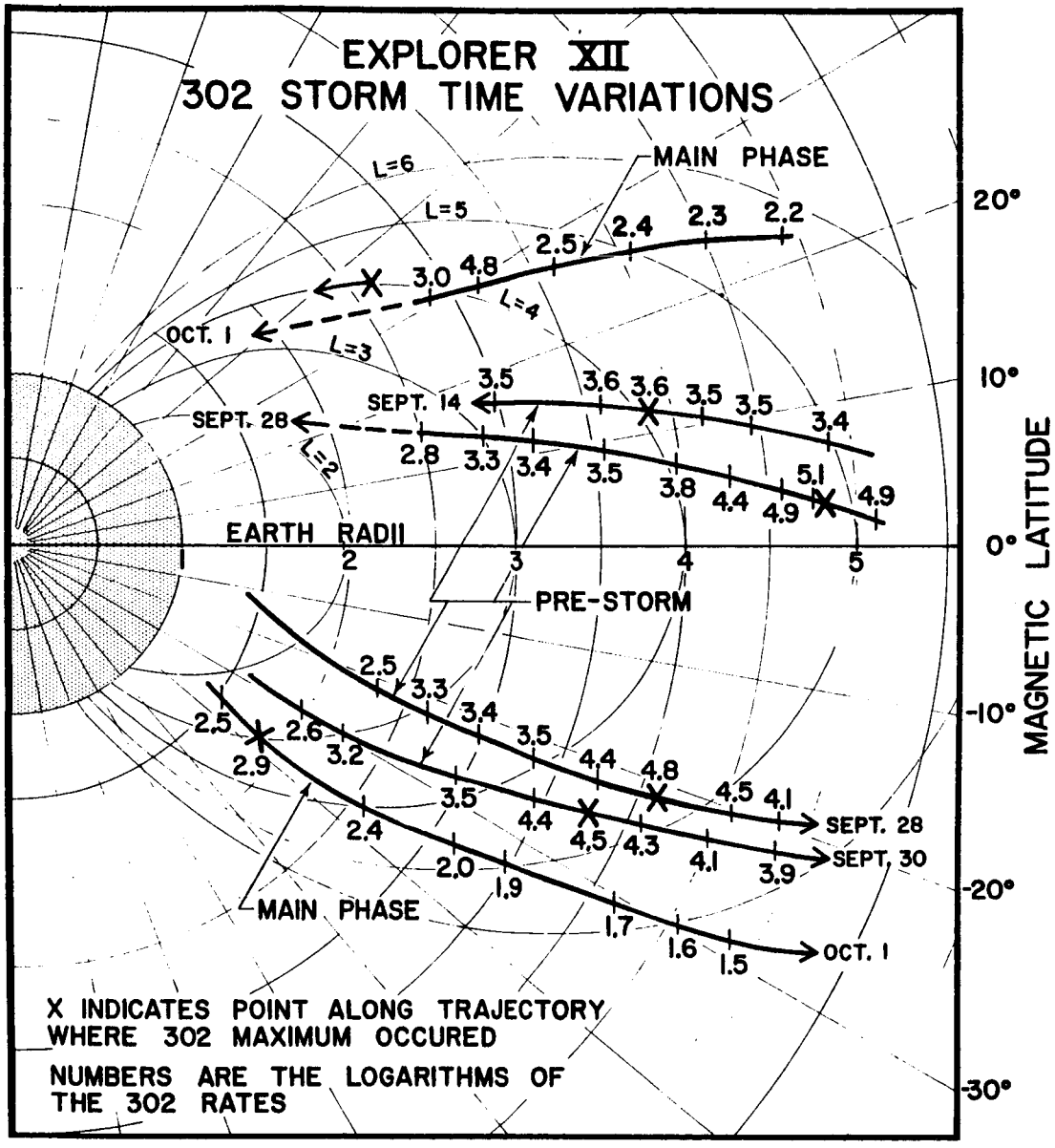
EXPLORER XII
302 STORM TIME VARIATIONS
MAIN PHASE
L=6
L=5
L=4
L=3
L=2
OCT. 1
SEPT. 14
SEPT. 28
SEPT. 30
EARTH RADII
PRE-STORM
MAIN PHASE
MAGNETIC LATITUDE
20°
10°
0°
-10°
-20°
-30°
X INDICATES POINT ALONG TRAJECTORY WHERE 302 MAXIMUM OCCURED
NUMBERS ARE THE LOGARITHMS OF THE 302 RATES

Figure 16

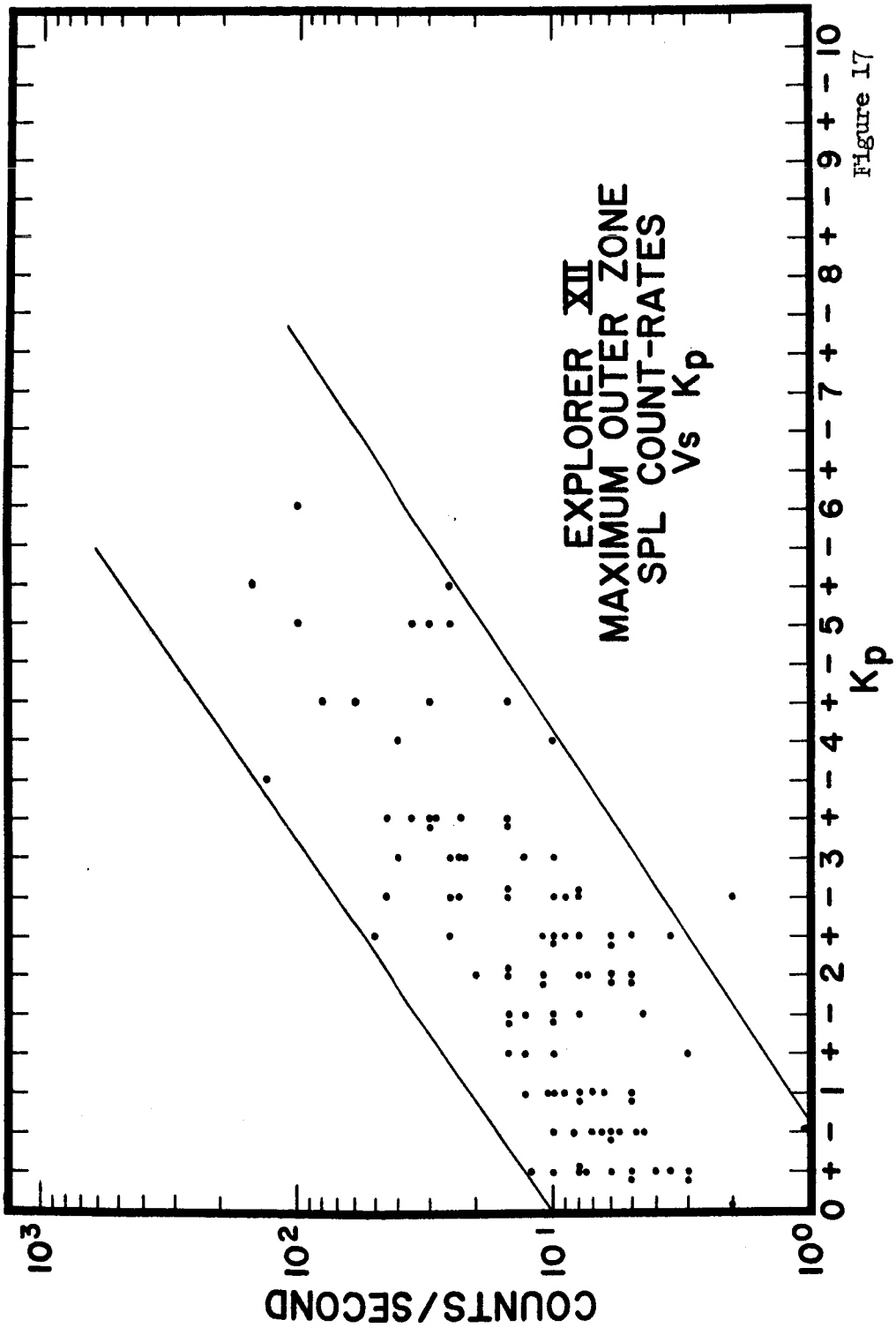
EXPLORER XII
MAXIMUM OUTER ZONE
SPL COUNT-RATES
Vs Kp
COUNTS/SECOND
10^3
10^2
10^1
10^0
0 + - 1 + - 2 + - 3 + - 4 + - 5 + - 6 + - 7 + - 8 + - 9 + - 10
Kp

Figure 17

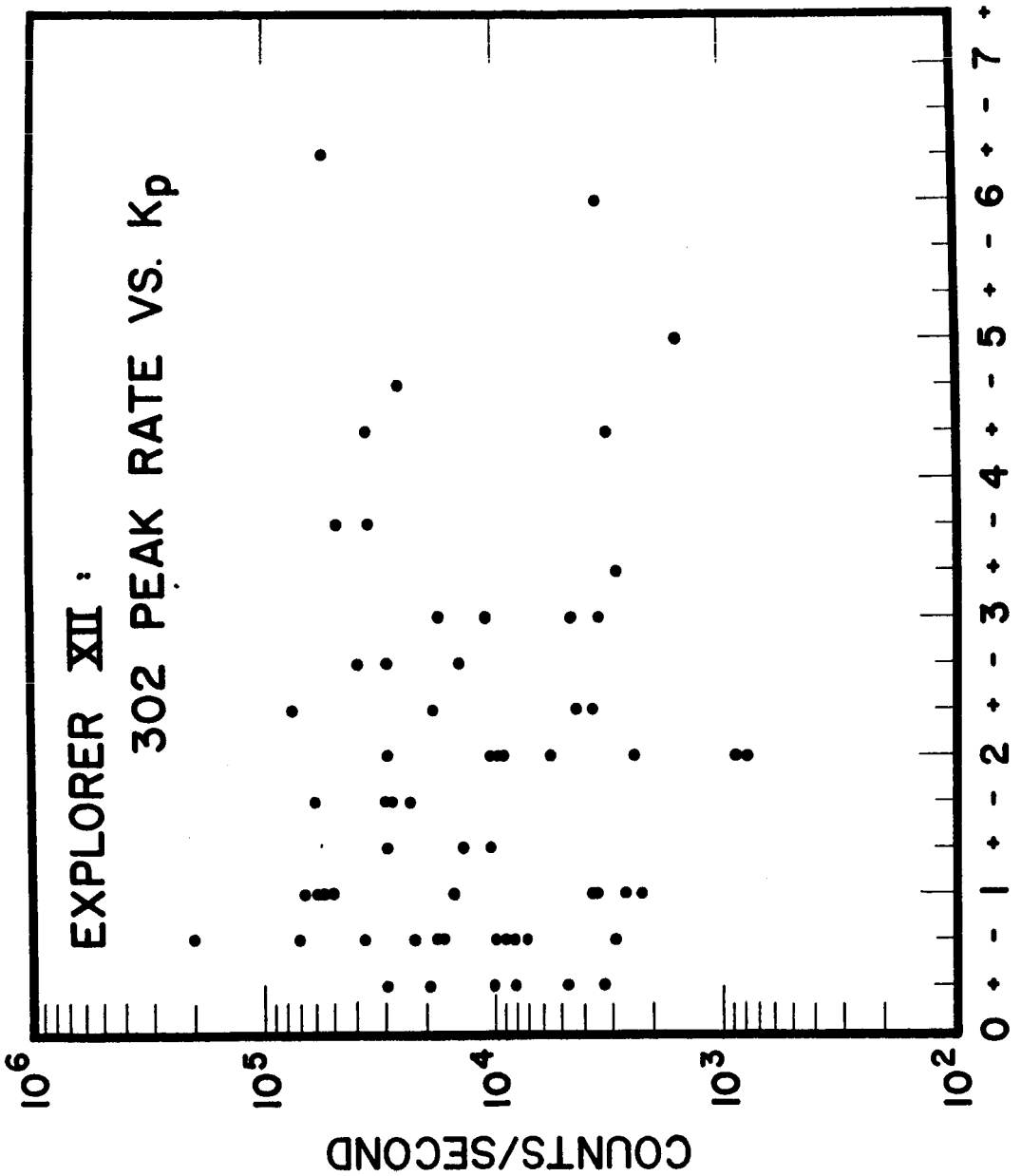
EXPLORER XII :
302 PEAK RATE VS. Kp
COUNTS/SECOND
10^6
10^5
10^4
10^3
10^2
0 + - 1 + - 2 + - 3 + - 4 + - 5 + - 6 + - 7 +
Kp

Figure 18

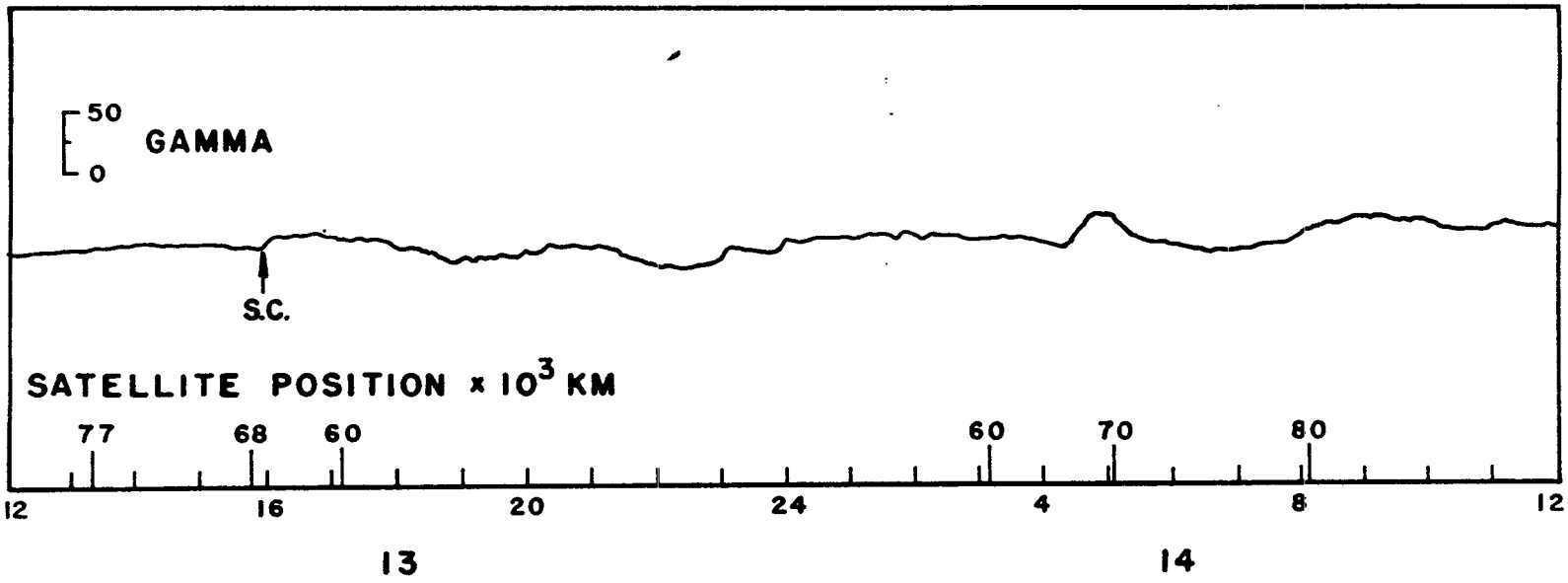
SAN JUAN MAGNETOGRAM
HORIZONTAL COMPONENT
50
0
GAMMA
S.C.
SATELLITE POSITION x 10^3 KM
77
68
60
60
70
80
12
16
20
24
4
8
12
13
14
SEPTEMBER

Figure 19

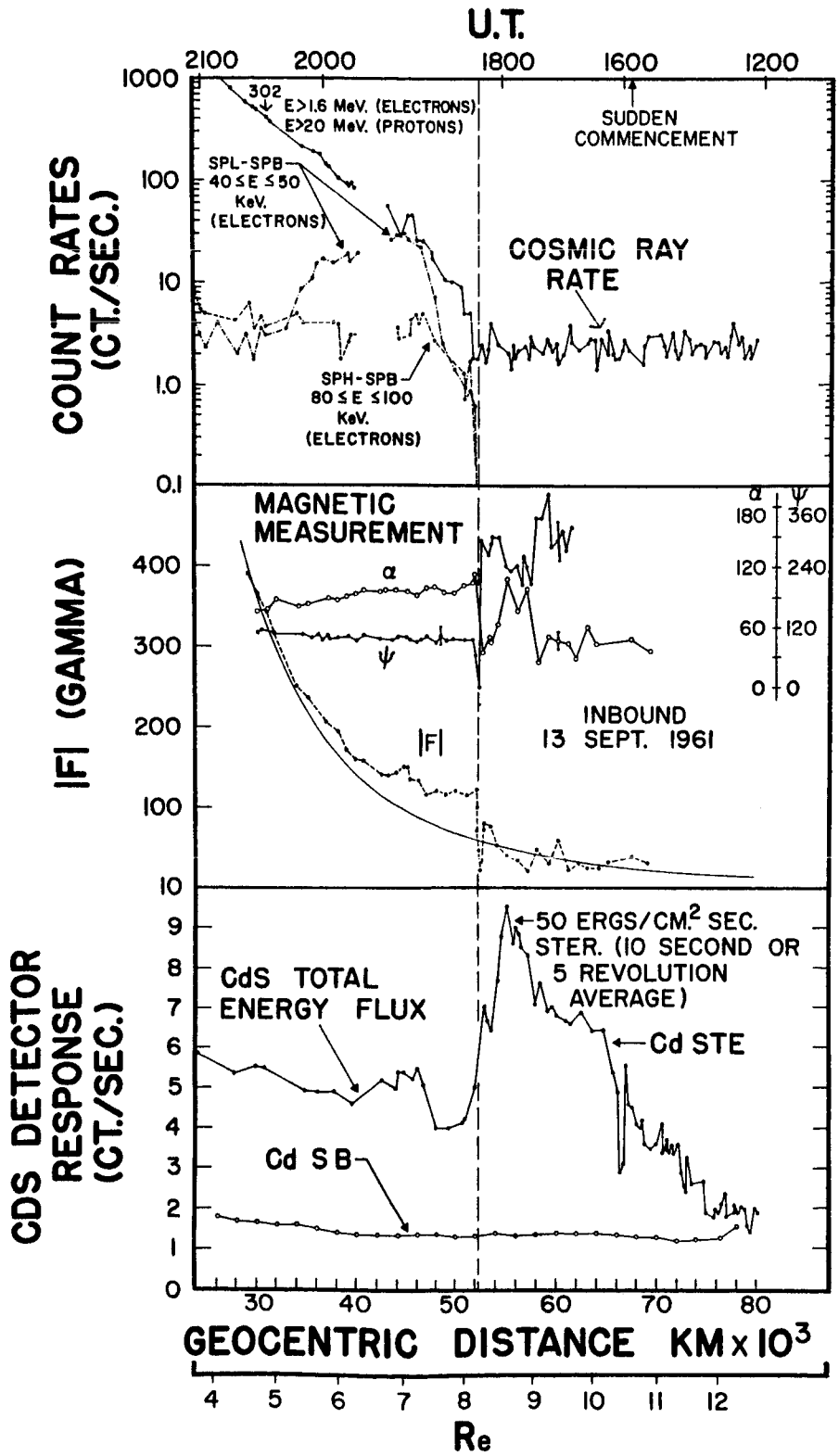
U.T.
2100
2000
1800
1600
1200
1000
100
10
1.0
0.1
COUNT RATES (CT./SEC.)
302
E>1.6 MeV. (ELECTRONS)
E>20 MeV. (PROTONS)
SUDDEN COMMENCEMENT
SPL-SPB
40 ≤ E ≤ 50 KeV. (ELECTRONS)
COSMIC RAY RATE
SPH-SPB
80 ≤ E ≤ 100 KeV. (ELECTRONS)
MAGNETIC MEASUREMENT
α
ψ
|F|
INBOUND 13 SEPT. 1961
400
300
200
100
10
|F| (GAMMA)
180
120
60
0
360
240
120
0
9
8
7
6
5
4
3
2
1
0
CDS DETECTOR RESPONSE (CT./SEC.)
CdS TOTAL ENERGY FLUX
50 ERGS/CM.2 SEC. STER. (10 SECOND OR 5 REVOLUTION AVERAGE)
Cd STE
Cd S B
30
40
50
60
70
80
GEOCENTRIC DISTANCE KM x 10^3
4
5
6
7
8
9
10
11
12
Re

Figure 20

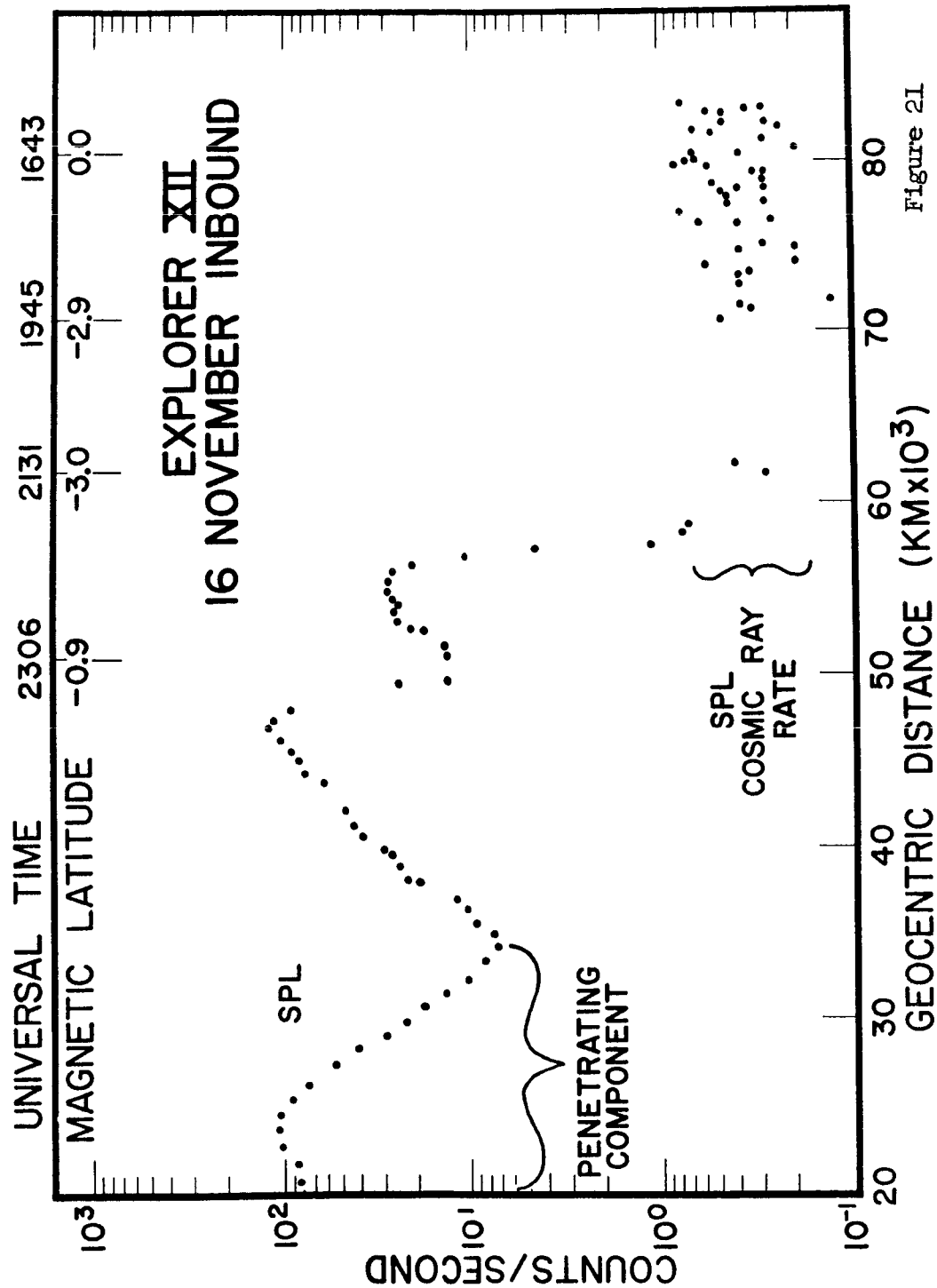
EXPLORER XII
16 NOVEMBER INBOUND
UNIVERSAL TIME 2306 2131 1945 1643
MAGNETIC LATITUDE -0.9 -3.0 -2.9 0.0
COUNTS/SECOND
GEOCENTRIC DISTANCE (KM x 10³)
SPL
PENETRATING COMPONENT
SPL COSMIC RAY RATE

Figure 21

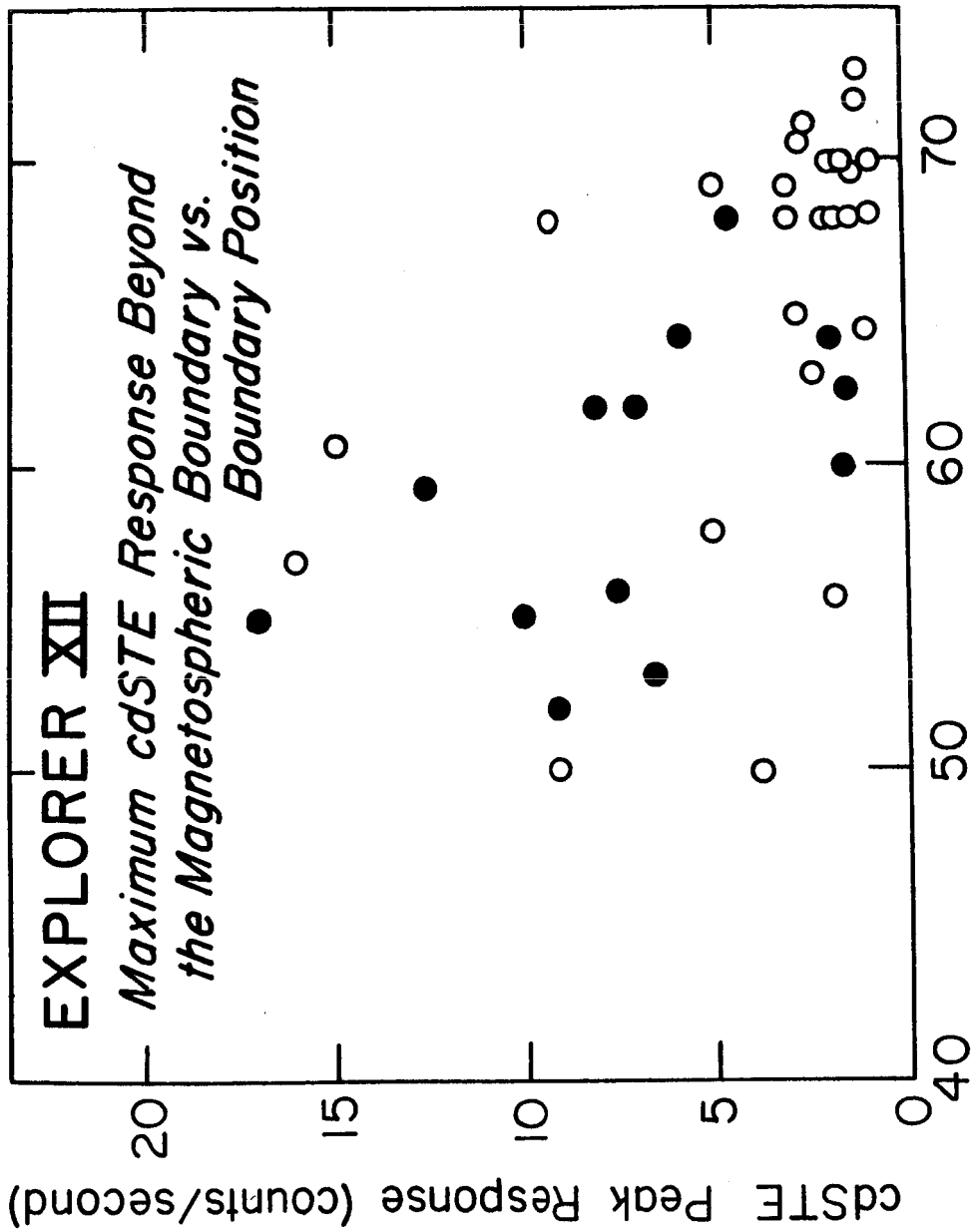
EXPLORER XII
Maximum cdSTE Response Beyond
the Magnetospheric Boundary vs.
Boundary Position
cdSTE Peak Response (counts/second)
0
5
10
15
20
40
50
60
70
Magnetospheric Boundary Position
(KM x 10³)

Figure 22

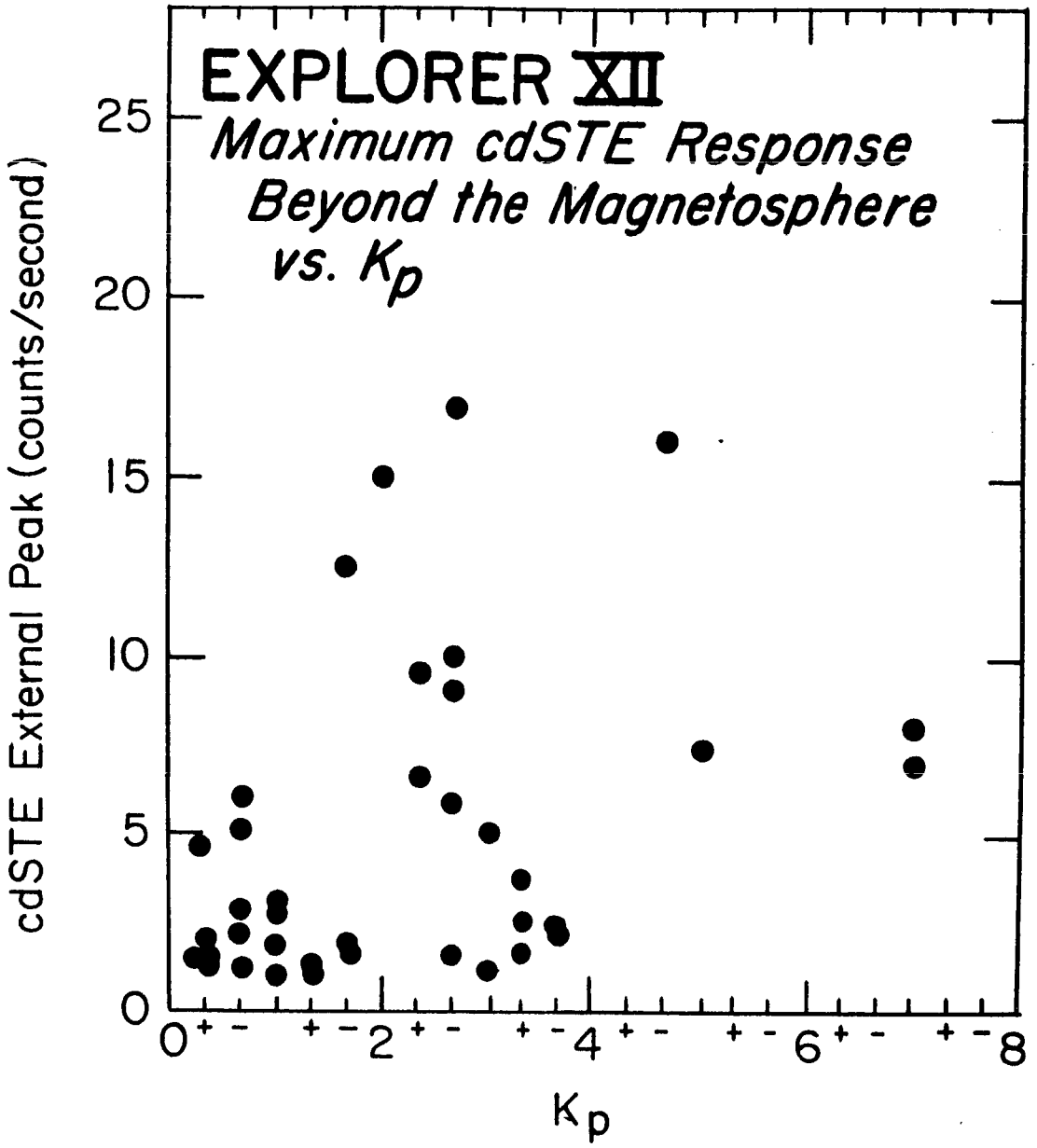
EXPLORER XII
Maximum cdSTE Response
Beyond the Magnetosphere
vs. Kp
cdSTE External Peak (counts/second)
0
5
10
15
20
25
0+ - + -2+ - + -4+ - + -6+ - + -8
Kp

Figure 23

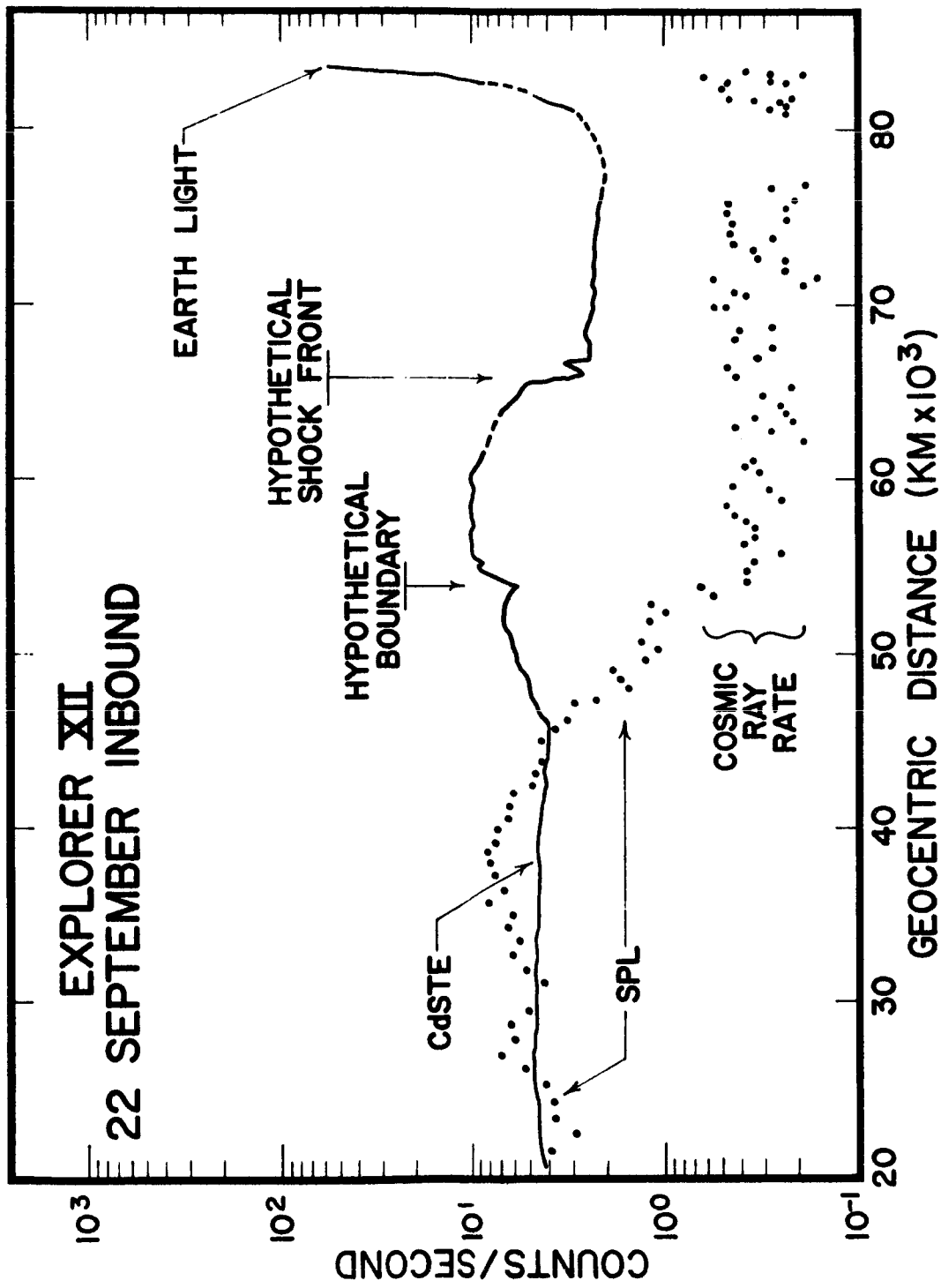
EXPLORER XII
22 SEPTEMBER INBOUND
EARTH LIGHT
HYPOTHETICAL SHOCK FRONT
HYPOTHETICAL BOUNDARY
CdSTE
SPL
COSMIC RAY RATE
COUNTS/SECOND
GEOCENTRIC DISTANCE (KM x 10³)
10³
10²
10¹
10⁰
10⁻¹
20
30
40
50
60
70
80

Figure 24

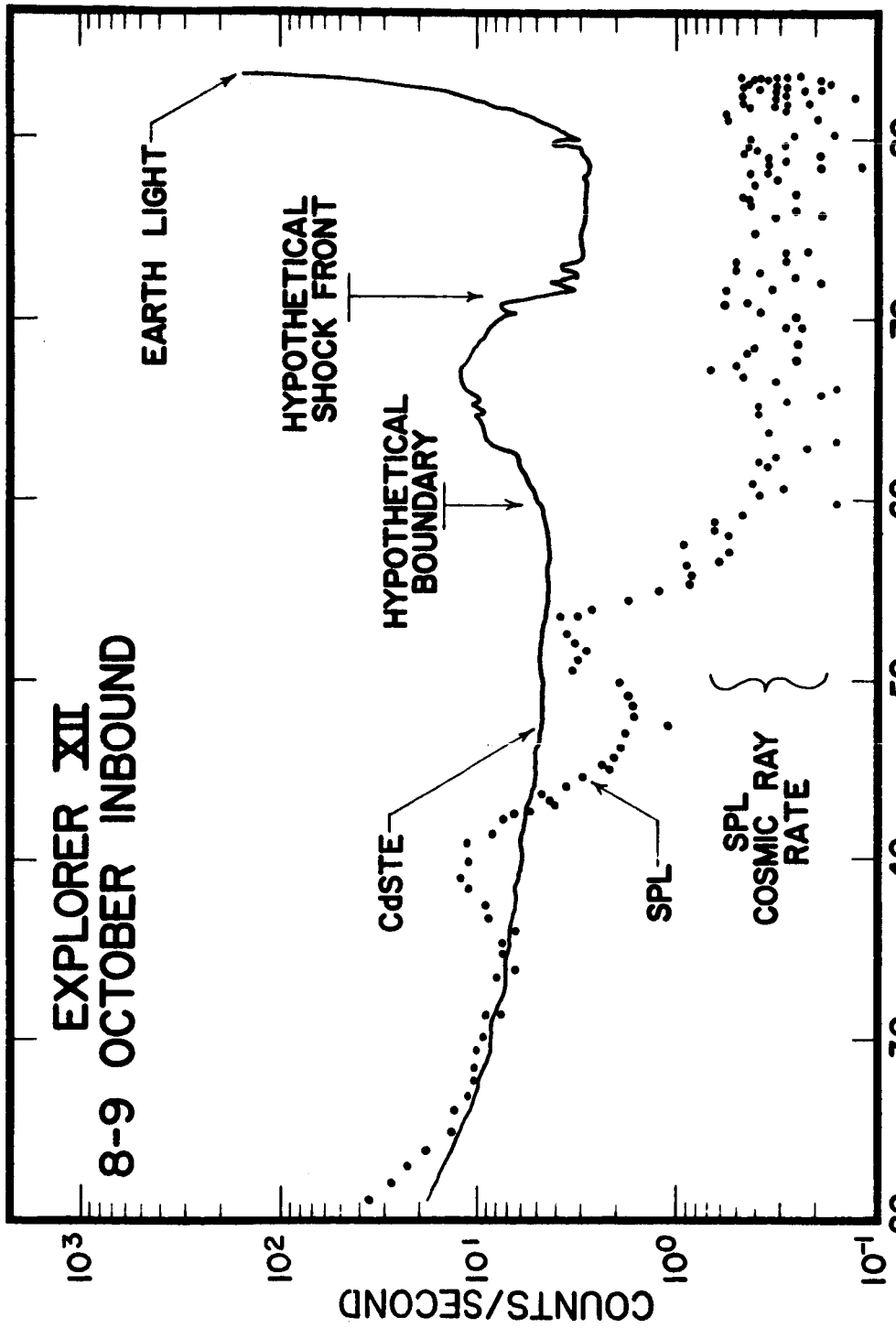
EXPLORER XII
8-9 OCTOBER INBOUND
EARTH LIGHT
HYPOTHETICAL SHOCK FRONT
HYPOTHETICAL BOUNDARY
CdSTE
SPL
SPL COSMIC RAY RATE
COUNTS/SECOND
GEOCENTRIC DISTANCE (KM x 10³)

Figure 25

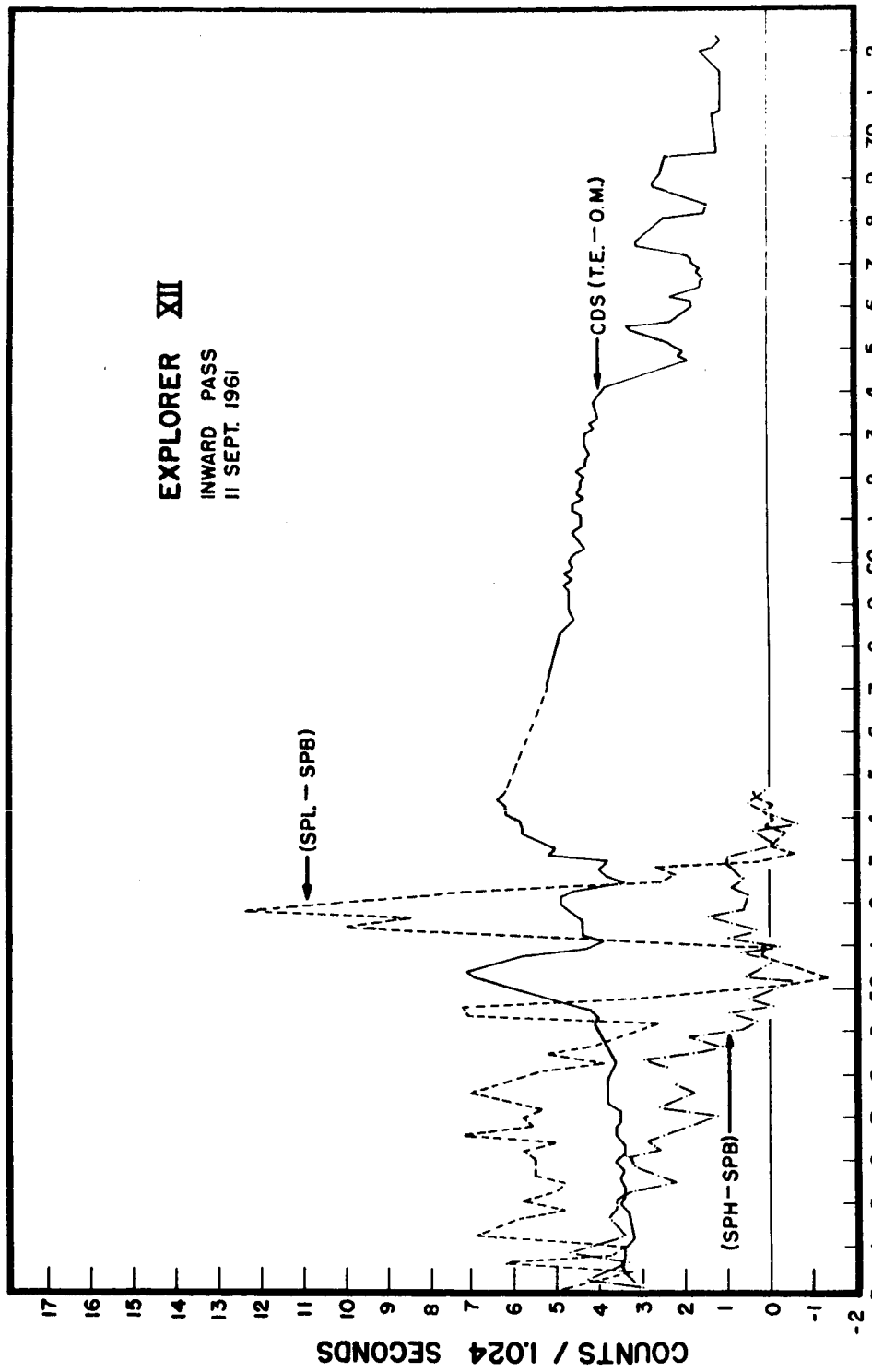
EXPLORER XII
INWARD PASS
11 SEPT. 1961
(SPL – SPB)
CDS (T.E. – O.M.)
(SPH – SPB)
COUNTS / 1.024 SECONDS
RADIAL DISTANCE IN 10^3 KM

Figure 26

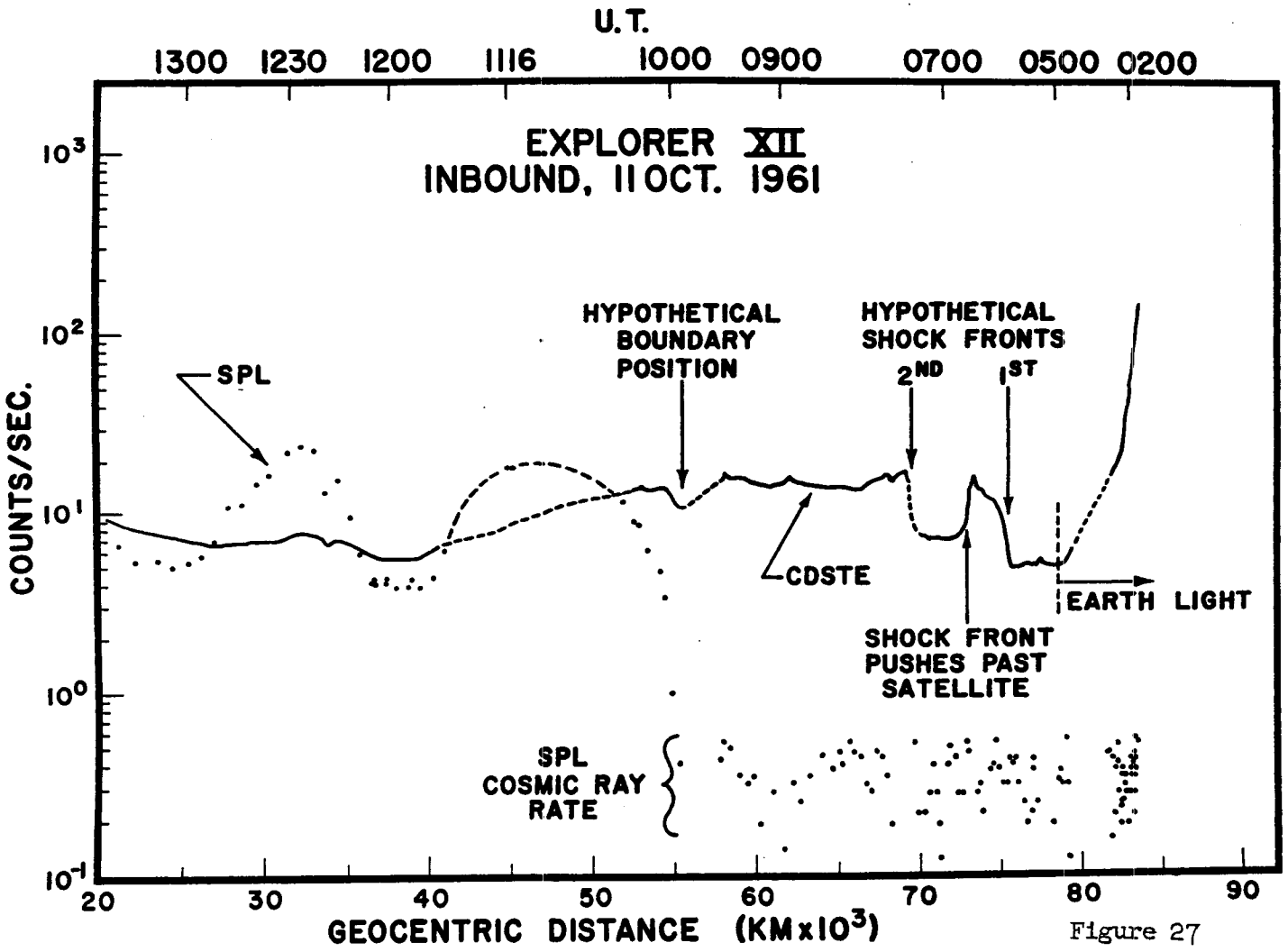
U.T.
1300 1230 1200 1116 1000 0900 0700 0500 0200
EXPLORER XII
INBOUND, 11 OCT. 1961
COUNTS/SEC.
10^3
10^2
10^1
10^0
10^{-1}
SPL
HYPOTHETICAL BOUNDARY POSITION
HYPOTHETICAL SHOCK FRONTS
2ND
1ST
CDSTE
EARTH LIGHT
SHOCK FRONT PUSHES PAST SATELLITE
SPL COSMIC RAY RATE
20 30 40 50 60 70 80 90
GEOCENTRIC DISTANCE (KM x 10^3)

Figure 27

EXPLORER XII

RADIAL POSITION OF THE MAGNETOSPHERIC BOUNDARY AS MEASURED BY TRAPPED ELECTRONS (SPL-SPB) COMPARED WITH D_{st}(H).

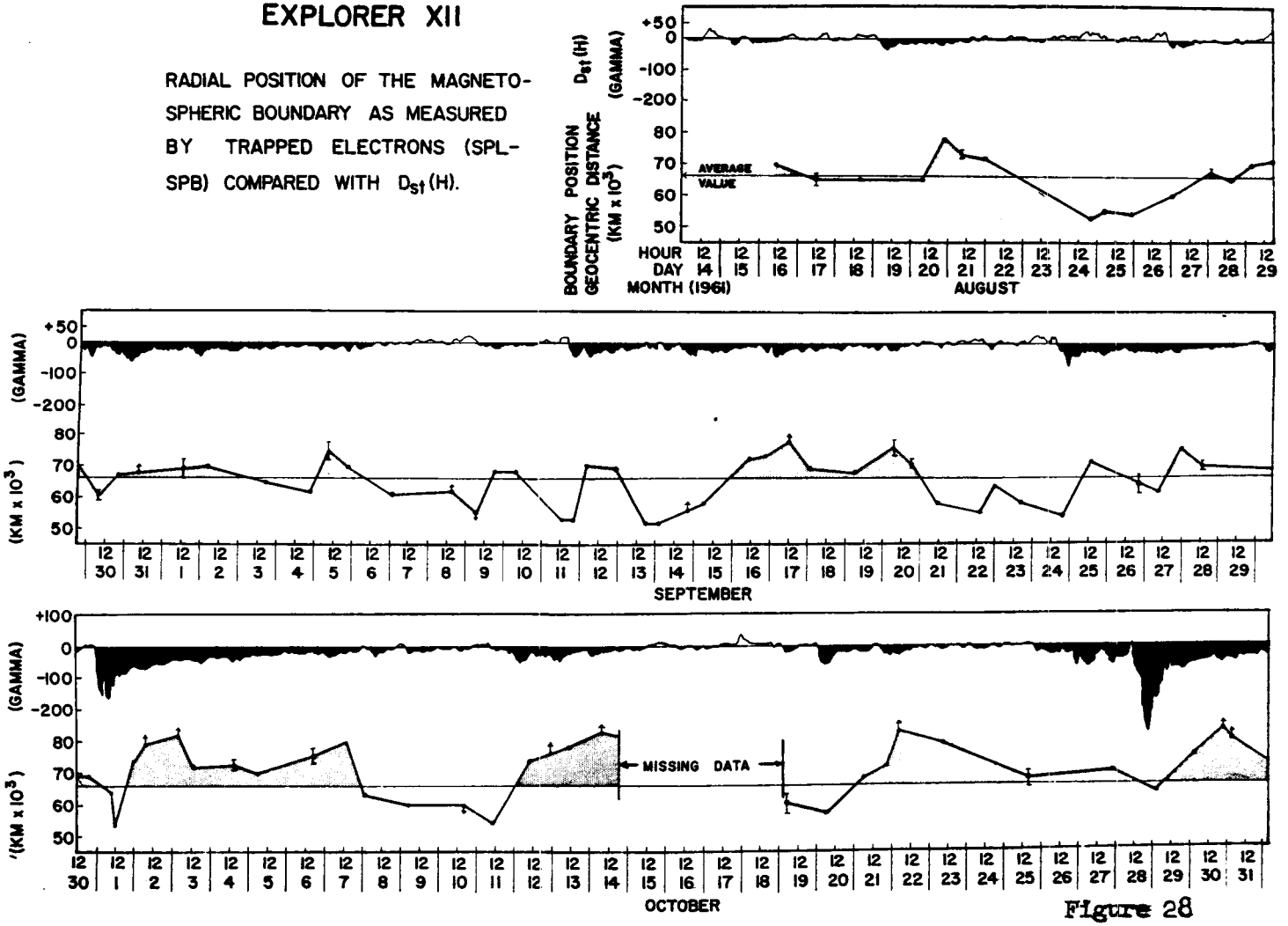

Figure 28

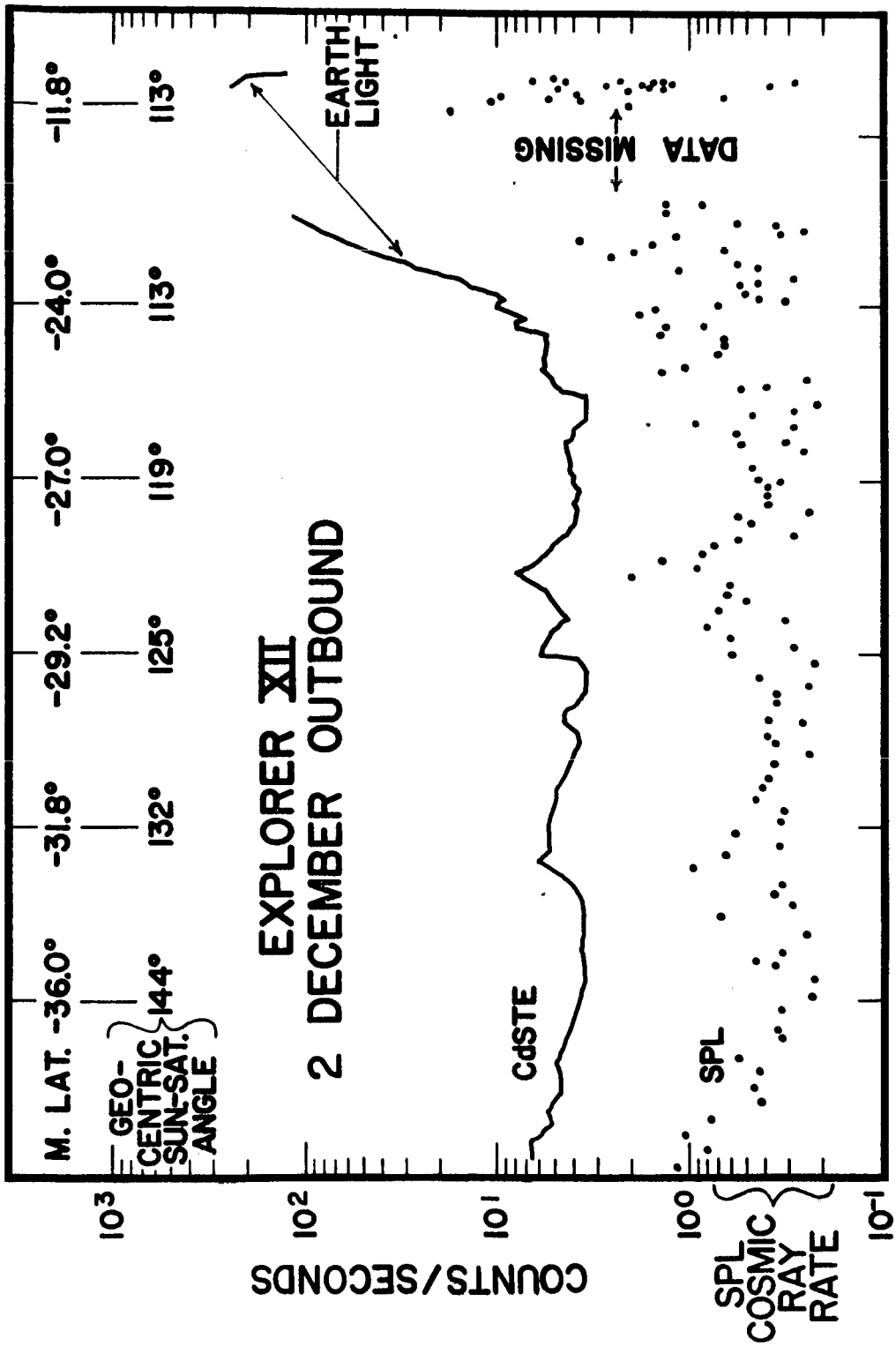
EXPLORER XII
2 DECEMBER OUTBOUND
EARTH LIGHT
DATA MISSING
CdSTE
SPL
M. LAT. -36.0° -31.8° -29.2° -27.0° -24.0° -11.8°
GEO-CENTRIC SUN-SAT. ANGLE 144° 132° 125° 119° 113° 113°
COUNTS/SECONDS
10^3
10^2
10^1
10^0
10^{-1}
SPL COSMIC RAY RATE
20 30 40 50 60 70 80
GEOCENTRIC DISTANCE (KM x 10^3)

Figure 29

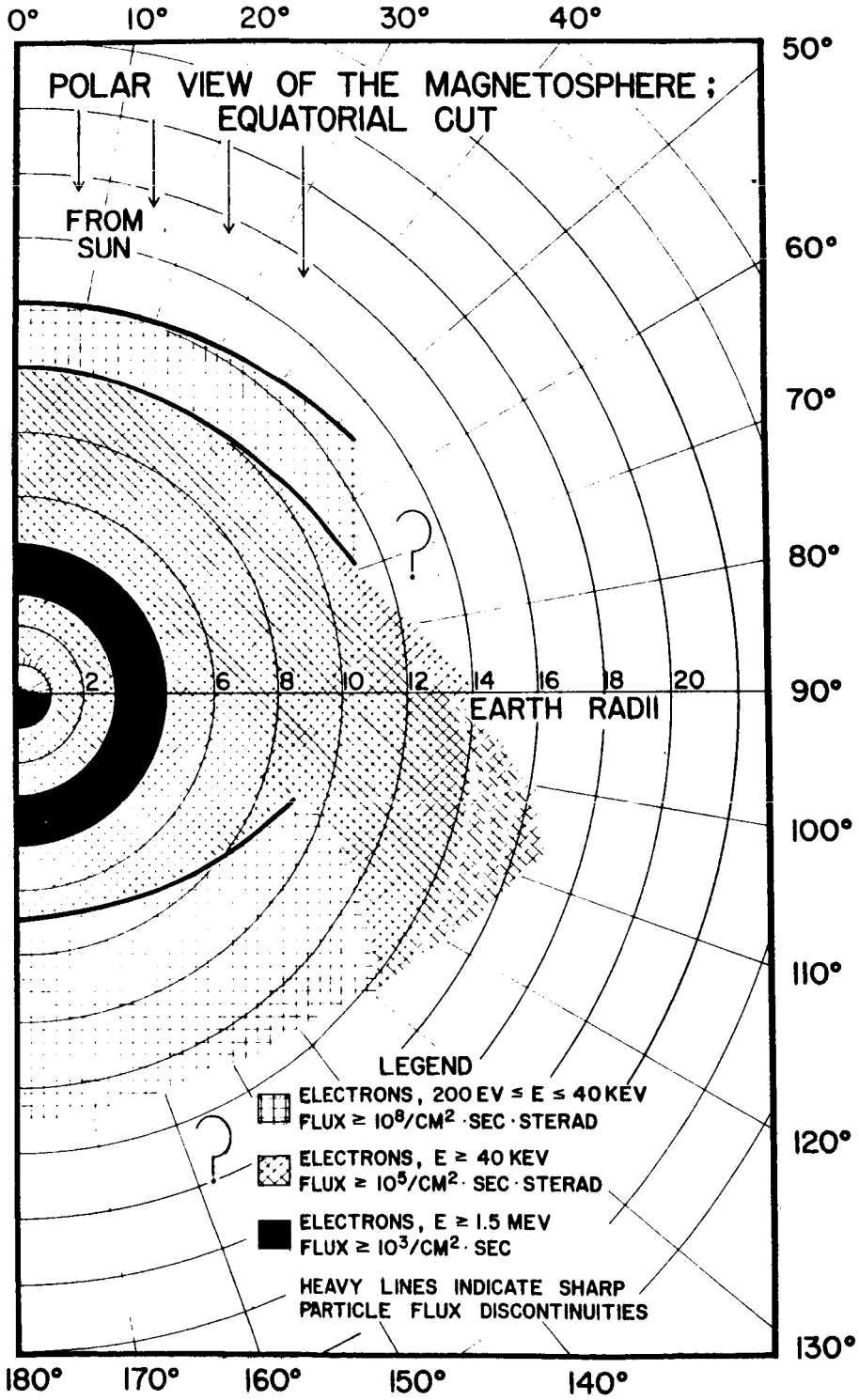
POLAR VIEW OF THE MAGNETOSPHERE;
EQUATORIAL CUT
FROM SUN
0°
10°
20°
30°
40°
50°
60°
70°
80°
90°
100°
110°
120°
130°
140°
150°
160°
170°
180°
2
6
8
10
12
14
16
18
20
EARTH RADII
?
?
LEGEND
ELECTRONS, 200 EV ≤ E ≤ 40 KEV
FLUX ≥ 10⁸/CM² · SEC · STERAD
ELECTRONS, E ≥ 40 KEV
FLUX ≥ 10⁵/CM² · SEC · STERAD
ELECTRONS, E ≥ 1.5 MEV
FLUX ≥ 10³/CM² · SEC
HEAVY LINES INDICATE SHARP
PARTICLE FLUX DISCONTINUITIES

Figure 30